Pediment formation and subsequent erosion in Gale crater: Clues to the climate history of Mars

A.B. Bryk [a,*], W.E. Dietrich [a], K.A. Bennett [b], V.K. Fox [c], C.M. Fedo [d], M.P. Lamb [e], E.S. Kite [f], L.M. Thompson [g], S.G. Banham [h], J. Schieber [i], J.A. Grant [j], A.R. Vasavada [k], A.A. Fraeman [k], L.A. Edgar [b], P.J. Gasda [l], R.C. Wiens [m], J.P. Grotzinger [e], K. Stack-Morgan [k], R.E. Arvidson [n], O. Gasnault [o], S. Le Mouélic [o], S. Gupta [h], R.M.E. Williams [p], R.Y. Sheppard [p,q], K.W. Lewis [s], D.M. Rubin [t], W. Rapin [r], M.N. Hughes [n], M. Turner [s], S.A. Wilson [j], J.M. Davis [h], R.E. Kronyak [k], L. Le Deit [o], L.C. Kah [d], J. Frydenvang [u], R.J. Sullivan [v], C.C. Bedford [m], E. Dehouck [w], H.E. Newsom [x,1], M.C. Malin [y]

[a] University of California, Berkeley, CA, USA
[b] U. S. Geological Survey Astrogeology Science Center, Flagstaff, AZ, USA
[c] Carleton College, Northfield, MN, USA
[d] University of Tennessee, Knoxville, TN, USA
[e] Division of Geological & Planetary Sciences, Caltech, Pasadena, CA, USA
[f] University of Chicago, Chicago, IL, USA
[g] University of New Brunswick, Planetary and Space Science Centre, Fredericton, Canada
[h] Imperial College, London, UK
[i] Department of Geological Sciences, Indiana University, Bloomington, IN, USA
[j] Smithsonian National Air and Space Museum, Washington, DC, USA
[k] Jet Propulsion Laboratory, Caltech, Pasadena, CA, USA
[l] Los Alamos National Laboratory, Los Alamos, NM, USA
[m] Purdue University, West Lafayette, IN, USA
[n] Washington University in St. Louis, St. Louis, MO, USA
[o] Université de Nantes, Nantes, France
[p] Planetary Science Institute, Tucson, AZ, USA
[q] Institut d'Astrophysique Spatiale, Orsay, France
[r] Institut de Recherche en Planétologie et Géodynamique, Toulouse, France
[s] Johns Hopkins University, USA
[t] University of California, Santa Cruz, CA, USA
[u] Globe Institute, University of Copenhagen, Copenhagen, Denmark
[v] Cornell Center for Astrophysics & Planetary Science, Cornell University, Ithaca, NY, USA
[w] Université Claude Bernard Lyon1, LGL-TPE, UMR 5276, CNRS, ENSL, UJM, Villeurbanne, France
[x] University of New Mexico, Albuquerque, NM, USA
[y] Malin Space Science Systems, San Diego, CA, USA

ARTICLE INFO

ABSTRACT

Evidence of paleo-rivers, fans, deltas, lakes, and channel networks across Mars has prompted much debate about what climate conditions would permit the formation of these surface water derived features. Pediments, gently sloping erosional surfaces of low relief developed in bedrock, have also been identified on Mars. On Earth, these erosional landforms, often thought to be created by overland flow and shallow channelized runoff, are typically capped by fluvial sediments, and thus in exceptionally arid regions, pediments are interpreted to record past wet periods. Here we document the Greenheugh pediment in Gale crater, exploiting the observational capability of the Curiosity rover. The absence of a fluvial cap suggests that the pediment was likely cut by wind erosion, not fluvial processes. The pediment was then buried by an aeolian deposit (Stimson sandstone) that mantled the

* Corresponding author.
  E-mail address: bryk@berkeley.edu (A.B. Bryk).
[1] Deceased.

lower footslopes of Aeolis Mons (informally known as Mt. Sharp). This burial terminated active wind erosion, preserving the pediment surface (as an angular unconformity). Groundwater was present prior-to, during, and shortly after Stimson deposition, perhaps contributing to lithification and certainly to early diagenesis. Post lithification, wind erosion first cut canyons in the northern most footslopes (north of Vera Rubin ridge). Unlithified gravels were deposited in these canyons, likely due to runoff from Mt. Sharp. Boulder-rich fluvial and debris flow deposits built a > 70 m thick sequence (Gediz Vallis ridge) on the southern Greenheugh pediment. Continued wind erosion left elevated patches of gravel on the northern footslopes, and exposure age dating shows that erosion essentially ceased before 1 Ga (but possibly much earlier). Erosion to the south led to emergence of Vera Rubin ridge, retreat of the Greenheugh pediment, and the formation of Glen Torridon valley. Hence, this footslope environment of Mt. Sharp records climate-driven periods of wind erosion, aeolian deposition (and groundwater activity), surface runoff and sediment deposition, followed by further significant wind erosion that declined to present very slow rates. This likely occurred during the late Hesperian and possibly into the Amazonian.

1. Introduction

The Greenheugh pediment is a 2.8 km^2 erosional remnant of distinct planar sloping topography at the northern footslope of Mt. Sharp in Gale crater (Figs. 1 and 2). While the landform had been mapped and its origin discussed based on satellite imagery (Malin and Edgett, 2000;
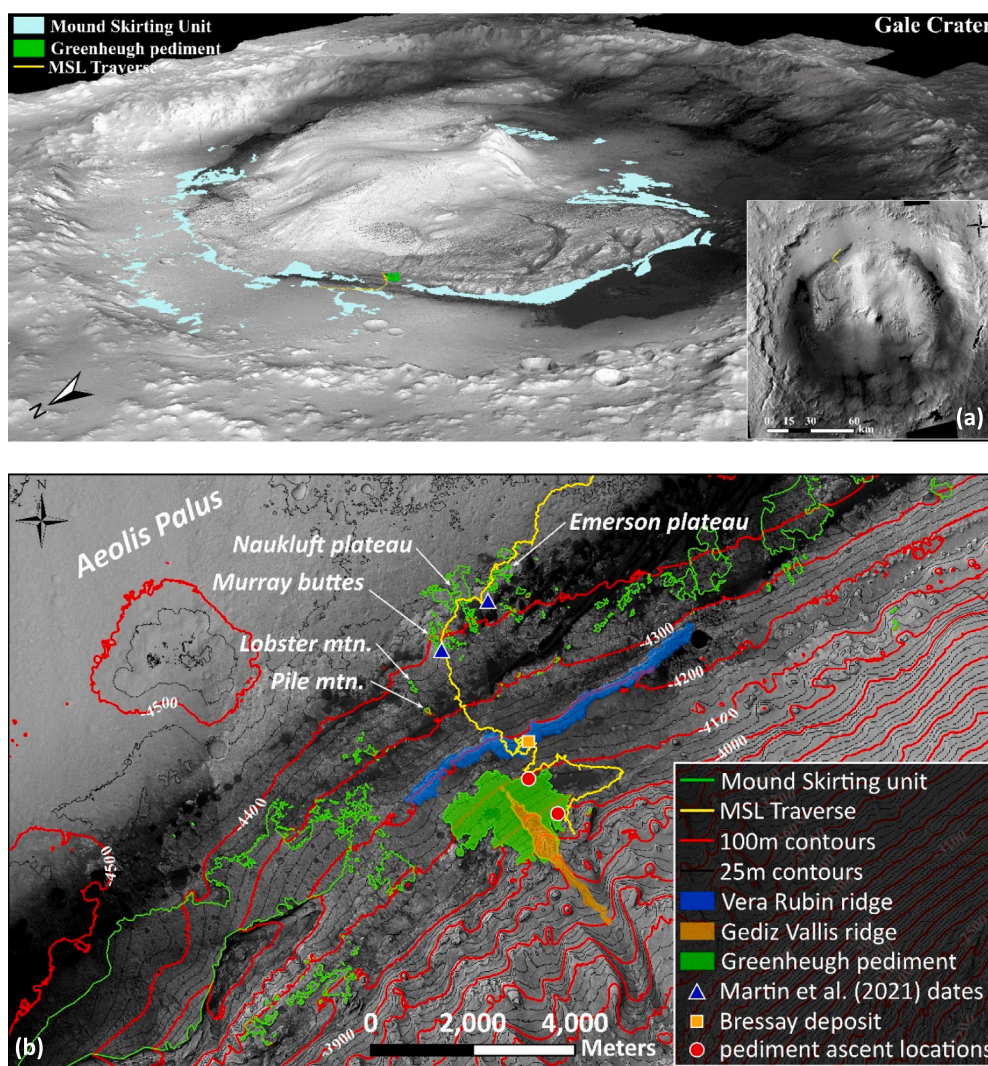

Fig. 1. Context maps of Gale crater and northern Mt. Sharp. a) 3D and map (inset) view of Gale crater made using imagery from the Context Camera (CTX) instrument on board the Mars Reconnaissance Orbiter (MRO) (Malin et al., 2007). The Greenheugh pediment is highlighted in green along with Curiosity's traverse (yellow) and the Mound skirting unit (teal) mapped by Anderson and Bell (2010) (light blue). b) Map of the northern footslopes of Mt. Sharp showing 25 (black) and 100 (red) meter HiRISE contours on a shaded relief image. Data from: McEwen et al. (2007), Calef III and Parker (2016), and Parker and Calef III (2016). The Greenheugh pediment is shown shaded in green, Vera Rubin ridge in blue, and the Gediz Vallis ridge in orange. Outline in green is a compilation of our own orbital mapping as well as: Mound Skirting unit features south of Aeolis Palus mapped by Anderson and Bell (2010) and Siccar Point group features mapped by Fraeman et al. (2016); Stack et al. (2017); Kronyak et al. (2019); Watkins et al. (2022); Banham et al. (2018); Banham et al. (2022). Pediment ascent locations, the Bressay heterolithic deposit as well as locations for radiometric exposure a (Martin et al., 2021) are also indicated on the map along the MSL traverse (yellow). HiRISE image credit: NASA/JPL/University of Arizona. (For interpretation of the references to colour in this figure legend, the reader is referred to the web version of this article.)

Anderson and Bell, 2010; Fraeman et al., 2016), it was only recognized as a pediment recently by the Mars Science Laboratory (MSL) mission's science team, which navigated the Curiosity rover along the eastern margin and ascended it in two locations. The term pediment is most generally defined as a gently sloping erosional surface of low relief developed on bedrock typically flanking a mountain range or escarpment (e.g., Dohrenwend and Parsons, 2009). Pediments on Earth often look similar to alluvial fans or bajadas in surface morphology, but are distinctly different in the subsurface. Whereas fans typically represent thick sequences of sediment, which can be accommodated by normal faulting for example, pediments are normally veneered with only a few meters of detritus, most if not all of which has been transported across the beveled pediment surface (King, 1953). Terrestrial field observations (e. g., Parsons and Abrahams, 1984) and numerical modeling (e.g., Howard, 1997) suggest pediments form through fluvial processes that spread laterally across the pediment surface, removing sediment supplied from upslope as well as eroding the bedrock surface. It is the beveled bedrock surface that is considered the pediment surface, which may or may not have a cap of mobilized detritus. Deep weathering may facilitate erodibility of the bedrock and influence the gradient of the pediment surface (Pelletier, 2010; Twidale, 2014). Typically, pediments flank a mountain or escarpment, which provides a source of sediment and runoff. Most studies have noted pediments in arid zones on Earth, and abandoned pediments are given particular attention (e. g., Hall et al., 2008). This is because abandoned pediments in arid regions that currently produce little or no runoff are sometimes considered indicators of a climate history of wetter times producing fluvial runoff capable of cutting and eroding a pediment (e. g., Oberlander, 1974).

Pediments have been mapped on Mars from satellite images and their presence has been used as evidence of fluvial activity, and given their low slope and relief, have been considered areas of very slow erosion (e. g., Cawley and Irwin III, 2018). In Endeavour crater, NASA's Opportunity rover provided the first ground-based observations of a pediment on Mars. However, the feature was not observable in cross-section and

there was not sufficient evidence to suggest what processes formed the pediment (Hughes et al., 2019). Inspection of the Greenheugh pediment by the Curiosity rover has now provided an opportunity to specifically investigate these processes, place it in the evolutionary history of Gale crater, and assess whether distinct links could be established with potential climatic drivers (and thus the climate of Mars).

Here we first review previous work on the Greenheugh pediment and associated deposits and then add observations on the pediment properties as ascertained from ascending the pediment on both the north and south sides as well as driving along its eastern margin (Figs. 1–3). We use rover-based observations and High Resolution Imaging Science Experiment (HiRISE) imagery to reconstruct the full extent of the pediment and its subsequent erosional history. This leads to a discussion where we address the following questions:

1. What processes formed the Greenheugh pediment (i.e., the beveled bedrock surface underlying the Stimson capping unit)?
2. What was the likely full extent of the Greenheugh pediment before erosional removal of the Stimson cap began?
3. What were the sources of sediment that formed the Stimson capping unit?
4. What caused the Greenheugh pediment downslope escarpment to retreat, leaving an elevated erosional remnant?
5. What influence did the pediment formation and subsequent burial have on the diagenetic evolution of the underlying bedrock and overlying caprock?
6. What are the likely climate conditions that favored the formation and subsequent burial and erosional degradation of the Greenheugh pediment and its capping deposits.

From this analysis, we build a rich time-history that calls for probable links to Martian climate history but also to possible roles of internal erosion and deposition dynamics.

Fig. 2. Footslope of Mt. Sharp looking towards the south. The Greenheugh pediment is shown shaded in green, Vera Rubin ridge in blue, and the Gediz Vallis ridge in orange. Outline in green is a compilation of our own orbital mapping as well as: Mound Skirting unit features south of Aeolis Palus mapped by Anderson and Bell (2010) and Siccar Point group features mapped by Fraeman et al. (2016); Stack et al. (2017); Kronyak et al. (2019); Watkins et al. (2022); Banham et al. (2018); Banham et al. (2022). The Amapari Marker Band (Milliken et al., 2010; Weitz et al., 2022) is shown (purple) as well as locations for radiometric exposure ages (Martin et al., 2021) are also indicated on the map along the MSL traverse (yellow). HiRISE image credit: NASA/JPL/University of Arizona. HiRISE image credit: NASA/JPL/University of Arizona. (For interpretation of the references to colour in this figure legend, the reader is referred to the web version of this article.)

Fig. 3. View of footslope looking towards the south. The MSL traverse (yellow) onto and around the Greenheugh pediment (green outline) is also included. HiRISE image credit: NASA/JPL/University of Arizona. (For interpretation of the references to colour in this figure legend, the reader is referred to the web version of this article.)

2. The Greenheugh pediment in context

2.1. Regional context

Early mapping efforts in Gale crater using orbital data collectively defined a variety of crater floor units based on texture, thermal inertia, albedo, and spectrally derived mineralogy (Malin and Edgett, 2000; Milliken et al., 2010; Anderson and Bell, 2010; Thomson et al., 2011; Le Deit et al., 2013). The most well-known of these is the Mound Skirting unit (MSu) first defined by Anderson and Bell (2010) (Fig. 1a). The MSu consists of apparent depositional features found draping the basal slopes of Mt. Sharp, the floor of Gale crater, and on the northern slopes of Gale crater. These inferred deposits commonly are dark-toned crater preserving ('pockmarked') surfaces that often form decameter escarpments and commonly exhibit *E*-W linear ridges of uncertain origin (Fig. S1 in Supporting Information S1; Kah et al., 2013; Milliken et al., 2014; Buz et al., 2017; Kronyak et al., 2019; Bretzfelder et al., 2024). Upslope of the MSu, in the vicinity of the Greenheugh pediment, the northern margin of Mt. Sharp forms large (tens to hundreds of meters high) topographic steps characteristic of layered sedimentary deposits of varying erosional resistance undergoing scarp retreat. These steps are further dissected by NW-SE trending valleys including Gediz Vallis (Figs. 1–3). Emanating from some of these valleys along the northern half of Mt. Sharp are layered degraded fan deposits (e.g., the Gediz Vallis ridge), which have been reported as resting stratigraphically above the MSu and may have been influenced by the presence of large ephemeral lakes (Anderson and Bell, 2010; Palucis et al., 2016). Near the base of Mt. Sharp centered roughly below Gediz Vallis, the modern topographic surface has a broad inclined conical shape, extending north from near the mouth of Gediz Vallis to the Murray buttes and east-west over 20 km laterally (see Fig. 1b -4400, −4300, −4200, and − 4100 m contours; Fig. 2). This hump-like feature has an amplitude of ~200-250 m over the ~20 km width of the feature. Located near the apex of it lies the much smaller Greenheugh pediment. (Figs. 1; 2).

2.2. Description of the pediment and previous work

The Greenheugh pediment is a long-recognized landform from orbital data along the lower slopes of Mt. Sharp (Malin and Edgett, 2000; Thomson et al., 2008; Anderson and Bell, 2010; Palucis et al., 2016; Fraeman et al., 2016; Bryk et al., 2019a, 2020). Early examination of this feature by Malin and Edgett (2000) suggested that the Greenheugh pediment records an unconformity representing a period of non-deposition during the construction of Mt. Sharp, which was subsequently deeply buried and then exhumed during net erosion of Mt. Sharp. Later authors hypothesized that the unconformity formed much later after substantial denudation of Mt. Sharp and was then buried by fan deposits (now known as the Gediz Vallis ridge). The pediment, which may have never been deeply buried, was then exposed through subsequent aeolian erosion (Thomson et al., 2008; Anderson and Bell, 2010; Palucis et al., 2016).

Today, the Greenheugh pediment is recognized as the upslope extension of an erosional surface preserved under a dark-toned resistant capping unit, the Stimson formation, (Williams et al., 2018; Bryk et al., 2019a; Banham et al., 2018, 2021, 2022; Bedford et al., 2020, 2022). Visited by Curiosity in three locations (prior to arriving at the pediment) and observed at a distance from many others, the aeolian Stimson formation currently comprises the only formation in the Siccar Point group (Fig. 4a-c; Fig. S3 and S4 in Supporting Information S1; Fraeman et al., 2016; Williams et al., 2018; Bryk et al., 2019b; Banham et al. (2018); Banham et al. (2022); Bedford et al., 2020, 2022). The buried erosional surface (the pediment) truncates sediments of the Mt. Sharp group (MSg) deposited during Mt. Sharp construction and as such defines a major unconformity now known as the basal Siccar Point group (SPg) unconformity (Bryk et al., 2019b; Banham et al., 2022). This unconformity clearly shows the pediment as an eroded surface formed after construction of Mt. Sharp and preserved by the Stimson. Remnants of the pediment appear to extend to the north of Vera Rubin ridge. The erosional surface is roughly parallel to current topography at the
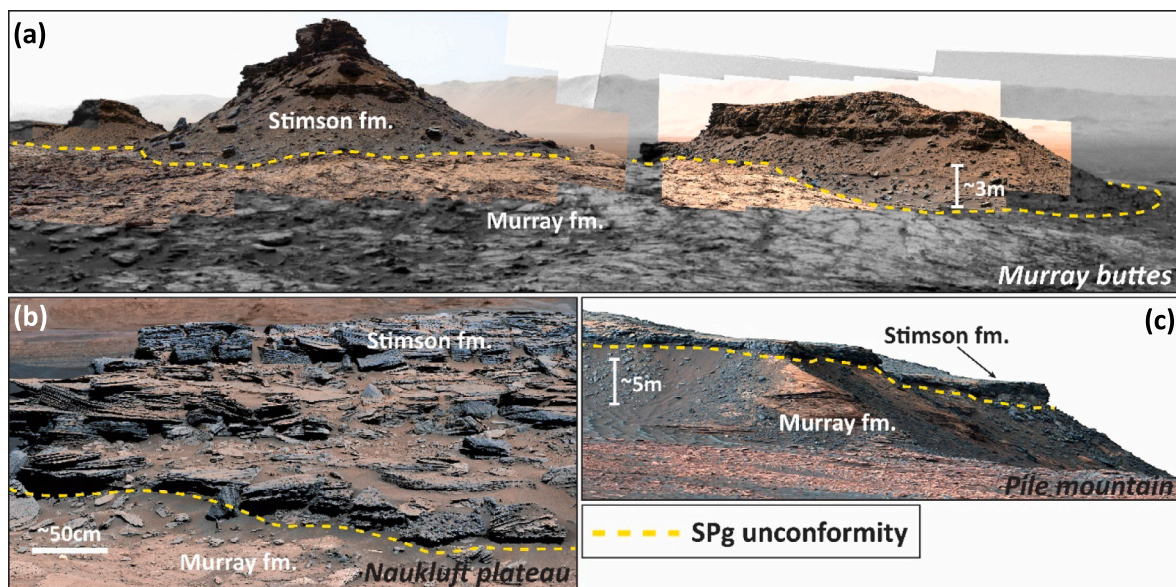
Fig. 4. Mastcam images showing areas exposures to the north (and downslope from) the Greenheugh pediment. Locations for a) Murray buttes, b) Naukluft plateau, c) Pile mountain are shown in Figs. 1b and 2. The basal Siccar Point group (SPg) unconformity (yellow dashed line) separates the Stimson formation (SPg) from the Murray formation within the Mt. Sharp group (MSg). Image credit: NASA/JPL-Caltech/MSSS. See Table S1 in Supporting information S3 for image sequence identifiers. (For interpretation of the references to colour in this figure legend, the reader is referred to the web version of this article.)

regional scale and thus likely records an erosion period when the lower slopes of Mt. Sharp were stripped to approximately the current topography prior to deposition of the Stimson fm. (Watkins et al., 2022). For simplicity in this paper, we will use the term "Greenheugh pediment" to also refer to the topographic feature comprised of the beveled bedrock surface mantled by the Stimson formation. Because the Stimson mantle is thin, the underlying pediment surface and current topographic surface are similar.

The Greenheugh pediment today covers ~2.8 km^2, and progressively declines in slope from 25 % to 12 % over a downslope distance of ~1600 m. Near the −4040 m contour, there is a break in slope, below which the surface slope is more variable but averages to a nearly consistent value of ~12 % (Figs. 5a; 6a, b). This range in slopes for the Greenheugh pediment is characteristic of typical values reported for pediments on Earth where bedrock erosion is due to surface water runoff (Dohrenwend and Parsons, 2009). As seen in Fig. 5b, the Stimson surface has retained many small impact craters and, bordering Gediz Vallis ridge, the surface is organized into a well-defined washboard-like pattern of low-amplitude ridges (Figs. 5b; 7a, b). The washboard pattern characterizing the top of the Stimson at the Greenheugh pediment is locally unique to the landform and contains two dominant ridge orientations. The major ridges are oriented *E*-W with an average azimuth of 107 degrees and an average wavelength of 14 m. The secondary ridges are roughly orthogonal to the primary ridges exhibiting an average azimuth of 200 degrees and an average wavelength of 9 m (Fig. S1a, b in Supporting Information S1). Amplitude in both cases is usually less than 0.5 m, with the secondary ridges generally showing slightly lower amplitude. The intersection of these two ridge/swale features gives rise to an apparent interference pattern that is typical of the polygonal 'washboard' appearance observed by HiRISE (Fig. 5b).

3. Rover-based inspection of pediment erosional boundary and capping unit

As part of the ascent of Mt. Sharp, the Curiosity rover deviated onto the northern edge of the pediment, then drove around its eastern edge and asfcended onto the southern edge of the pediment (Fig. 8). Our work relied primarily on imagery generated by Curiosity's Mastcam 34- and 100-mm lens cameras (Malin et al., 2017; Bell III et al., 2017), long-

distance imaging by the ChemCam long distance Remote Micro-imager (ChemCam LD RMI) (Maurice et al., 2012; Wiens et al., 2012), the Mars Hand Lens Imager (MAHLI) camera (Edgett et al., 2012; Yingst et al., 2016), and the rover's navigation cameras (Navcam) (Maki et al., 2012).

Chemical and mineralogical data referenced herein were generated from Curiosity's Chemistry Laser Induced Breakdown Spectroscopy (ChemCam LIBS) and Remote Micro Imager (ChemCam RMI) (Maurice et al., 2012; Wiens et al., 2012), the Alpha-Particle X-Ray Spectrometer (APXS) (Gallert et al., 2015), the Chemistry and Mineralogy (CheMin) instrument (Blake et al., 2012), and the Sample Analysis at Mars (SAM) instrument (Mahaffy et al., 2012).

All orbital mapping was completed in ArcGIS using the HiRISE (McEwen et al., 2007) MSL Gale Merged Orthophoto Mosaic 25 cm/ pixel base map generated by Calef III and Parker (2016). Elevation data were derived from HiRISE stereo pair products calibrated to Mars Global Surveyor (MGS) Mars Orbiter Laser Altimeter (MOLA), by Parker and Calef III (2016). Topographic profiles (e.g., Figs. 6b) the polar histogram (Fig. S1b in Supporting Information S1), the Mound Skirting Unit reconstruction video (Video S11 in Supporting Information S1), and the reanalysis of Watkins et al. (2022) data (Fig. S13 in Supporting Information S1) were completed in MATLAB. Figures showing all of Gale crater (Fig. 1) were produced using ArcGIS from data collected by the Context Camera (CTX) on board the Mars Reconnaissance Orbiter (MRO) (Malin et al., 2007).

3.1. Northern exposure and ascent (tower butte location)

Figure 9 shows the northern ascent area and the northern margin of the pediment along which Curiosity traversed between Tower butte and Bloodstone hill. Fig. 10 provides context views of the northern margin of the pediment taken during Curioisty's exploration of Glen Torridon (Fig. 3; Bennett et al., 2023). Stimson formation rocks occur in prominent cliff forming outcrops above the poorly-exposed SPg unconformity. Blocks shed from the Stimson variably mantle the exposed Mt. Sharp group sediments. Notably, these boulders rarely extend beyond the base of the escarpment (Fig. 10a, b) – thus suggesting either rapid destruction over short distances away from the cliff face, or possible episodic (non-steady state) scarp retreat (see sections 3.2 and 5.4). At Tower butte,
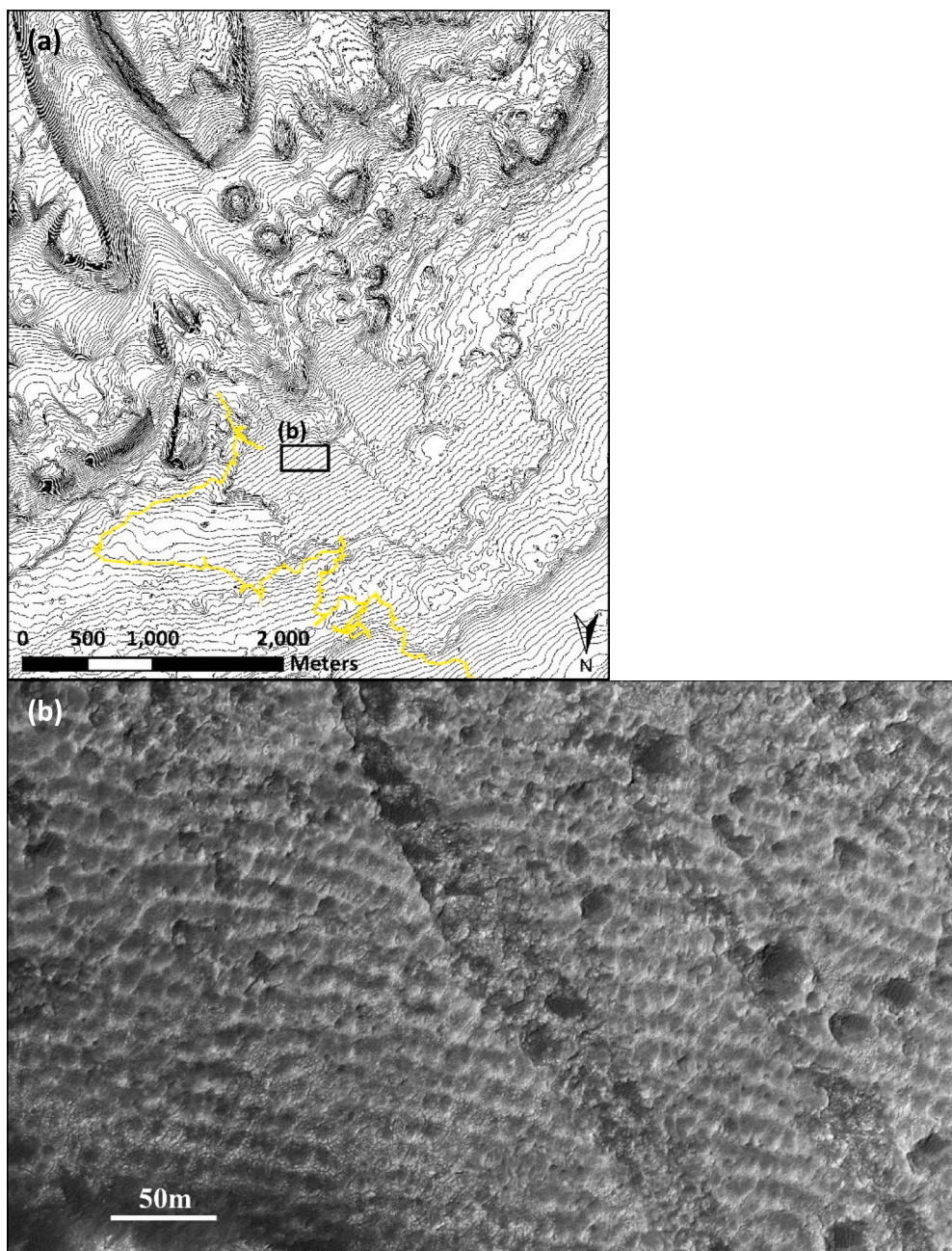
Fig. 5. Greenheugh pediment a) Topographic map (10 m contours) of the Greenheugh pediment and surrounding area. Yellow line is the Curiosity path; b) HiRISE orthoimagery inset showing the washboard pattern characteristic of the Stimson at the Greenheugh pediment. HiRISE image credit: NASA/JPL/University of Arizona. (For interpretation of the references to colour in this figure legend, the reader is referred to the web version of this article.)

Curiosity encountered a prominent light-toned topographic shelf, which was ultimately chosen for the Hutton drill site (Fig. 10b).

At this shelf, which lies below the unconformity, Curiosity observed abundant diagenetic features including dark-toned nodules, blue-gray bedrock coloration, as well as sub-vertical light- and dark-toned veins that were not seen crossing the unconformity into the overlying Stimson (Fig. 11; Fig. S5 in Supporting Information S1). Exposure of the unconformity was rare as it was almost everywhere covered in modern aeolian sand or obscured by scree (Fig. 10b). Near the ascent location, the best exposure of the SPg unconformity was found at the Moray Firth outcrop (Figs. 10b; 12). Here the SPg erosional surface is relatively smooth, with local variations smaller than 20 cm. At this location it cuts across the laminated Glasgow member of the Carolyn Shoemaker formation (Fig. S3 in Supporting Information S1). Above the unconformity,

no evidence for water-transported sands or gravels, which typically mantle terrestrial pediments, was observed. Instead, it was overlain by the aeolian Stimson formation (e.g., Banham et al., 2022). Along the ascent location, an unusual texture was noted that consisted of discontinuous bedded-to-massive sandstone characterized by occasional matrix supported clasts (up to 1 cm in diameter) and centimeter scale spherules (Fig. 11b, c). The unit exhibited a gradational upper contact with the more typical cross-bedded Stimson and did not appear to indicate transport by water.

Within the Stimson fm., three distinct intervals (Fig. 12) were identified at the ascent location that correspond to subtle but consistent lithologic differences (Banham et al., 2022). The first interval above the unconformity (Gleann Beag interval) is characterized by decimeter to half meter scale trough cross-stratification, abundant nodules, and one
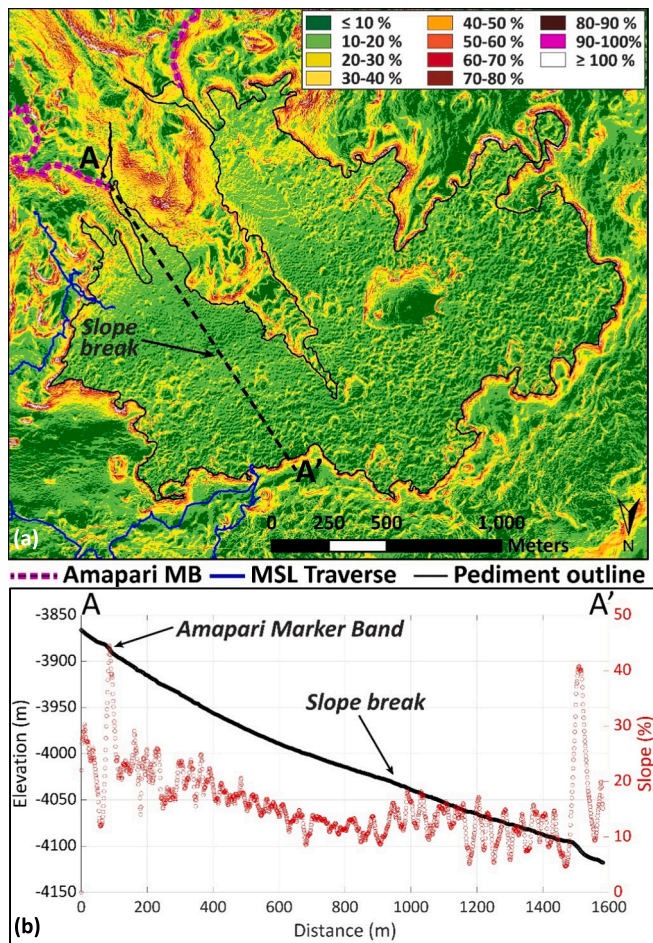
Fig. 6. Slope map and associated long-profile at the Greenheugh pediment. a) Slope map from HiRISE-derived topography with the Amapari Marker Band (MB) overlain in purple and the MSL traverse in blue. b) Elevation and slope profile A-A' taken from the SE side of the pediment perpendicular to topography. Note in the profile the locations of slope anomalies at the Northern edge of the pediment, near the center of the profile (labeled slope break) and at the Amapari Marker Band (Purple dashed line in (a) (Milliken et al., 2010; Weitz et al., 2022). HiRISE image and topographic data source credit: NASA/JPL/ University of Arizona. (For interpretation of the references to colour in this figure legend, the reader is referred to the web version of this article.)

location small mudstone clasts incorporated in the sandstone sediment. The nodules are chemically indistinguishable from the surrounding Stimson and appear to exist as clusters of preferentially cemented rounded sand grains (Fig. S6 in Supporting Information S1; Thompson et al., 2022b). Nodule abundance varies within the unit and can be observed extending into the upper intervals of the Simson as occasionally discreet fingers or tendrils of nodularized sandstone. The next interval above the nodular Stimson (labeled the Ladder interval) is comprised of platy weathering aeolian sandstone with abundant pinstripe laminations and large planer foresets (including thicknesses of up to 0.8 m and laterally traceable bedding over >70 m). The Ladder interval represents some of the largest preserved sedimentary structures observed by Curiosity. Finally, the top of the Stimson south of Tower butte (labeled the Edinburg interval) includes the Edinburgh drill site (Fig. 10) and is comprised of blocky-weathering trough cross-bedded aeolian sandstone (Fig. 12; Banham et al., 2022).

Upon ascending the pediment escarpment, Curiosity crossed the degraded top of the Stimson arriving at the Machir Bay outcrop – the highest elevation gained during the northern ascent (Figs. 10b, and 13a). Mastcam and ChemCam RMI surveys of the top surface of the pediment revealed patches of blocky-weathering Stimson in the

nearfield (green shading in Fig. 13a, b) and Curiosity's first distant observations of the washboard pattern (Fig. 13c). It is possible the blocky-weathering (Edinburgh) interval observed here near Tower butte are remnant pieces of the once more continuous washboard texture. Further imaging of the Stimson top indicated an absence of foreign clasts as may have originated from a likely once more extensive Gediz Vallis ridge to the south (Bryk et al., 2019b).

Western butte lies adjacent to the Greenheugh pediment NW of Tower butte. Curiosity visited the eastern plateau known as "the shoulder" of Western butte and ascended as far as was safe towards the capping unit on the West side of the butte (Fig. 9). There, anticipating an encounter with a disconnected former piece of Greenheugh pediment, the rover instead encountered a dark rubbly deposit of unconsolidated boulders resting on a north-sloping surface (Fig. 10a). The boulders were both physically and chemically distinct from the Stimson formation observed at Tower butte, and their origin remains unclear (Fig. S7 in Supporting Information S1).

3.2. Exposure along transect from north to south

East of Bloodstone hill (Fig. 9), Curiosity circumnavigated the Sands of Forvie during which time the team extensively imaged the Eastern margin of the Greenheugh pediment (Fig. 8). Although cover by modern sand and scree made full exposure of the contact rarely visible along this transect, the boundary was generally planar and the Stimson was a relatively constant thickness (Fig. 14). The smooth (Fig. 14a, c) to slightly wavy (Fig. 14b) contact lacked local troughs characteristic of fluvial incision, and no evidence for water sorted sediments (sand or gravel) was observed.

The escarpment varied in relief but was typically 10 m high with a 1-3 m thick Stimson cap and variable scree coverage. Occasional patches of thick (10-30 cm) scree indicate a residual colluvial mantle, previously deposited that then subsequently experienced net erosion (Fig. 15). We also observed similar patches on the isolated Stimson capped buttes downslope and north of the pediment (at Pile mountain) (Fig. S4 in Supporting Information S1) and perhaps along the North side of Western butte (Fig. 10a; Fig. S7 in Supporting Information S1). Along the rover path following the eastern side of pediment, occasional distinct blue/ gray colored clasts interpreted to be Stimson blocks were encountered. At the maximum distance (1.2 km) from the eastern side of the pediment where the rover path turned and headed west (Figs. 1b; 8), several Stimson blocks up to 100 mm long were found along this section of the traverse. Imaging along the track to the west, also revealed the blue/ gray rocks of the Stimson on top of Rafael Navarro mountain. (Fig. 8; Fig. S8 in Supporting Information S1). Together these observations suggest that the pediment was once more laterally extensive.

South of the Sands of Forvie, Curiosity drove along the southeast margin of the pediment passing Siccar Point towards Maria Gordon notch and the southern pediment ascent location at Blackcraig (Fig. 8). Along a 90 m long outcrop to the north of Maria Gordon notch, Dietrich et al. (2022) found a distinct zone of deformed Stimson fm. sediments directly above the SPg unconformity (Fig. 16a, b). The unit is typically less than 1 m thick and exhibits a range of textures from massive bedding to convolute laminations. The upper contact with the overlying cross-bedded Stimson is typically sharp and non-planar (Fig. 16c) with the overlying laminations occasionally deflecting away from or towards the contact (Fig. 16d). Several vertical surfaces (fracture planes) within the overlying cross-bedded Stimson appear to contain a coating of sediment that may have been injected upward from the basal unit (Fig. 16e). Close inspection of tumbled blocks of this basal unit (Fig. 16f-h) enabled contact science which revealed that although the sedimentary textures within the rock were distinct, the typical grainsize and chemistry of the basal unit is identical to the overlying cross-bedded Stimson (Dietrich et al., 2022). Together, these observations suggest a soft sediment deformation mechanism for the basal Stimson fm. likely through the presence of water saturation at a time when the unit was not fully
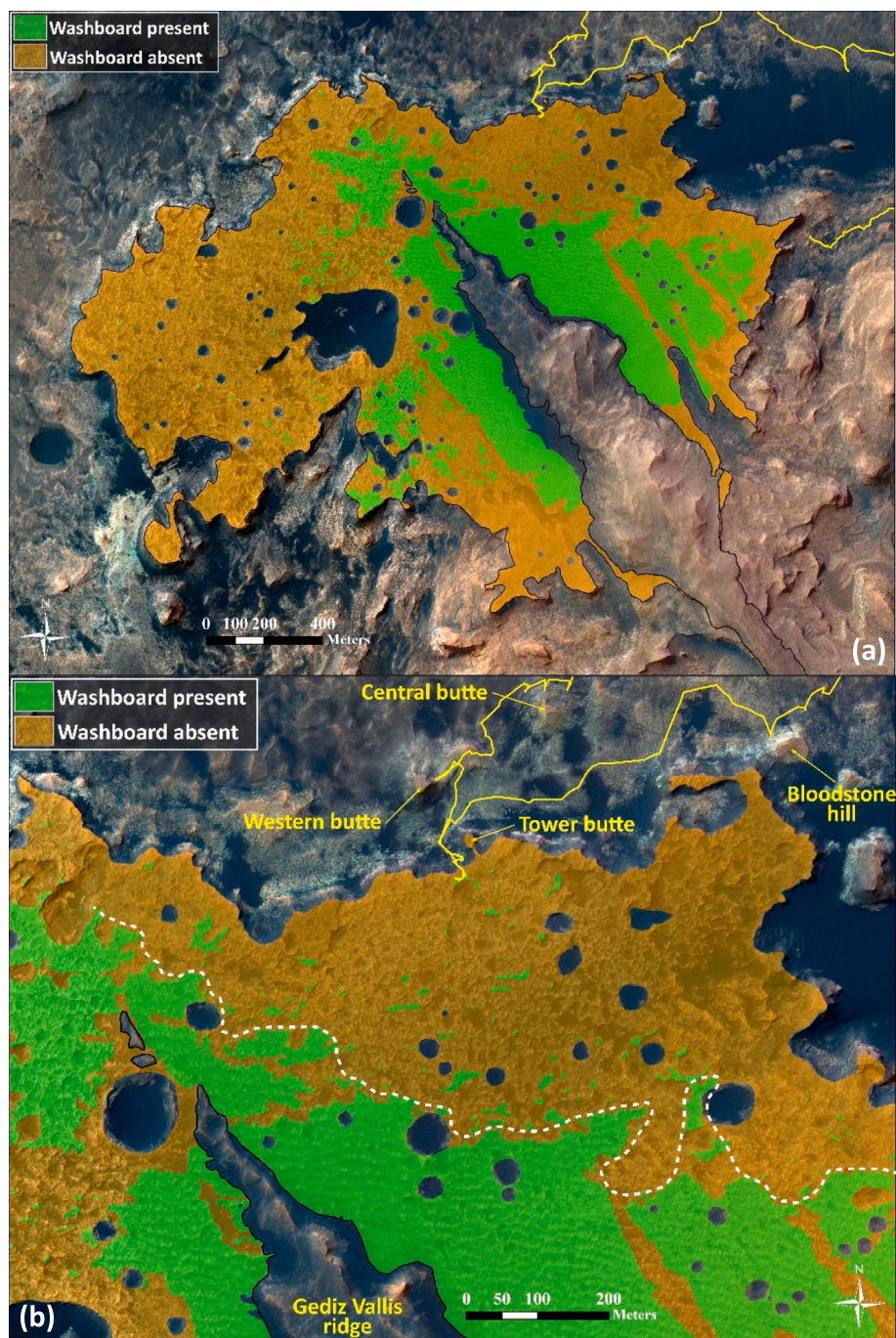
Fig. 7. Washboard pattern mapped from HiRISE orthoimagery showing areas of 'intact' washboard (green) and areas of non-washboard Stimson (orange). a) full pediment map. b) Inset showing the NE pediment area including the approximate boundary (white dashed line) between coherent washboard and the lower Stimson units. HiRISE image credit: NASA/JPL/University of Arizona. (For interpretation of the references to colour in this figure legend, the reader is referred to the web version of this article.)

lithified (see also Fig. S15 in Supporting Information S1). This interpretation is supported by the results of Banham et al., 2024, from data collected further west and higher within the Stimson stratigraphy.

Near the southern pediment ascent location, Maria Gordon notch is a 14 m vertical exposure of stratigraphy of the Port Logan member of the Mirador formation (see Fig. S3 in Supporting Information S1 for stratigraphic nomenclature), which is here unconformably cut by the pediment and overlain by the Stimson (Figs. 17 and S9 in Supporting Information S1). At Maria Gordon notch, Curiosity observed a dramatic change in outcrop colour from red near the base to gray at the top (Fig. S9 in Supporting Information S1). The colour transition occurs

roughly at an elevation of -3971 m and was not observed elsewhere at that elevation suggesting it may be related to the presence of either the SPg unconformity or the overlying Stimson formation, rather than due to a primary depositional change. Like the ascent at Tower butte, the strata below the unconformity at Maria Gordon outcrop exhibit extensive veination in a variety of orientations. These veins were not observed crossing the unconformity into the overlying Stimson (Fig. S9 in Supporting Information S1).

Curiosity's traverse from the northern to the southern pediment margins allowed us to observe the pediment surface descending down across 315 m of elevation drop and truncating at least 6 distinct
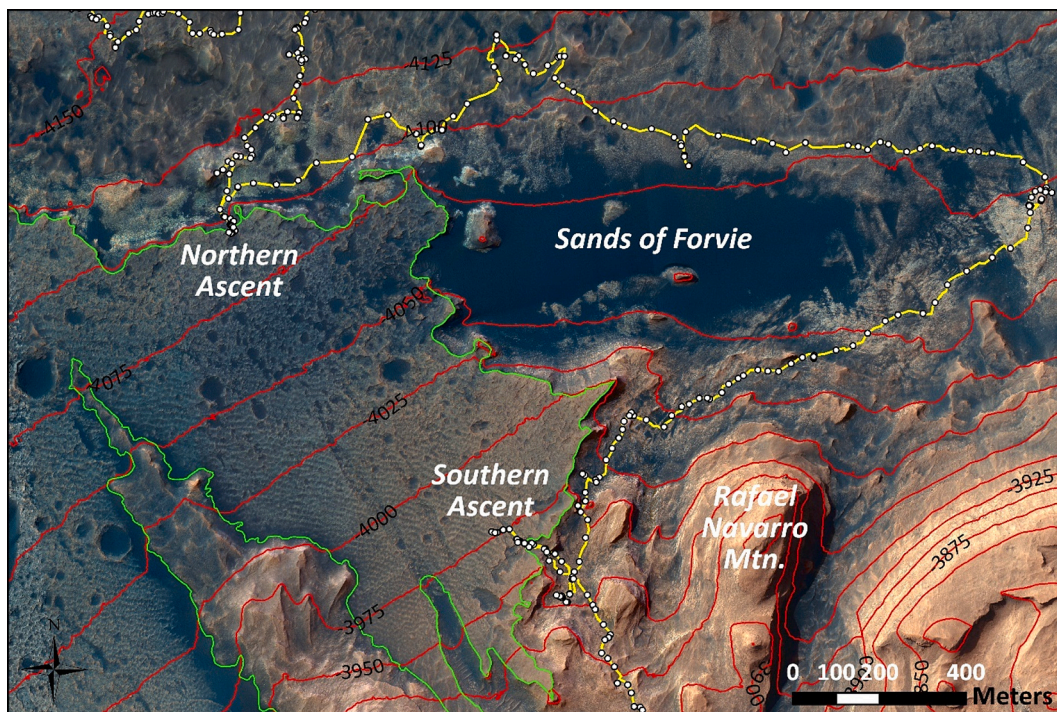
Fig. 8. Map of the eastern side of the Greenheugh pediment showing the two ascent locations northern (Tower butte) and southern (Blackcraig) as well as the MSL traverse around the Sands of Forvie. HiRISE image credit: NASA/JPL/University of Arizona.
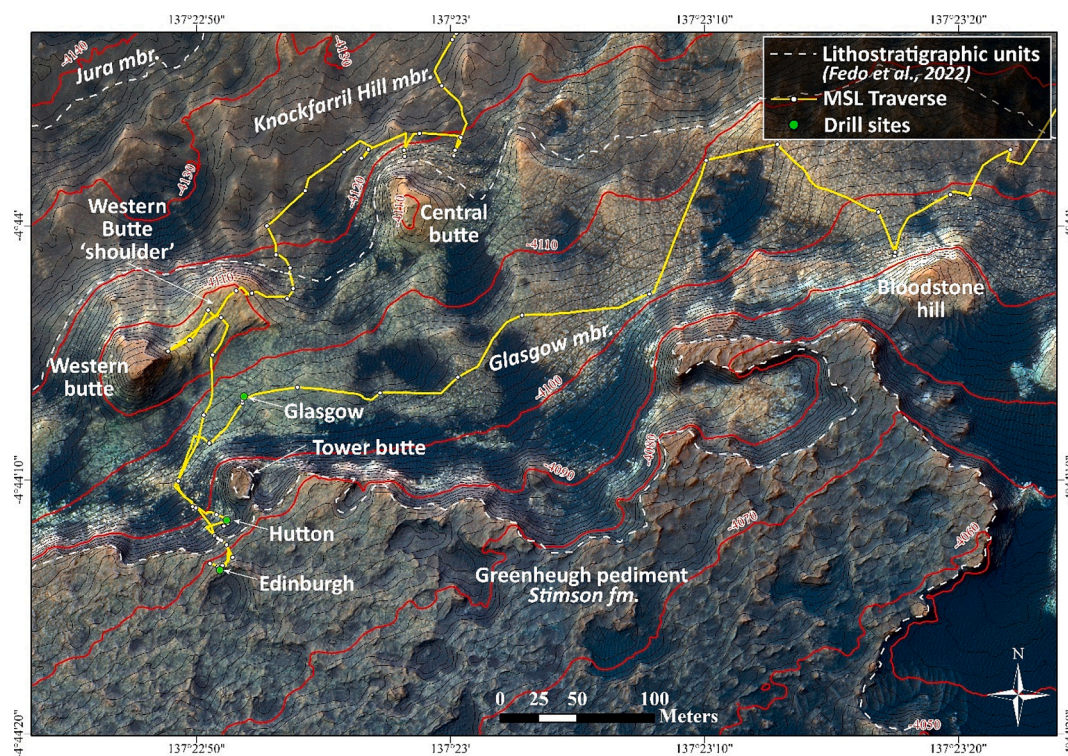
Fig. 9. Northern edge of the Greenheugh pediment showing the ascent location near Tower butte as well as the eastern traverse along the northern margin of the pediment. Note: stratigraphic members are defined after Fedo et al. (2022). HiRISE image credit: NASA/JPL/University of Arizona.

lithologies (Fig. S3 in Supporting Information S1). Everywhere the unconformity (pediment surface) along the margin of the Greenheugh pediment was observed, the topographic variation along it was minimal (<0.5 m amplitude). This regional planarity is consistent with observations of the SPg unconformity away from the pediment (made at

Emerson, Naukluft and Murray Buttes) although local topographic variability was much greater (Watkins et al., 2022). The unconformity at the regional scale can therefore be observed smoothly cutting across nearly 630 m of elevation and every lithologic unit identified by the rover above (and possibly including) the Bradbury group (Fig. S3 in
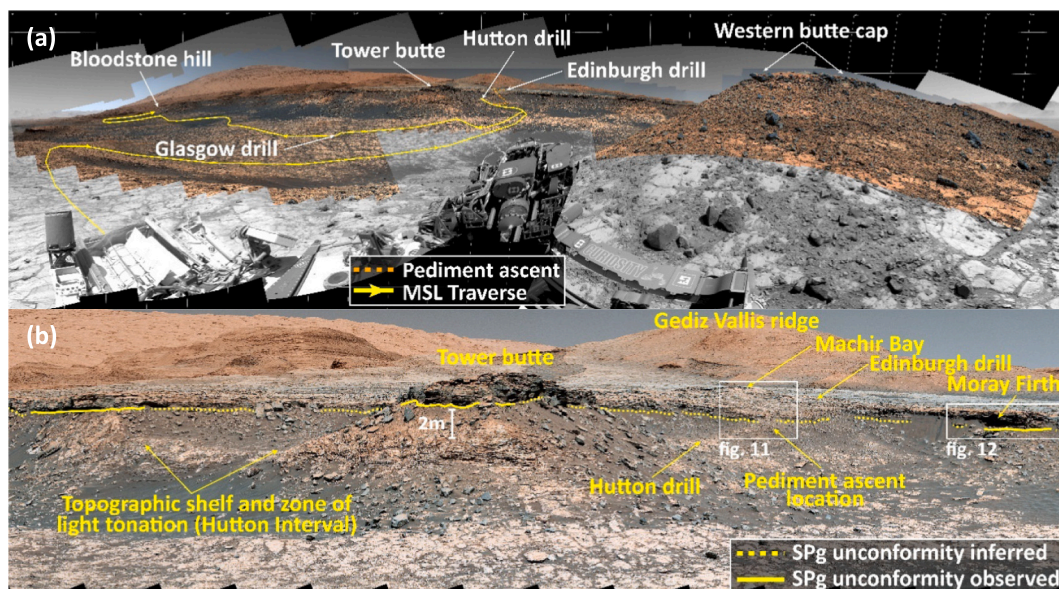
Fig. 10. Mastcam imagery overlain on Navcam imagery taken from the northeast 'shoulder' of Western butte towards the Greenheugh pediment and centered on Tower butte a) Context (180°) view of pediment ascent area as viewed from the shoulder of Western butte. The pediment ascent location, Hutton, Edinburgh and Glasgow drill sites, and Bloodstone hill can also be seen along the MSL traverse (yellow/orange) (mixture of M100 and Navcam imagery). b) Closer view of the ascent area at Tower butte. Image credit: NASA/JPL-Caltech/MSSS. See Table S1 in Supporting information S3 for image sequence identifiers. (For interpretation of the references to colour in this figure legend, the reader is referred to the web version of this article.)

Supporting Information S1; Williams et al., 2018).

3.3. Southern exposure and ascent at Blackcraig

Curiosity made a second ascent of the Greenheugh pediment along the Southeastern margin at the Blackcraig outcrop (Fig. 17; Fig. S10 in Supporting Information S1). The unconformity was poorly exposed because it was often covered by modern wind-blown sand. However, in rare instances where the unconformity was observed, there was again no evidence for local fluvial incision and or water-worn clasts above the unconformity. The stratigraphy of the Stimson near Blackcraig shared several similarities with the ascent at Tower butte, but with some notable differences. The base of the section contains cross-bedded platy weathering aeolian sandstone with occasional nodular zones. Above this there is a discontinuous zone of massive to convolute laminated sandstone (Banham et al., 2024). This interval is laterally discontinuous and reminiscent of the deformed basal unit observed east of Maria Gordon Notch, except that where present it occurred above the lowermost coherently cross-bedded Stimson, rather than directly above the unconformity. One location in this interval contained possible evidence for fluid escape structures, although the rover could not get close enough to confirm. Above this, the Stimson assumed a blocky texture similar to that at Tower butte (Fig. 18; Fig. S10 in Supporting Information S1).

Curiosity continued beyond Blackcraig downslope along the pediment surface on one of several NW-SE trending wind scoured furrows that dissect the top of the Stimson (Figs. 8; 17). Upon exiting this furrow, Curiosity first encountered an intact expanse of the washboard pattern identified from HiRISE (Figs. 5; 7; 18; 19). The pattern of orthogonal ridges and swales is clearly visible in Mastcam data. Unexpectedly, the Mastcam data also revealed a finer-scale texture that characterized the surface of the washboard ridges (Fig. 19). The new and widespread (Fig. 19a inset) texture, given the informal descriptive term 'gatorback terrain' consists of blocky-weathering Stimson bedrock that has been molded into roughly evenly spaced decimeter-scale blocks the majority of which remain attached to the bedrock. The blocks are fracture bound and exhibit a consistent ventifaction pattern with a preferred azimuthal orientation of ~235 degrees (Figs. 18; 19a). The 'troughs' of the washboard pattern consisted of swales covered with loose sand as well

as scattered Stimson derived stones in size from pebbles, cobbles, to boulders. In some swales, the gatorback blocks could be seen poking through the regolith (Fig. 19a). At both ascent locations, cross-sectional observations of the washboard pattern were rare. In addition, the extreme ventifaction and blocky surface texture defining the gatorback terrain made identifying a relationship between the gatorback terrain, the washboard, and the stratigraphy of the Stimson difficult. However, along the trough margin where Curiosity ascended the pediment, there was a single location where Mastcam data suggested a possible link between the decameter-scale washboard pattern and the layering within the Stimson (Fig. 19b).

Close inspection of the gatorback blocks revealed some similarity in chemistry with other areas of the Stimson, but several elements differed from typical basaltic Stimson (Thompson et al., 2022a). Grain size data were sparsely available due to wind polishing of the incipient boulders, but the available measurements indicated a finer-grained Stimson than was found at Tower butte (Banham et al., 2022). As with the Tower butte ascent area, detailed imaging of the top of the Stimson again yielded no evidence of foreign clasts away from the Gediz Vallis ridge.

Figure 20 compares generalized schematic stratigraphic sections observed by Curiosity in the Blackcraig area with that from Tower butte. In contrast with the Tower butte area, the stratigraphy of the Stimson near Blackcraig is more variable with zones of deformation and nodules occurring inconsistently at variable stratigraphic levels across the ascent area. In general, the sedimentary facies are similar at the two ascent locations. At several locations along the margin of the Greenheugh pediment, Curiosity enabled observations of a discontinuous bedded-to-massive sandstone characterized by occasional matrix supported centimeter-scale clasts and spherules outcropping near the base of the Stimson (Figs. 11; 16 g, h; S15 in Supporting Information S1). Two hypotheses explain the occurrence of this facies. The most likely explanation for this unit is laterally variable soft sediment deformation within the lowermost Stimson prior to lithification. Deformation likely resulted from groundwater flow through un- or semi-consolidated Stimson sediments and may have been aided by meteor impacts (Dietrich et al., 2022). A second possibility is that some parts of this facies – particularly where coarser clasts and spherules are present (Fig. 11c) – could represent a lag deposit remaining from the pre-Stimson aeolian
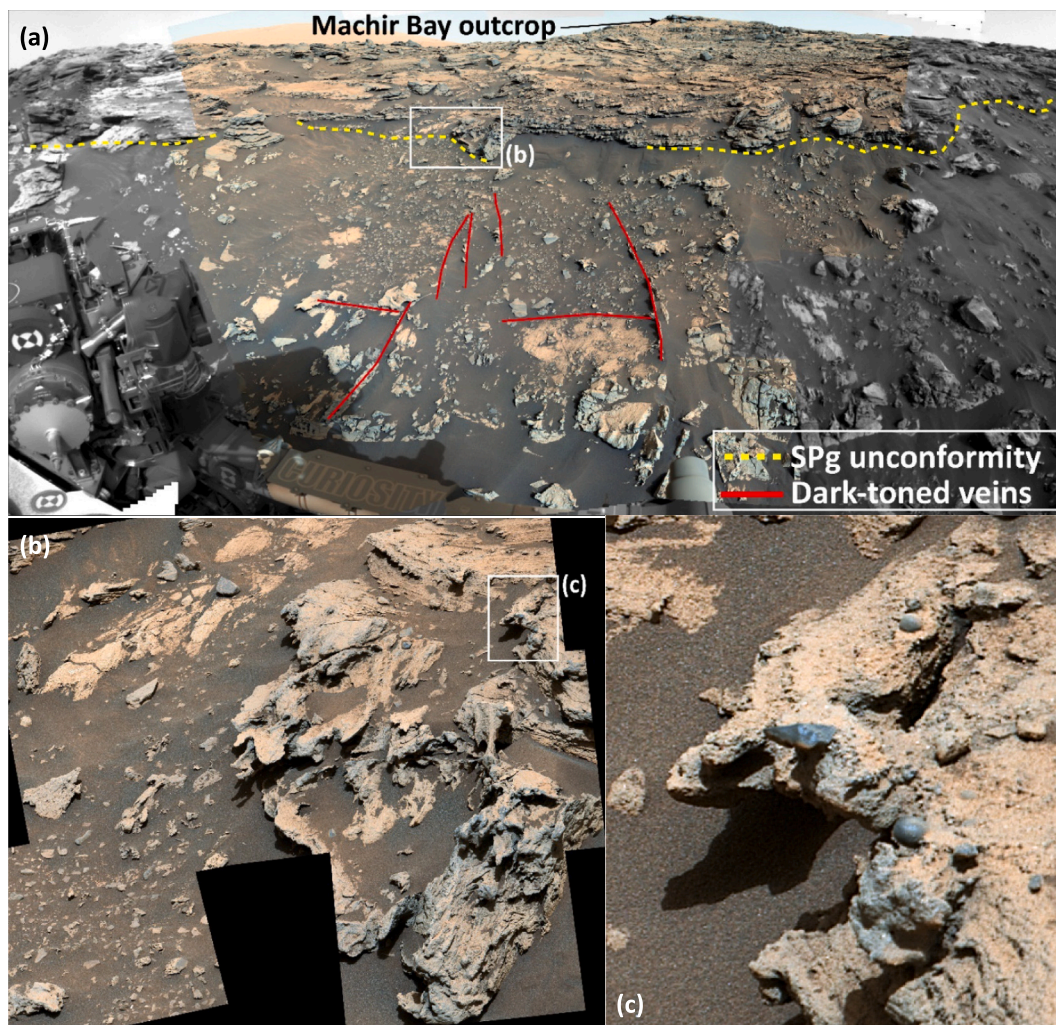
Fig. 11. The Tower butte pediment ascent area. a) pediment ascent location including SPg unconformity (yellow dashed lines) and dark vein traces in the Glasgow member (red). b) Hutton's section target and the apparent coarse basal pediment unit. c) Inset showing in situ spherules and cm-scale clasts within the basal Stimson unit. Image credit: NASA/JPL-Caltech/MSSS. See Table S1 in Supporting information S3 for image sequence identifiers. (For interpretation of the references to colour in this figure legend, the reader is referred to the web version of this article.)
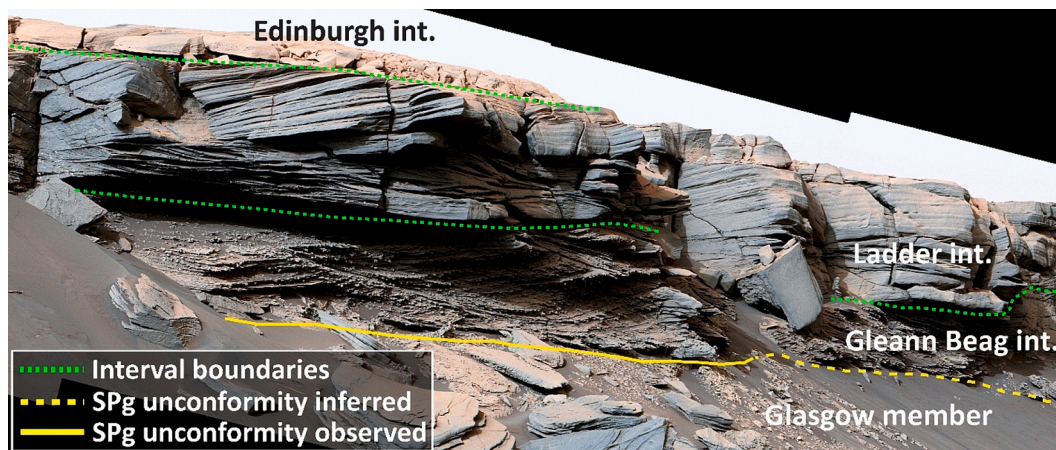
Fig. 12. Greenheugh pediment showing the SPg unconformity and Stimson stratigraphic intervals ("int.") as defined by Banham et al. (2022). Image credit: NASA/JPL-Caltech/MSSS. See Table S1 in Supporting information S3 for image sequence identifiers. Note the Stimson cliff in this image is ~1.5 m thick.

denudation phase of Mt. Sharp. These two explanations are not mutually exclusive, and it is possible Curiosity has encountered features like this in the past (e. g. the top of Western butte) but without the science team realizing their connection to the Stimson (Fig. S7 in Supporting Information S1).
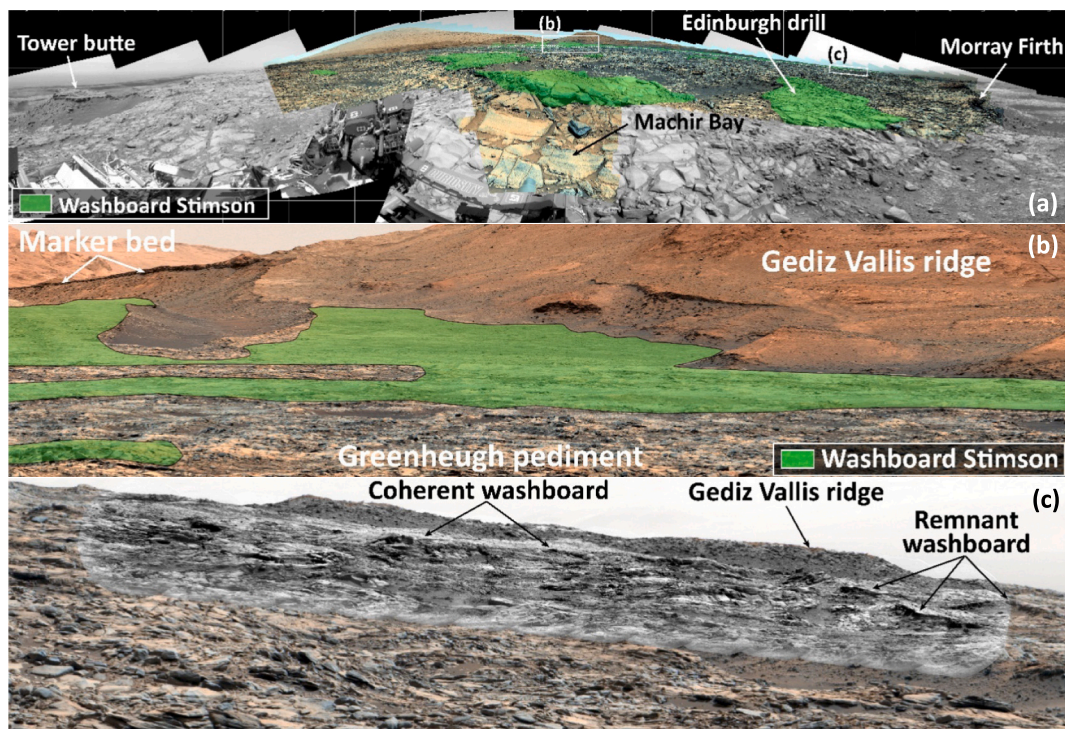
Fig. 13. Top surface of the Stimson-mantled Greenheugh pediment looking south towards Mt. Sharp. a) Green area indicates pieces of preserved washboard structure. b) Boundary between preserved washboard surface near the Gediz Vallis ridge and degraded Stimson (no colour). c) Inset from (a) showing Mastcam and ChemCam RMI imagery of the distal Gediz Vallis ridge as well as areas of coherent and remnant washboard below. Image credit: NASA/JPL-Caltech/MSSS. See Table S1 in Supporting information S3 for image sequence identifiers. (For interpretation of the references to colour in this figure legend, the reader is referred to the web version of this article.)

4. Greenheugh pediment reconstruction and erosional history

4.1. Estimated current thickness of the Stimson

In order to estimate current thickness of the Stimson across the pediment we used a combination of mapping along the exposed edge and then a projection across the entire surface (Fig. 21). Locations along the pediment margin that included both a topographic inflection of the contact and a change in HiRISE false colour image tone were chosen as approximate locations for the SPg unconformity (red dots in Fig. 21). Direct mapping of the unconformity was not possible due to poor exposure. However, approximate location data were checked with rover-based imagery where it was available. A thin-plate projection (Pohjola et al., 2009) was then used to interpolate the unconformity across the aerial extent of the pediment. This surface subtracted from the modern topographic surface (from HiRISE 1 m topography provided by Parker and Calef III, 2016 and Calef III and Parker, 2016) yields a rough estimate of the thickness of the modern Stimson and how it varies across the Greenheugh pediment (Fig. 21).

The map indicates the Stimson thickness remains between ~1 and 5 m around the perimeter of the escarpment and is in general agreement with Curiosity's direct observations of the northern, eastern, and southeastern margins of the pediment (Figs. 14 to 16; Banham et al., 2022). Thickness may be greatest (reaching 10 m) near the center of the pediment, but averages only 2.3 m thick over the entire landform. This area of greatest thickness depends on the reliability of the projection, and there is considerable uncertainty. The greatest thickness, however, does roughly correspond to the best-preserved washboard surface (Figs. 7; 21). The interpolated thicknesses in general agree with thickness data reported at previously visited Stimson outcrops (Banham et al., 2018; Williams et al., 2018) as well as with Mastcam observations along Curiosity's circumnavigation of the pediment escarpment. Nonetheless, the actual thickness of the Stimson cover in the center of the pediment is

unknown and so this projection at the center of the feature can be considered a suggestion.

Most of the Stimson at the Greenheugh pediment does not exhibit the coherent washboard texture (Fig. 7). Isolated outcrops of washboard indicate the feature once likely covered the pediment surface and has subsequently experienced erosion regardless of formation mechanism. The current Stimson surface thus represents a second, currently active beveled bedrock surface. Satellite imagery shows the washboard pattern extending to the edge of the Gediz Vallis ridge on both sides of the outcrop. At neither ascent location were foreign blocks visible across the pediment, indicating effective elimination of Gediz Vallis shed clasts by strong wind erosion across the pediment. Nonetheless, as noted above, foreign clasts were found beyond the Sands of Forvie, over 1.2 km from the edge of the pediment. It is also possible that foreign clasts from the former Gediz Vallis ridge may be visually indistinguishable from the rubbly Stimson top at the pediment.

4.2. Former extent of the Greenheugh pediment

At every location, ground-based observations indicate the SPg unconformity is capped by the dark-toned and often cliff-forming aeolian Stimson sandstone (Figs. 4, 10, 14–16; Banham et al., 2018, 2021, 2022; Watkins et al., 2022). Effectively, the Stimson deposit preserves a paleo erosion surface. Paleorelief along the unconformity varies among Stimson outcrops. Watkins et al. (2022) performed geometric analysis of the SPg unconformity along the northern Stimson outcrops previously encountered by Curiosity (Murray buttes, Naukluft and Emerson plateaus, Figs. 1b and 2). Exposure of the unconformity in these areas was good, typically occurring at the base of buttes, thus enabling accurate measurements of paleorelief of up to ~10 m locally. Despite these areas of local relief, Watkins et al. (2022) found broad agreement between the modern topographic surface and the preserved paleosurface. In contrast, the unconformity at the Greenheugh pediment (upslope of Vera Rubin
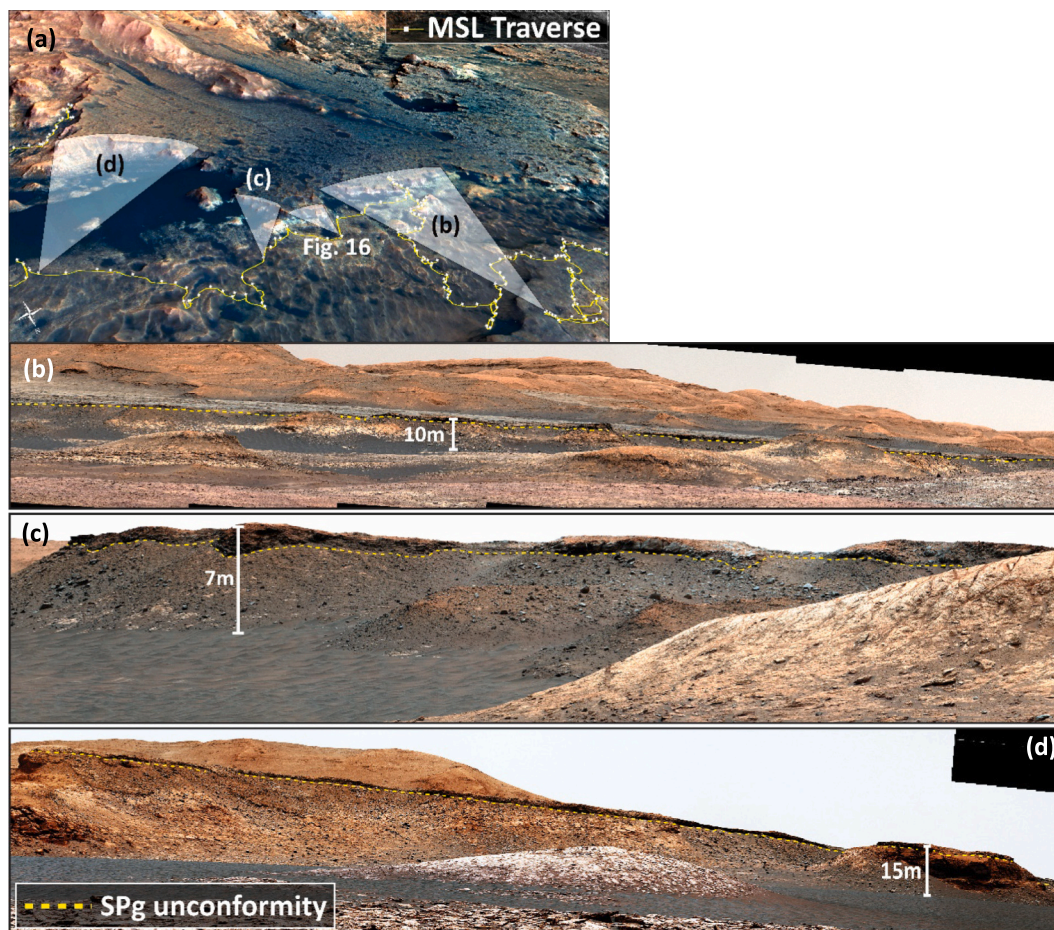
Fig. 14. Exposure of the SPg unconformity along the northern and eastern margin of the Greenheugh pediment. a) Mastcam location and look angles for Mastcam mosaics in b-d. b) Northern margin of the pediment. c) Northeast margin of the pediment. d) Eastern extent of the pediment escarpment south of Siccar point showing planar SPg unconformity and patches of regolith mantle flanking the escarpment. HiRISE image credit: NASA/JPL/University of Arizona. Mastcam image credit: NASA/JPL-Caltech/MSSS. See Table S1 in Supporting information S3 for image sequence identifiers.
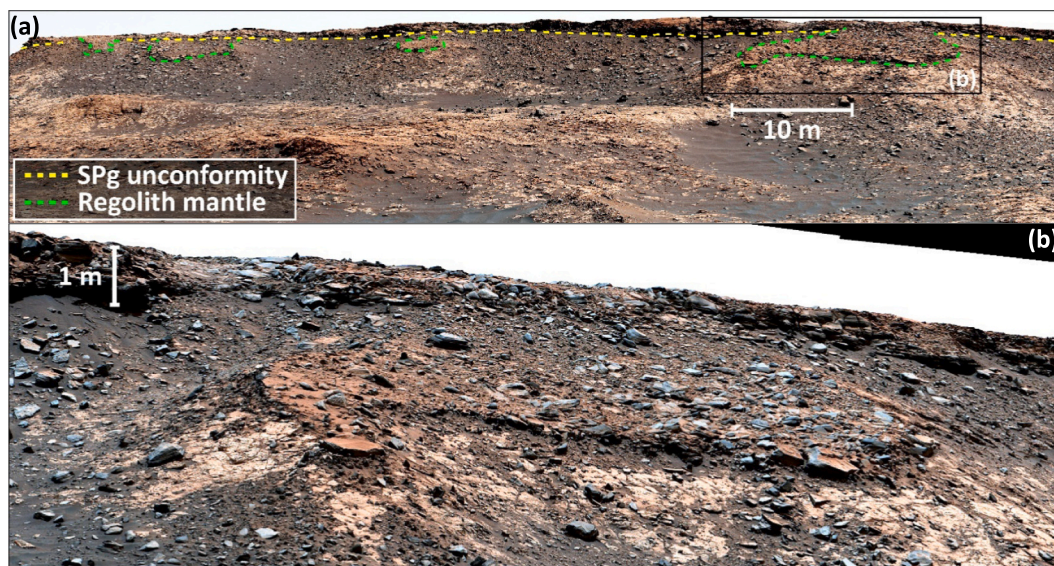
Fig. 15. Pediment exposure west of Bloodstone hill (see Fig. 14a for look angle). a) Residual scree slope mantle (green dashed lines) along the pediment margin that suggest episodic or differential scarp retreat. b) A closer view of the mantle patch Image credit: NASA/JPL-Caltech/MSSS. See Table S1 in Supporting information S3 for image sequence identifiers. (For interpretation of the references to colour in this figure legend, the reader is referred to the web version of this article.)
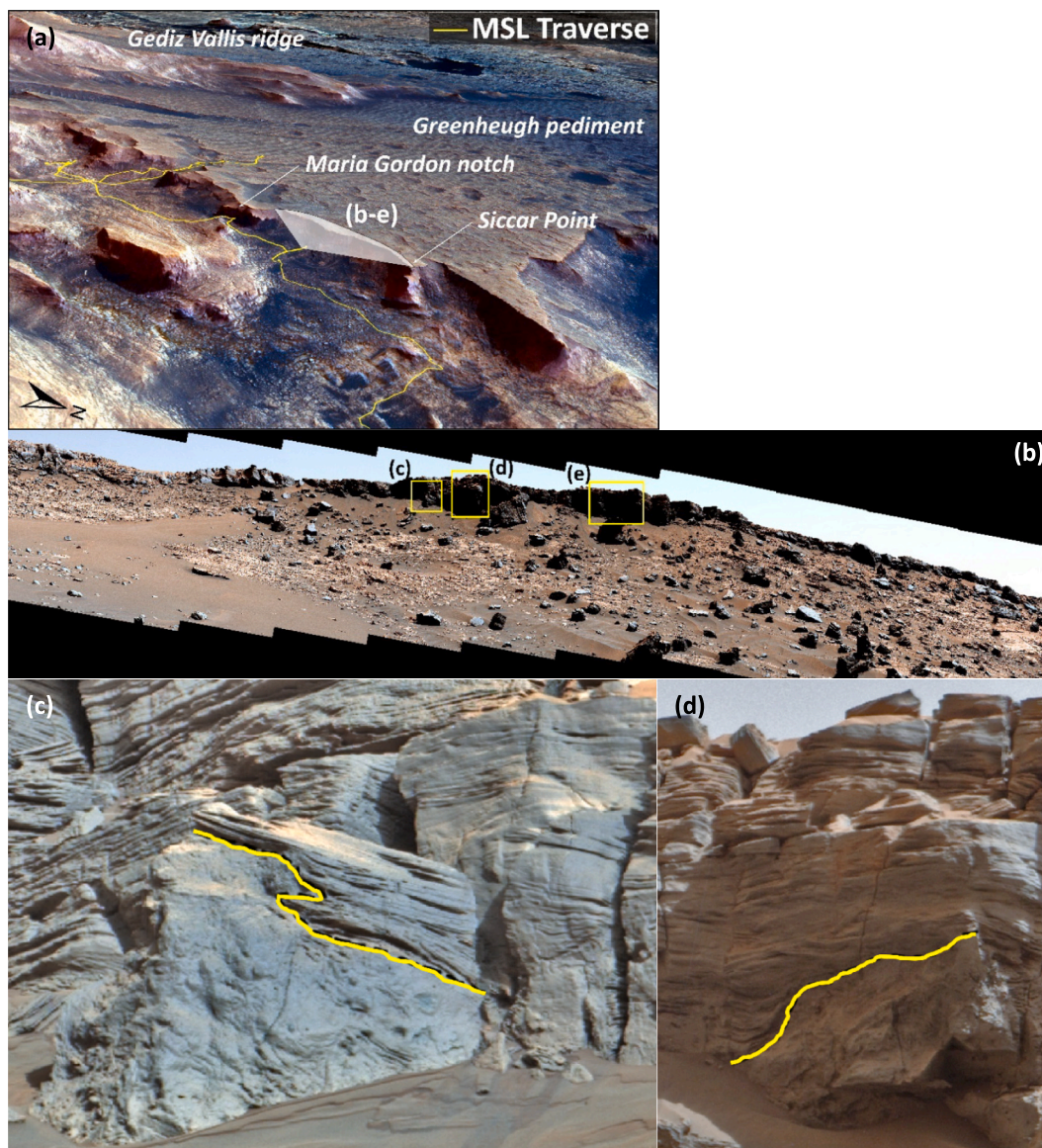
Fig. 16. Pediment escarpment exposure revealing soft sediment deformation features in the lower Stimson. a) 3D view of the outcrop exposure located between Siccar Point and Maria Gordon notch. (b-e) Mastcam mosaics of the basal Stimson (b) showing loss of coherent bedding, as well as the irregular boundary between the deformed sediments and the undisturbed upper layers including evidence for possible fluid escape paths. (f-h) Mastcam mosaics of tumbled blocks accessed for chemical analysis and grain size measurements. HiRISE image credit: NASA/JPL/University of Arizona. Mastcam image credit: NASA/JPL-Caltech/MSSS. See Table S1 in Supporting information S3 for image sequence identifiers.

ridge) occurs near the top of the escarpment and is poorly exposed, most commonly covered by scree and modern wind-blown sand. Direct measurements of paleorelief (where possible) were never greater than 1 m indicating even stronger correspondence between the modern topographic surface (top of the Stimson) and the unconformity at the Greenheugh pediment (Fig. 14). The total range in thicknesses among Stimson outcrops (on the contiguous Greenheugh pediment and in the isolated outcrops to the north) observed using both HiRISE and Curiosity imagery is relatively narrow – averaging 2.8 m and never exceeding 12 m (Fig. 21; Banham et al., 2018). We found no exposures to the north in the crater floor that would indicate that the Stimson capped pediment once extended much beyond the Naukluft plateau area (Fig. 1) and was a deposit of great thickness.

Together these observations paint a consistent regional picture of the Stimson formation. The modern Stimson formation is a thin, laterally extensive, crater preserving, mesa forming unit with major outcrops concentrated at the base of Mt. Sharp (Figs. 1–3). The observed Stimson outcrops correspond to areas previously mapped from orbit as areas of Mound Skirting unit (Anderson and Bell, 2010) and in situ as the Siccar Point group (Fraeman et al., 2016; Stack et al., 2017; Kronyak et al., 2019; Watkins et al., 2022; Banham et al., 2018, 2021 and 2022). These outcrops include the more remotely observed area of the Emerson plateau, to the east of the rover transect, where a clear dark toned cliff forming unit is visible (Fig. S14 in Supporting Information S1). Hence, we propose that south of Aeolis Palus, the Mound Skirting unit and the Siccar Point group are both represented by the Stimson formation deposited on a paleosurface (now recognized as the SPg unconformity) that unifies Stimson-capped buttes (e.g., Murray buttes, Naukluft and Emerson plateaus; Figs. 3 and 4) with the Greenheugh pediment. This pedimentation surface thereby records a period when net erosion shifted to net deposition along the base of Mt. Sharp.

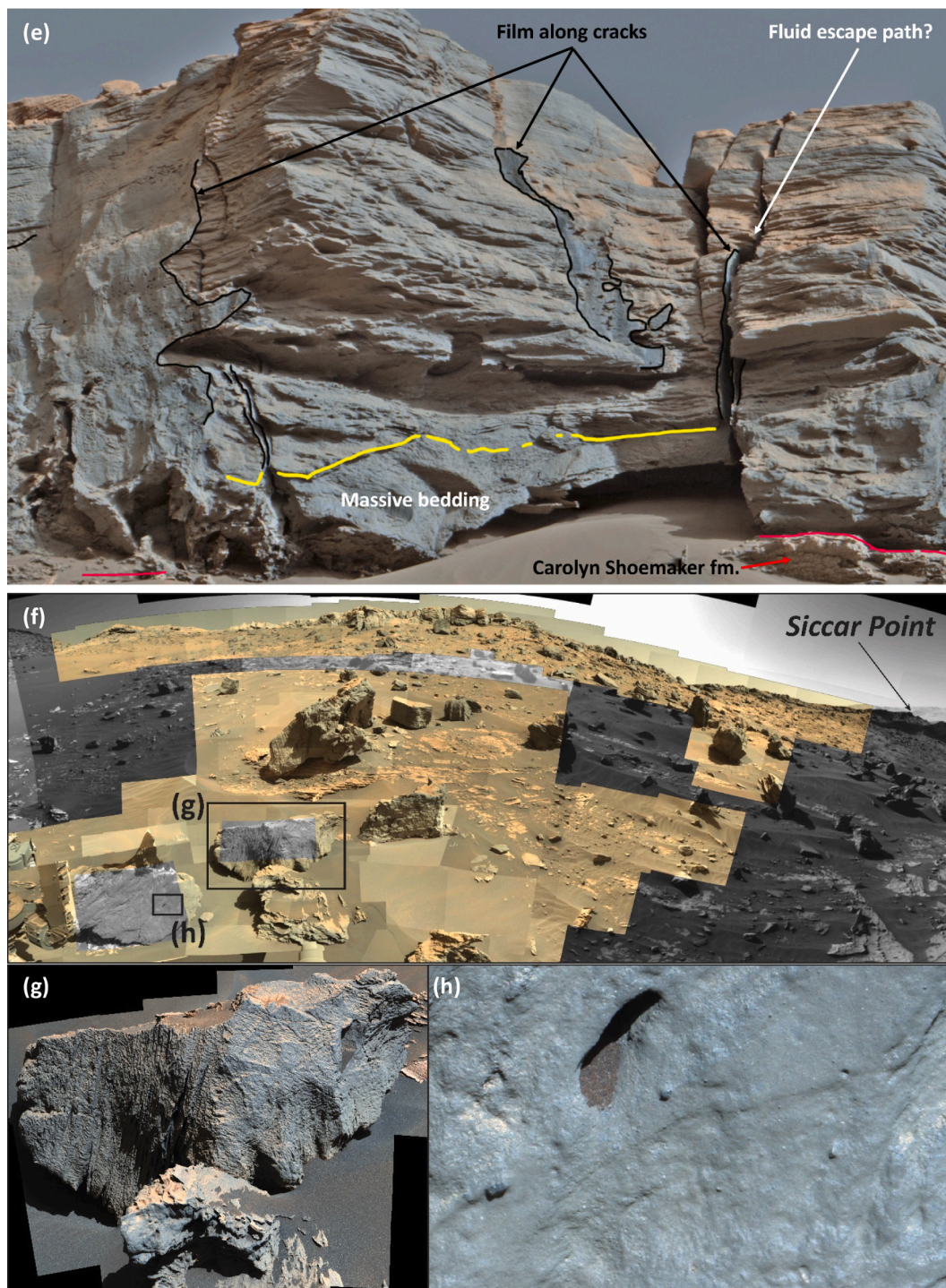On the basis of this hypothesis, we made a projection of the full

Fig. 16. (*continued*).

extent of the Greenheugh pediment in the region of the MSL traverse (Fig. 22a). We included an extensive patch of Mound Skirting unit to the west for which we lack rover-based observations, but, given its proximity to the current Greenheugh pediment, may have been part of the same contiguous feature. In order to make the map, the modern Mound Skirting unit outcrops (Fig. 22a green outlines) were interpolated across the basin using a thin plate projection (Pohjola et al., 2009) through data chosen from the top surface of each outcrop. Everywhere the rover observed the Stimson, the topographic (top) surface was roughly parallel to the unconformity and the average thickness of the unit is 2.8 m. Therefore, the top surface of the Stimson, although a somewhat eroded

feature itself, represents a reasonable approximation for the pediment cap at the regional scale. To be consistent, we added this thickness to the top of Vera Rubin ridge (VRR) in the final map. This reconstructed surface matches the local projection of the pediment north to the Murray buttes (Fig. 22b; Bryk et al., 2020; see also Fraeman et al., 2020). The northern extent of the paleosurface is constrained by visible outcrops. The low relief, beveled bedrock surface of the northern floor of Gale (Aeolis Palus) could also be called a pediment, but given the break in slope, it is likely a different surface than what we have mapped in this reconstruction (Fig. 22a).

The Greenheugh pediment reconstruction follows modern
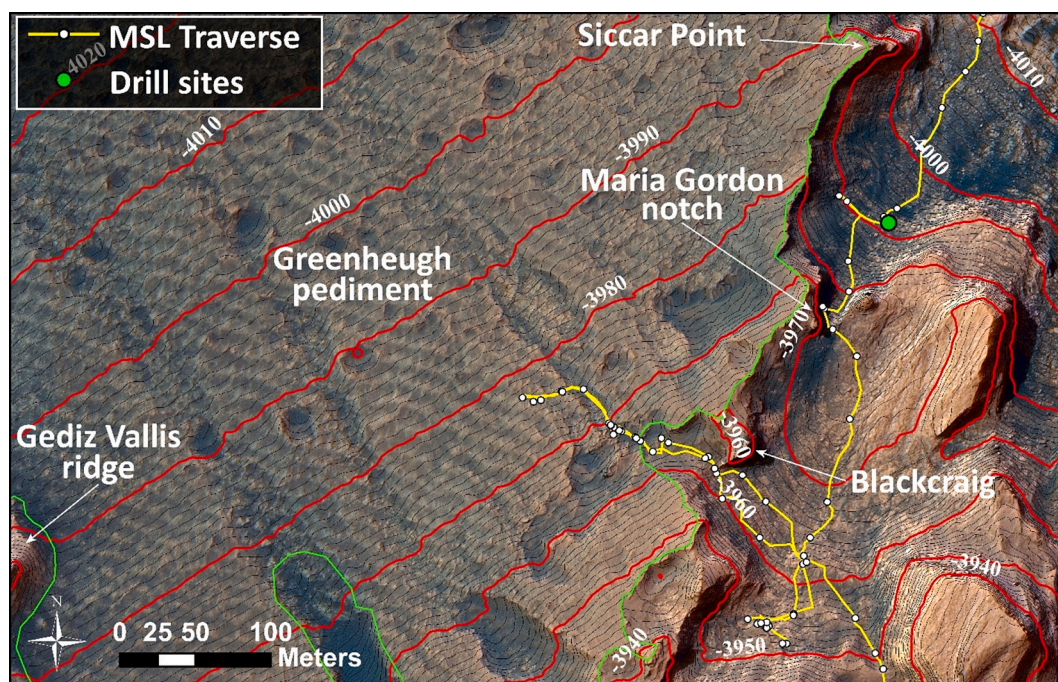
Fig. 17. Map showing the Southern pediment ascent at Blackcraig. The green line delineates pediment edge and the yellow line indicates the rover path. HiRISE image credit: NASA/JPL/University of Arizona. (For interpretation of the references to colour in this figure legend, the reader is referred to the web version of this article.)
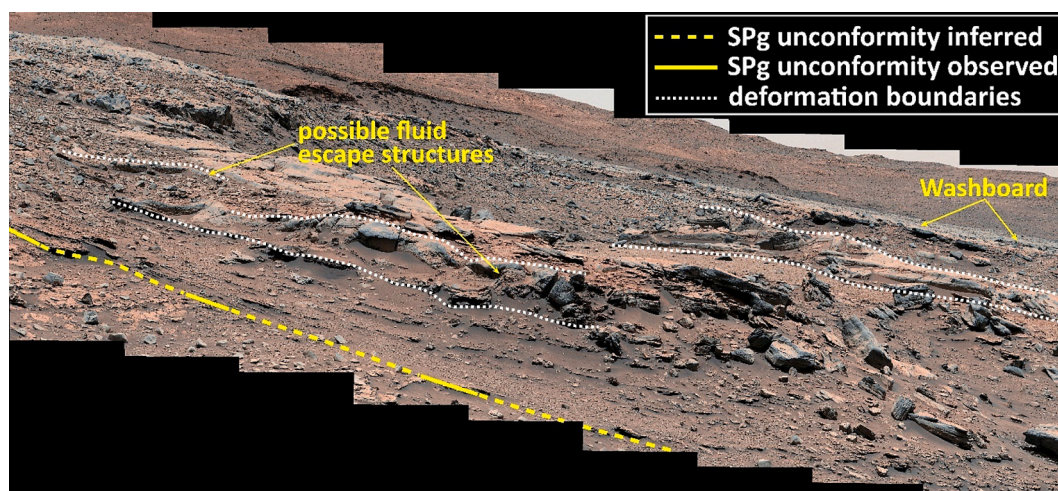
Fig. 18. Exposure of an alteration zone in the Stimson facies at the Blackcraig ascent location (see Banham et al., 2024). Note exposures of coherent washboard in the distance and fluid escape structures bounded above and below by typical Stimson cross-bedding. Mastcam image credit: NASA/JPL-Caltech/MSSS. See Table S1 in Supporting information S3 for image sequence identifiers.

topography at the regional scale (see contour similarities between Figs. 1–2 and 22a). Notably, the reconstructed surface (and thus the Greenheugh pediment) follows the topographic form of the inclined conical surface or topographic hump that spans nearly the entire MSL mission traverse up Mt. Sharp (Fig. 1; Video S11 in Supporting Information S1).

4.3. Sequence and pattern of erosional destruction of the pediment

By subtracting the current topography (Fig. 1b) from the reconstructed Greenheugh pediment surface (contours in Fig. 22a), we document the spatial pattern of erosion of the pediment and underlying bedrock (Fig. 23). The depth contours in Fig. 23 indicate the amount of erosion that has occurred since the deposition and lithification of the Stimson. The map reveals significantly more post-Stimson erosion near the mountain front than away from it as would be predicted by slope-wind erosion models (e.g., Kite et al., 2016). East of the Greenheugh pediment the depth of post-Stimson erosion exceeds 145 m into underlying bedrock in some locations (Fig. 23). The region SE and upslope of the Greenheugh pediment was excluded from the reconstruction as there are no Stimson outcrops to guide the projection. It is unknown whether the Stimson once extended this far up Mt. Sharp.

Several observations suggest that post-lithification of the Stimson, significant net erosion of the pediment was initiated in the northern footslopes and spread upslope. The rover's journey crossed into Stimson-capped aligned bluffs bordered by broad Murray bedrock floored valleys as it entered the Emerson plateau (Fig. 1). Curiosity then traveled across the Naukluft plateau nearly along contour for ~2 km before turning
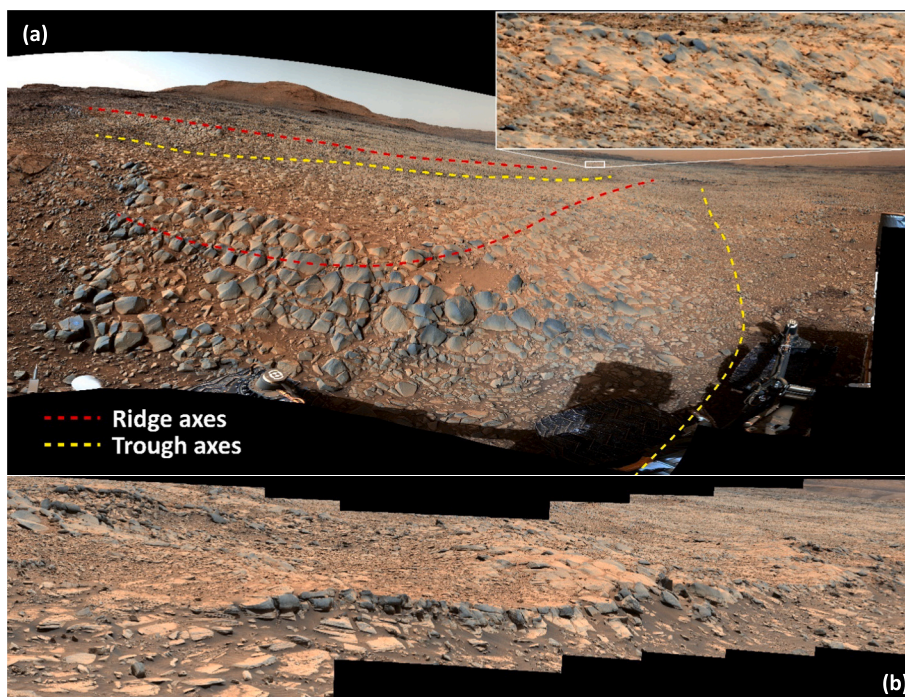
Fig. 19. Pediment surface at the Blackcraig ascent area a) Ridges (red) and troughs (yellow) and prominent ventifaction pattern ("gatorback") characteristic of intact washboard Stimson. Inset shows gatorback pattern present near the base of the Gediz Vallis Ridge b) A cross-sectional view of the washboard pattern suggesting a relationship between the topography Stimson internal stratigraphy. Mastcam image credit: NASA/JPL-Caltech/MSSS. See Table S1 in Supporting information S3 for image sequence identifiers. (For interpretation of the references to colour in this figure legend, the reader is referred to the web version of this article.)
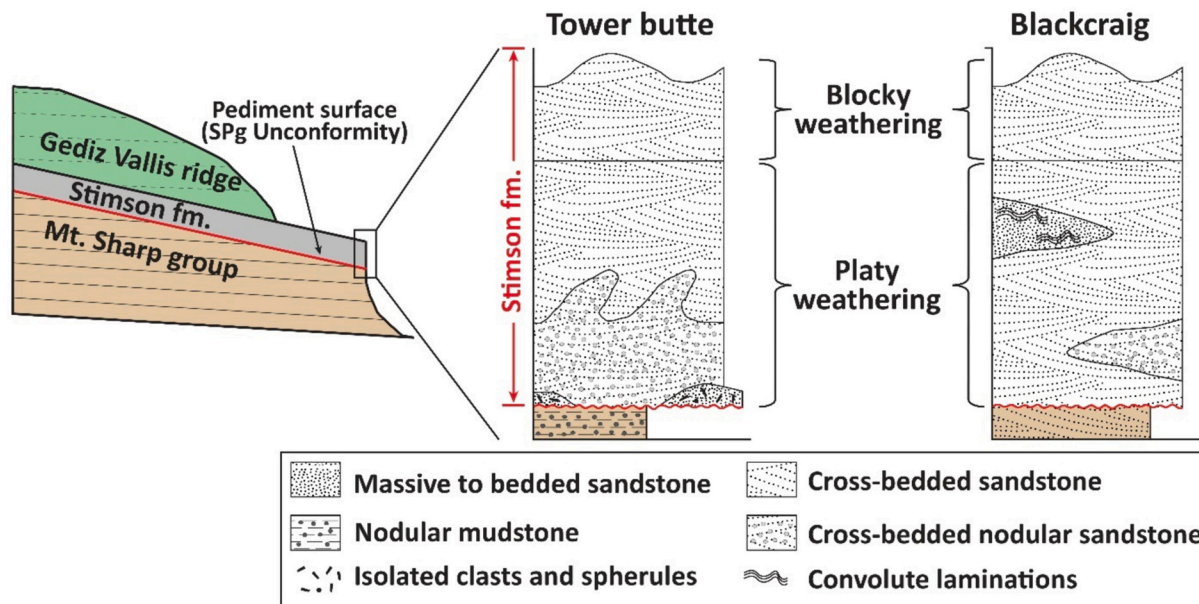
Fig. 20. Schematic cross-section and generalized stratigraphic column of the Stimson on the Greenheugh pediment and the underlying uppermost Glasgow member at Tower butte and Blackcraig. Synthesis figure for pediment ascent stratigraphy.

south towards the Murray buttes area (Figs. 1–2; 4a, b) towards VRR. This eroded landscape revealed the topography of the pediment boundary between the Murray and Stimson (the SPg unconformity) which tended to be near the base of the bluffs (Banham et al., 2018, 2021; Watkins et al., 2022). Wiens et al., 2020 describe that at three locations the rover passed unconsolidated heterolithic deposits of gravel and boulders. One of the deposits (Blackfoot) lay on both Stimson and Murray bedrock and the outcrop was bordered by 4 m deep canyons (Fig. 24a; Wiens et al., 2020 Supplemental Fig. 1–1). A second

(Brandberg) lay on just the Murray and on its north side was a bench, the north edge of which dropped 10 m. The third site (Bimbe), farthest south and west, lay on the sloping eroded topographic surface underlain by the Murray formation. These gravel and boulder deposits therefore, were deposited after significant dissection and butte retreat had occurred here, but some erosion continued after deposition. The heterolithic deposits may have been much more extensive and thicker after initial deposition. Based on inspection of these deposits in the field, we used HiRISE imagery to make a map of the possible occurrence of other like
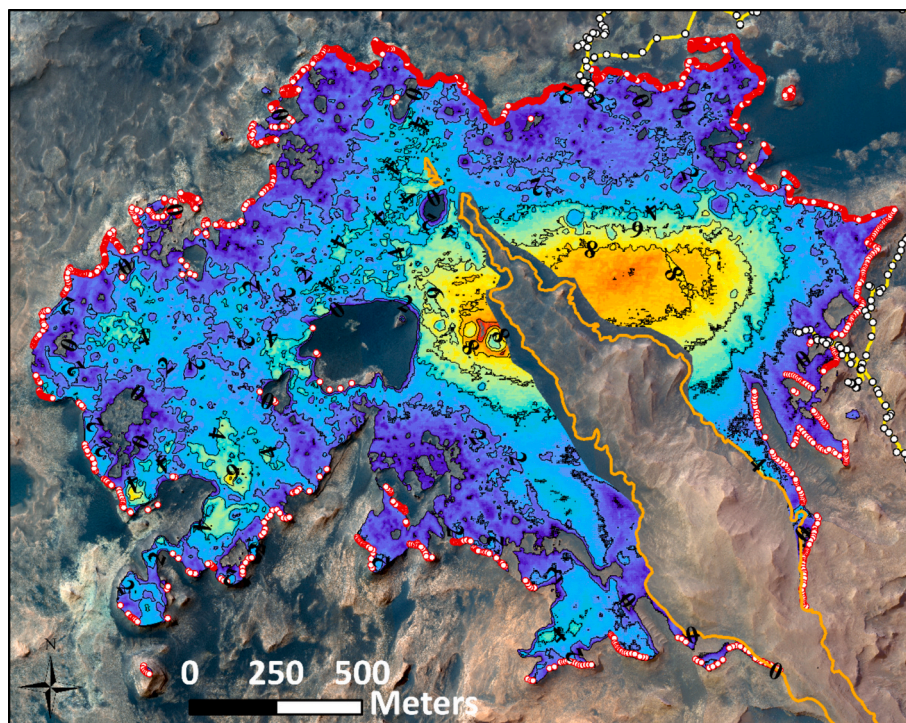
Fig. 21. Contoured thickness map of the Stimson formation on the Greenheugh pediment. Red dots indicate locations where the SPg unconformity could be reliably identified due to both a topographic inflection and a change in HiRISE false colour image tone. Locations were confirmed with Mastcam where possible. Thicknesses in the interior pediment was derived from a thin plate approximation. HiRISE image credit: NASA/JPL/University of Arizona. (For interpretation of the references to colour in this figure legend, the reader is referred to the web version of this article.)

deposits (Fig. 24a). Those most like the field sites observed with Curiosity lie in or close to the projected former extent of the pediment (Figs. 22; 23). A fourth unconsolidated gravel patch (see 'Bressay' in Fig. 24a) was subsequently encountered on VRR (Fraeman et al., 2020). The deposit is 40 m long, approximately 15 m wide, and is heterolithic with highly variable grain size (Fig. S12 in Supporting Information S1). It appears to lie in a subtle trough that crosses the narrow Vera Rubin ridge. The deposit rests directly on the exposed diagenetically altered erosion resistant bedrock of VRR and is aligned in the downslope direction. Wiens et al. (2020) note that the lithologic composition seems distinct from the heterolithic patches to the north.

For these sediments (including Bressay) to have crossed Vera Rubin ridge and been transported to Murray buttes, the pediment would have been still topographically connected to VRR (although the Stimson cap would likely have been removed). This then suggests that significant erosion at and north of Vera Rubin ridge as well as removal of the Stimson at VRR, and deposition of the heterolithic unit preceded the development of the Glen Torridon trough between VRR and the Greenheugh pediment. Wiens et al. (2020) offer several hypotheses for the transport processes that generated these deposits, which includes fluvial or debris flows, raising the possibility that deposits record the onset Gediz Vallis ridge fan construction.

Upslope of Vera Rubin ridge, wind erosion caused 8 m of vertical incision along the north facing bluff edge as the pediment escarpment retreated southward. To either side of the modern Greenheugh pediment, the erosion cut progressively deeper as it approached the steeped slopes to the south, possibly greater than 145 m, overall much greater than erosional incision north of Vera Rubin ridge (Fig. 23).

At two northern locations along the bluff floor adjacent to the former pediment, Martin et al. (2021) obtained exposure age dates from drill samples, both indicating ages of about 1 billion years. At Mojave (Figs. 1–2; 24b) the sample was taken 40 m from the basal edge of the bluff. At Quela, closer to Vera Rubin ridge (Figs. 1–2; 24b) the drill sample was just 5 m away from the edge. A 50 m long heterolithic

deposit, lying 1 to 4 m above the current Murray formation exposed floor, lies just to the north of the Quela bluff (Fig. 24b). Martin et al. (2021) concluded that these exposure age dates indicate that over at least the last billion years there had been essentially no vertical erosion and only 5 to 40 m of bluff retreat. These rates are far less than needed to explain the dissected landscape south of Vera Rubin ridge. The simplest interpretation is that there had been a significant decline in erosion rates along the northern footslopes by at least 1 billion years ago. This is in contrast to the much greater depth of erosion upslope of Vera Rubin ridge on either side of the preserved pediment, including canyon incision by over 100 m forming large yardangs on the slopes (Fig. 23).

5. Discussion

5.1. Processes that formed the Greenheugh pediment

On Earth, it is widely accepted that over large distances, preserved erosional surfaces (unconformities) are polygenetic and time-transgressive, meaning that although these surfaces today are laterally continuous, distinct areas of the surface have undergone cycles of denudation and burial at different times often by different processes (e. g., Vail et al., 1977; Fairbridge and Finkl, 1980; Karlstrom and Timmons, 2012). In fact, the only requirement for the creation of an erosional unconformity is that a landscape undergoing net erosion transitions to one undergoing net deposition. In Gale, the preservation of the Siccar Point unconformity by the Stimson formation enables us to study a former episode in the paleo-erosion history of northern Mt. Sharp. Essentially, the unconformity, although not a snapshot, gives us a glimpse at what the topography of Mt. Sharp looked like billions of years ago. Observations made with the Curiosity rover now enable us to understand the processes that produced that erosion surface.

There is no clear evidence for fluvial or glacial erosion processes preserved along the SPg unconformity at the Greenheugh pediment. This leaves wind erosion as the most probable erosion mechanism that
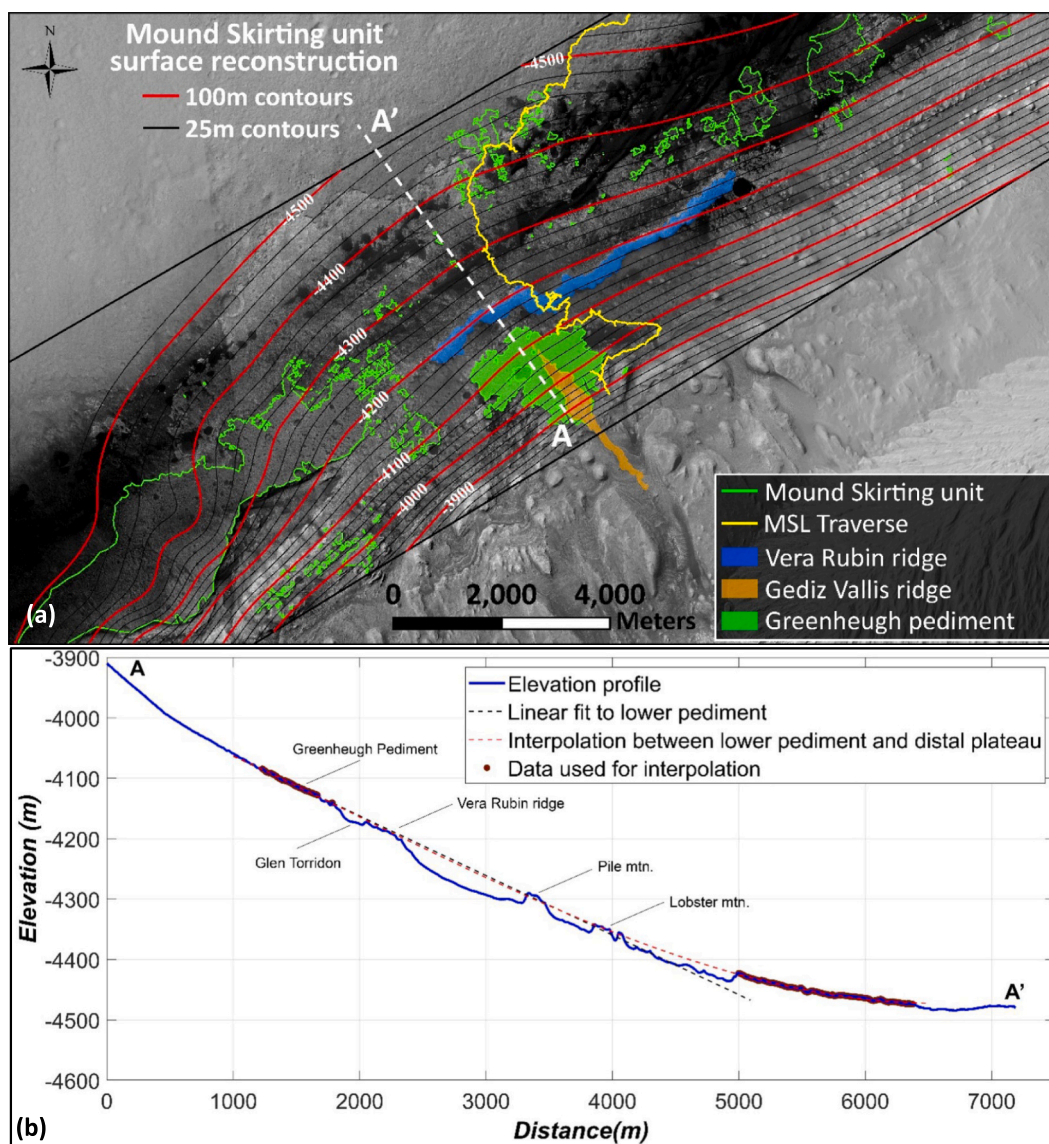
Fig. 22. Mound Skirting unit surface reconstruction prior to erosional dissection. a) HiRISE orthoimagery overlain with 25- and 100-m contours of the reconstructed Mound Skirting unit. Modern exposures of the Mound Skirting unit (equivalent to the SPg group in this area) are shown outlined in green. The Greenheugh pediment, Vera Rubin ridge, and the Gediz Vallis ridge are shaded in green, blue, and orange respectively. Projection assumes all the Mound Skirting Unit outcrops and Stimson mantled Greenheugh pediment were part of a footslope aeolian dune field (Stimson fm.). b) Topographic profile A-A' (see (a)) with labeled locations and two reconstructions (linear and 2nd order polynomial fits) of the Greenheugh pediment (Reproduced from Bryk et al., 2019b). Red dots indicate topographic data used for the polynomial fit. HiRISE image credit: NASA/JPL/University of Arizona. (For interpretation of the references to colour in this figure legend, the reader is referred to the web version of this article.)

created the pediment. Wind eroding bedrock, however, tends to etch out heterogeneities in bedrock properties and, through positive feedback in otherwise homogeneous material, cut canyons. Yardangs emerge, and smooth plains by wind alone would seem unlikely (Pelletier et al., 2018; Pelletier, 2018; Barchyn, 2018). Yardang-shaped hills do currently occur upslope of the southern edge of the pediment where the mean landscape slope steepens considerably (Figs. 1–3), but most of the reconstructed pediment surface lies below these features, which may be both lithologically different from lower Mt. Sharp and also subject to distinct wind patterns (Fig. 25; Dromart et al., 2021). Based on observations in Gale crater, Day and Kocurek (2016) proposed an erosional sequence in which wind dissection of bluffs progressively reduces an area to low gradient nearly planar "desert pavement", in which rocky plains are mantled by residual clasts. Neither the Greenheugh pediment contact surface with the Stimson, nor the current exposed bedrock surface of the eroded Stimson are marked by a mantle concentration of residual clasts.

The ascent of the rover from Murray Buttes also did not reveal areas of residual rock debris forming a pavement covering the underlying bedrock. Nonetheless, Day and Kocurek (2016) do propose a planation process by wind.

Watkins et al. (2022) reported total paleorelief values between 7 and 71 m along the Siccar point unconformity along the northern Stimson outcrops (Murray buttes, Naukluft and Emerson plateaus), concluding that the mechanism for erosion along the unconformity at these locations was wind scour. Removing the regional paleoslope of the unconformity at these outcrops and recalculating local paleotopography yields values averaging to only a few meters with a maximum of ~10 m over many tens of meters distance (Fig. S13 in Supporting Information S1). Despite this correction, paleotopography along the preserved unconformity north of the pediment is significantly greater than at the present Greenheugh pediment, where local topography along the unconformity was never greater than 1 m. It may be that along the northern edge of
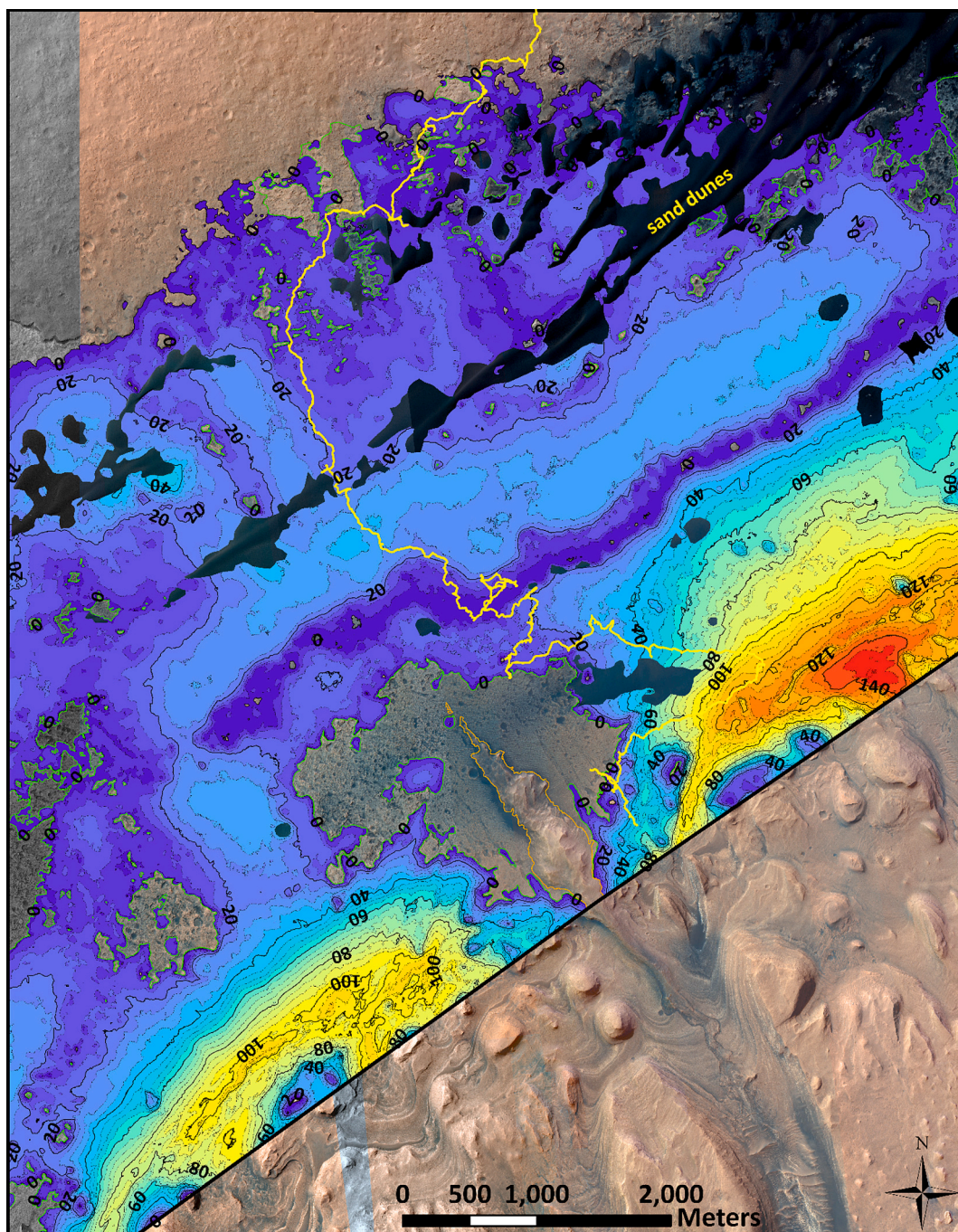
Fig. 23. Erosion depth below the projected top of the Mound Skirting unit (shown in Fig. 24) to the present Martian surface. Note depth contours are referenced to the top of the Stimson and thus do not account for the thickness of the Stimson, which averages 2.8 m across all areas it has been observed by Curiosity. Colour corresponds to specific erosion depth intervals. The region SE and upslope of the Greenheugh pediment was excluded from the reconstruction as there are no Stimson outcrops to guide the projection. HiRISE image credit: NASA/JPL/University of Arizona.

pediment projection (e.g., Murray buttes) wind had scoured subtle ridge and swale topography before Stimson deposition.

The relative smoothness of the regional projection (Fig. 24) unifies the pediment with the northern outcrops as a single regionally extensive contiguous surface overlain by the Stimson formation. Across the northwest slopes of lower Mt. Sharp, the process of erosion that cut this surface is most likely wind abrasion. In some places this resulted in an exceptionally smooth planation surface (i.e., at the Greenheugh pediment), while elsewhere local ~10 m scale topography was produced (e. g. at Murray Buttes) (Fig. 1; Watkins et al., 2022). The difference may have been caused by episodic and/or partial cover of the northern

outcrops by aeolian sands during the denudation phase or possibly due to differential hardness within the Murray as the pre-Stimson landscape lowered.

Upslope above the southern pediment margin as traversed by Curiosity, lithologic properties may have played a role in the enabling wind to scour without forming prominent (> meter-scale) yardangs in the lower slopes. Presently, the transition from lower slopes of Mt. Sharp, which are gently sloping with few local hills, to the yardang shaped upslope steep hills corresponds approximately to the lithologic transition from the mudstone (Murray and lower Carolyn Shoemaker formations) to sandier aeolian deposits (upper Carolyn Shoemaker to Mirador
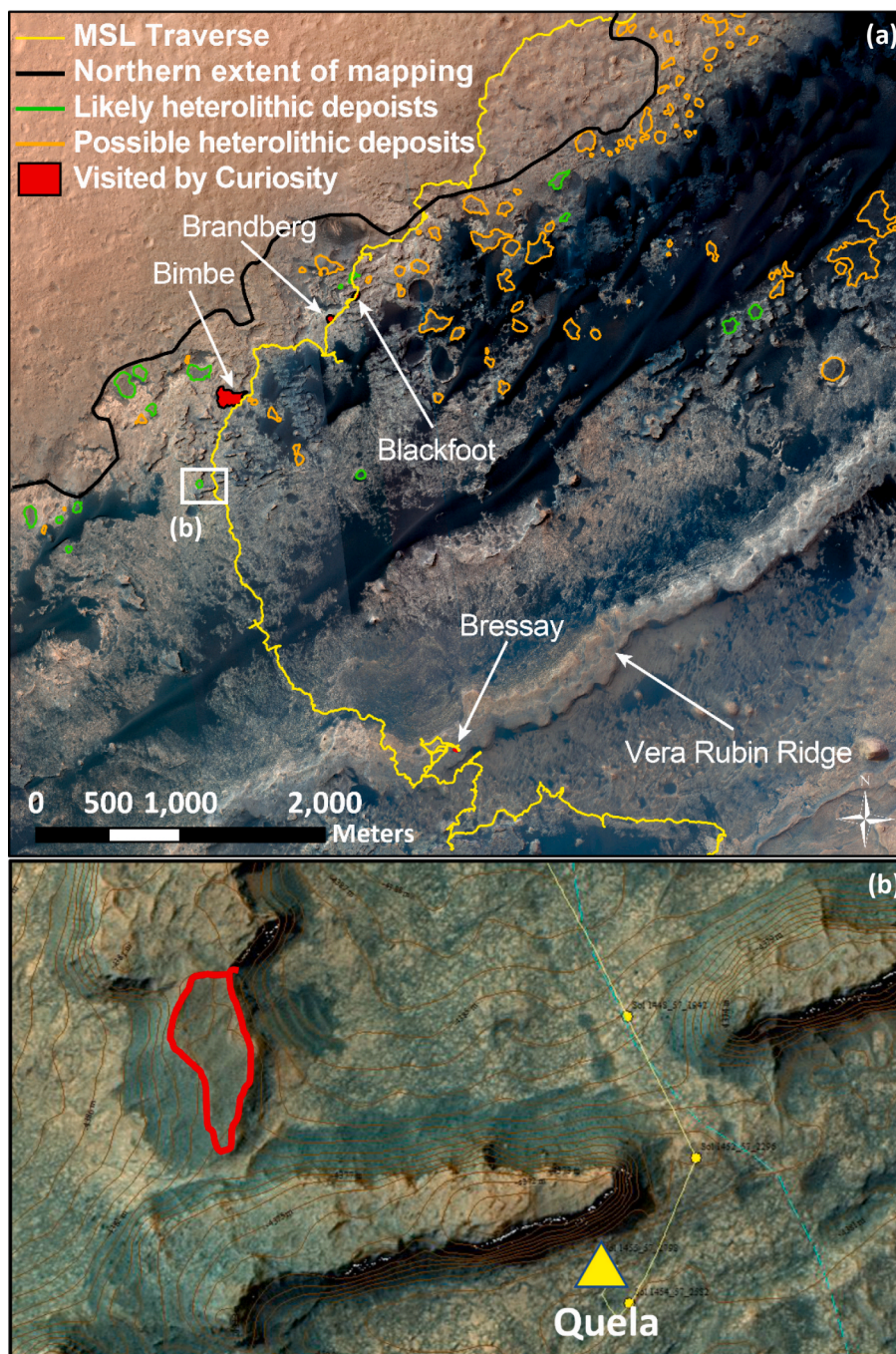
Fig. 24. Location of heterolithic units of unlithified gravel deposits. a) HiRISE orthoimagery overlain by likely (green), possible (orange) and visited (red) heterolithic units (e.g., Wiens et al., 2020). b) The Quela area where a heterolithic unit (red outline) is deposited on top of both the Murray and Stimson formations and Martin et al. (2021) report an exposure of 1 billion years (located at the triangle). HiRISE image credit: NASA/JPL/University of Arizona. (For interpretation of the references to colour in this figure legend, the reader is referred to the web version of this article.)

formations) (Fig. 25; Fig. S3 in Supporting Information S1). Although the prominent erosionally resistant 'Amapari Marker Band' unit lies above the Mirador fm. (Figs. 2; 25; Milliken et al., 2010; Kite et al., 2013; Weitz et al., 2022), the steepened hills extend to the north beyond the marker band outcrop, making its role less important in slope evolution. It may be that the mudstone of the Murray and lower Carolyn Shoemaker formations is sufficiently uniform and erodible, that low gradient erosional slopes are formed in it without yardang emergence.

Two other observations support wind abrasion origin of the Greenheugh pediment. First, post-Stimson erosion on the eastern side of the pediment has cut a wedge of increasing depth from Vera Rubin ridge to the steepened slopes of Mt. Sharp, to depths greater than 100 m (Fig. 23). This was likely done during a period free of any fluvial processes with the only erosive agent being wind. Although the currently active eroding surface is not a smooth plane, wind erosion, nonetheless, has not led to large yardang forms. An even smoother modern surface can be found on the north side of VRR (Figs. 1–2). Second, as noted above, the surface of the Greenheugh pediment is capped by the lithified Stimson formation, which over the majority (75 %) of the pediment surface has experienced sufficient erosion to be entirely missing the washboard pattern. Hence, the current top of the Stimson at the Greenheugh pediment defines a second, clearly wind scoured pediment
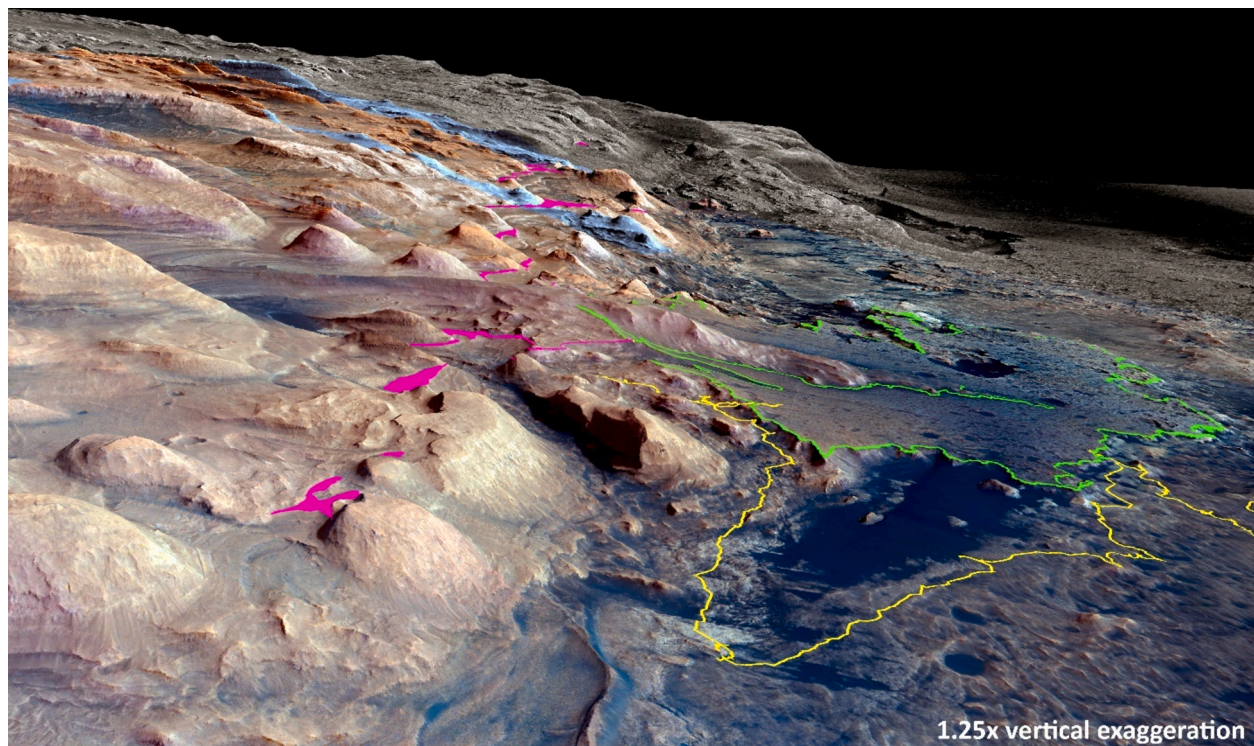
Fig. 25. A 3D HiRISE view of the NW margin of Mt. Sharp facing WSW including the Greenheugh pediment (green outline), Amapari Marker Band (purple), and Curiosity's traverse (yellow). Note the 1.25× vertical exaggeration. HiRISE image credit: NASA/JPL/University of Arizona. (For interpretation of the references to colour in this figure legend, the reader is referred to the web version of this article.)

surface. Although fluvial and debris flow deposits (Gediz Vallis ridge) did partially cover (at least) the Stimson, we found no evidence of fluvial wear on the surface at the rover ascent locations and no foreign sorted gravels away from the Gediz Vallis ridge.

Modeling predicts pediment formation by fluvial processes on Earth, especially under conditions of bedrock footslopes with fixed basal elevation (i.e., a stable lower boundary condition) (e.g., Howard, 1997.) Aeolian abrasion models for yardang formation after an initial seed topography have further explored yardang emergence and evolution (e. g., Pelletier et al., 2018). Exploration of the conditions under which wind abrasion alone can produce laterally extensive planar slopes without destabilizing into ridge and swale topography (and ultimately yardangs) will require a fully coupled wind shear and sediment transport and abrasion model (including lithologic controls on abrasion resistance), an effort that is beyond the scope of this study.

Our analysis has implications for interpreting pediment elsewhere on Mars. Although we cannot conclude that all pediments on Mars were formed by wind abrasion, our observations suggest that pedimentation by wind-abrasion is possible and may be common. Unless separate evidence suggests fluvial erosion, Martian pediment forms may not be a reliable indicator of past wet conditions. Future field studies identify evidence for fluvial erosion, then widely mapped Martian pediments should not be considered reliable indicators of past wet climate conditions.

5.2. Spatial extent of the Greenheugh pediment before erosional removal began

The regional reconstructions shown in Figs. 22 and 23 indicate a pre-Stimson surface of pedimentation that unifies the Greenheugh pediment with the northern outcrops (Murray buttes, Naukluft, and Emerson plateaus) and unconformably cuts across ~630 m of exposed Mt. Sharp stratigraphy. The preserved surface records at least part of the initial pre-Stimson denudation phase of Mt. Sharp, during which time the

majority of material that once filled northern Gale was removed. While it is obvious the layered sediments cut by the pediment surface (SPg unconformity) once extended far beyond their current positions (Figs. 2, 3, 25; Fig. S1 in Supporting Information S1), the depth of crater in-filling and thus the amount of material removed prior to- and during- pedimentation remains disputed (e.g., Lewis et al., 2019a, 2019b).

Our regional reconstruction of the Stimson upper surface (Fig. 22) (which reasonably parallels the SPg unconformity) now reveals that the regional paleotopography of the pedimentation surface conformed to the inclined convex surface (humped topography) that characterizes much of the modern landscape downslope of Gediz Vallis (Figs. 1–2; 22). The surface of this topographic feature exists today both as 1) a preserved surface (by the Stimson) that reflects at least part of the progressive denudation phase of Mt. Sharp that removed much of the upper mound stratigraphy, and 2) also today as a modern erosion surface. There is no evidence that it formed as a depositional feature (i.e., an alluvial, debris flow, or submarine fan). The most likely origin of the feature is that it is broad antiform formed due to differential compaction that has now been exhumed through wind abrasion. Searching higher on the mound for evidence of differential compaction could help further constrain the timing of deformation. The majority of Curiosity's traverse up Mt. Sharp has been along the axis of this feature, which given the scale of the landform and the subtle changes in bedding orientation, could explain some of the difficulties in comparing orbital and ground-based bedding orientation measurements at various locations across lower Mt. Sharp (Kite et al., 2013; Fraeman et al., 2013; Stein et al., 2020; Turner and Lewis, 2023).

The Greenheugh pediment may have been laterally more extensive than shown in Figs. 22 and 23. Given the pattern of wind transport (e.g., Day and Kocurek, 2016) around the base of Mt. Sharp and as reflected in the current Bagnold dune field, Stimson deposits may have extended well to the east and west, as suggested by the mapped Mound Skirting unit outcrops (Fig. 1; Anderson and Bell, 2010). Though likely of similar origin, we can't assess whether these more distant outcrops record

simultaneously active deposits (that would have preserved the erosional surface that is the Greenheugh pediment).

The proposed projection of the pediment (Fig. 23) is conservative and is supported by the downslope Stimson bluffs of the Murray Buttes, Naukluft, and Emerson plateaus and Stimson blocks found throughout Glen Torridon (Fig. 3), as well as along the easterly journey around the Sands of Forvie (Fig. 3) dune field (where probable Stimson blocks were found over 1.2 km from the current outcrop). The SPg unconformity definitely crossed Vera Rubin ridge and was likely a contiguous surface at the time the Stimson was deposited. There is a break in slope at the base of Mt. Sharp, to the north of which no Stimson capped outcrops have been observed. On the floor of Gale crater (Aeolis Palus to the north of the projected pediment extent), there is exposed bedrock that includes fluvial deposits, but not Stimson aeolian deposits (Williams et al., 2018). As noted above, some papers have proposed thick (100 s of meters) Stimson deposits to the north of our projection (e.g., Grotzinger et al., 2015), but we found no exposures to support this interpretation.

Based on spatial changes in bedform morphology recorded in the Stimson, Banham et al. (2021) suggest that the smaller scale bedforms found at the top of the Stimson and the Emerson plateau exposure (first rover encounter with Stimson at the base of Mt. Sharp) are typically what would occur at the distal edges of an erg (large dune field). This then points to a finite reach of the Stimson at the time when the deposit was preserved, supporting the idea that these locations (Greenheugh pediment and the Emerson plateau) were the up- and down-slope margins of the Bagnold-dunes-scale Stimson erg.

The Greenheugh pediment, along with the northern Stimson outcrops, exists because the capping Stimson sandstone was strongly cemented, creating a resistant unit over soft underlying sediments. This favored a bluff retreat mechanism in which the underlying softer rock is eroded, forcing the exposed capping Stimson to tumble downslope. Chemical analysis of both the lithified Stimson formation, and the modern Bagnold dunes suggests that a combination of magnetite (through the aqueous alteration of basaltic olivine), and amorphous silica are responsible for cementing the Stimson (Yen et al., 2017). We do not, however, know through which process(es) lithification occurred. Given the 10s of kilometers over which the Stimson has been observed, it is reasonable to suggest that the lithification process must have been regionally extensive. Finally, the absence of Stimson outcrops across Aeolis Palus suggests that either the Stimson erg did not extend far to the Northwest or that the lithification process hardening at least the basal Stimson, although widespread, did not extend far to the NW across the floor of Gale.

5.3. Source of sediment for the Stimson

What events reversed a long period of erosion (and pediment generation) to a condition of net accumulation of sediment along the footslopes of Mt. Sharp? Banham et al. (2022) report that the Stimson at the northern edge of the Greenheugh pediment and the measurements made north of Vera Rubin ridge indicate that the Stimson has a geometric mean grain size of 486 μm and 406 μm, respectively. These data come from MAHLI, which can collect images to within 10 mm of the surface yielding up to 16 μm/pixel (Edgett et al., 2012; Yingst et al., 2016 Banham et al., 2018 methodology). The reported mean grain sizes may be systematically high because, even with 16 μm pixel resolution, densely packed fine sand on unbroken rock surfaces is difficult to identify and measure individually: its presence goes largely uncounted. MAHLI imaging point locations without detectable large grains in the image were not subject to a grain size analysis. In contrast, Banham et al. (2018) reports the currently active Bagnold dunes along the northern footslopes are composed of 112-120 μm size sand (but here well sorted sands without any matrix are readily counted using MAHLI). Large variations in bedforms and transport directions (north, south, west) (from bottom to top of section) at the northern edge of the pediment at Tower butte differed from the primarily northerly direction in the northern footslope deposits (Banham et al., 2022). Bedford et al. (2022) note that the upper unit west-migrating dunes have a slightly different geochemistry and mineralogy from the lower deposits. All of the Stimson deposits are sandstones noted by their distinctive dark colour, wind abrasion resistance, and a fracture density that enabled large blocks to be released and tumble down bluffs during retreat.

As proposed above (section 5.2), it seems likely that the downslope outcrops of the Stimson capped bluffs correlate to the those exposed in the Greenheugh pediment (Figs. 22 and 23), thus unifying the Stimson as a once laterally contiguous unit. This, along with the scale of the dunes reported by Banham et al. (2018, 2021, 2022), suggests that the Stimson, rather than being an event that caused significant great depth of refilling of Gale, was in essence a greatly expanded version of the current Bagnold dune field, i.e., a dune field band along the lower slopes of Mt. Sharp. As noted above, this band may be contemporaneous with other units mapped as mound skirting unit elsewhere in Gale mapped by (Anderson and Bell, 2010; Fig. 1). The Stimson, then, at full extent may have been a large dune field that draped the lowest slope of north facing Mt. Sharp (possibly well up into Gediz Vallis) and extended at least about 4 km wide (North- South) across a 500 m elevation change, and laterally at least 10 km (and possibly much more). On the scale of Gale crater, much like the modern Bagnold dunes, the Stimson dune field would have been a relatively small feature. Because it is difficult to decipher the timing of events, it is possible that deposition and lithification occurred in various regions of the Stimson dune field at different times. Without direct correlation of time-synchronous features, we cannot definitively say the dune field covered the entire reconstructed Stimson unit all at once – although this is perhaps most likely.

Two hypotheses with very different significance can explain the Stimson capping event: internal dynamics within Gale crater resulting in a lag of sandy material, or an influx of sand into Gale crater from elsewhere. Progressive back wearing erosion of the northern face of Mt. Sharp and erosion of the basal floor of Gale in strong winds must have lifted out of the crater clay, silt and fine sand. This may have left the larger, mineral grains and lithic fragments composing the dark sands of Stimson, as found in the Bagnold Dunes, and as loose sand typically found darkening outcrops presently. Topographically-driven winds then could have concentrated the sands into Stimson sand dunes as a band along the base of Mt. Sharp. Day and Kocurek, 2016 describe how as the period of net erosion and exhumation of Gale develops, wind directions will change. Katabatic winds on the crater walls and the exposed Mt. Sharp mound would develop and a regional wind direction from the northern would be deflected around the mound. Such processes currently drive Bagnold dunes and have led to the development of 34 km long 15 km wide dune field along the western side of Gale floor (Day and Kocurek, 2016).

An example calculation examines this idea. Consider just the broad northern floor of Gale crater (where fluvial sandstones have been mapped by Williams et al. (2018)) to be a source area of sand entrainment (1050 km^2) which would then be deposited on an estimated pediment depositional area (66 km^2). And if we assume 15 m of original Stimson deposition, then it would take just 1 m of erosion in the source area to produce enough material for the Stimson formation, if the erosion was of similar sand size. If the source area is just 10 % coarse sand, then it would take 150 m of erosion to produce the 15 m of deposition. These numbers are obviously guesses but it illustrates that just erosion and concentration of residual sand grains could provide a residual mass capable of feeding the Stimson accumulation. The net erosion and then burial and concentration of a large dune field does require, nonetheless, atmospheric conditions capable of such work, which may have largely occurred during times of denser atmospheric conditions (Bridges et al., 2017). Furthermore, Day and Kocurek (2016) argue that the modern sand deposits found around the crater are only a small amount of the sand that would have been produced by progressive exhumation of Gale, hence past winds must have been sufficient to carry most sediment out of the crater.

The simpler argument, but one that calls for dynamics in external sourcing of sediment is to propose that Stimson sediment records a period of return to net deposition of sediment from external sources into Gale, where topographically directed (as described by Day and Kocurek (2016)) winds accumulate the sediment along the base of Mt. Sharp. Such a change in sediment input could be a response to an episode of glacial/fluvial activity on Mars that mobilized abundant sand, then ceased, providing a source of sediment for winds to carry across craters such as Gale. Such events have been proposed in the mid latitudes (e.g., Head et al., 2005; Souness and Hubbard, 2012). Hence, the Stimson capped pediment could record a climatic cycle of dry (net erosion-forming the pediment surface)-to wet (sand generation elsewhere) to dry (transport sand to the crater and net deposition). If one includes the subsequent (presumably water-mediated) lithification process, the soft-sediment deformation of the lowermost Stimson, and then later erosional backstripping, at minimum of one more wet-dry cycle is required. A still simpler explanation to initiate sediment deposition would be that a significant change in just the wind direction may have increased the transport of sand into Gale, turning the lower slope into a net depositional environment. A significant delivery from an external source could also lead to a much greater infill in Gale then is evident from current exposure of Stimson.

The Stimson mineral composition differs from contemporary Bagnold dune sediments. Two samples collected from the Bagnold dunes and one sand deposit collected near the landing site had olivine from 10 to 17 % and magnetite of 1 to 3 % (Ehlmann et al., 2017). Two drilled Stimson samples collected along the northern outcrops (excluding drill samples from zones of visibly strong alternation) had no olivine, but instead contained elevated magnetite (10 to 11 %). One sample (Edinburgh drill site) on the Greenheugh pediment had both elevated olivine (8.4 %) and magnetite (10 %) (Thorpe et al., 2022). These data suggest that the original Stimson composition may have been similar to the Bagnold dunes although with additional input from a more alkaline-rich (Na and K) source rock (Thompson et al., 2022a, 2022b). Post-depositional, diagenetic alteration of olivine to magnetite (which contributed to lithification) also occurred (Yen et al., 2017), but perhaps was simply incomplete at the Edinburgh sample site (Fig. 10b). These data, therefore, do not suggest that Stimson was derived from a fundamentally mineralogically foreign source although there may have been an additional source of e.g., olivine and potassium feldspar at the pediment that was either diagenetically altered, or never accumulated elsewhere in the Stimson. It is likely, however, that the modern Bagnold dunes are at least in part comprised of recycled Stimson fm.

The estimated scale of dunes in the Stimson ranges from 3 m tall and 45 m in wavelength to 20 m tall and 300 m in wavelength (Banham et al., 2018, 2021, 2022). Bridges et al. (2017) through field measurements and modeling, suggest that higher atmospheric density and warmer conditions than present would be needed to drive significant Bagnold field dynamics. The implication is that whether internal dynamics or external sourcing, present atmospheric conditions on Mars would be unable to generate sufficient erosion-generated sediment supply and nor mobilize large scale active dunes recorded in the Stimson formation. Bridges et al. (2017) who documented limited activity on the Bagnold dunes at the base of Mt. Sharp cite Haberle et al. (2003) in noting that near surface winds are a function in precession and eccentricity and suggest that obliquity excursions could lead to periods of greater dune activity. Haberle (2022) further explains the links between obliquity and climate change on Mars. In Gale, presently, modestly active dune fields are confined to the floor an edge of Mt. Sharp (Day and Kocurek, 2016 maps).

5.4. Processes that caused Greenheugh pediment to retreat becoming an elevated erosional remnant

The Greenheugh pediment area shifted from a location of net erosion, cutting the pediment surface, to net deposition and cessation of erosion as the Stimson sediment accreted on the pediment, and then back to net erosion, but this time through the lithified, erosion-resistant Stimson cap. This later phase of erosion (that still weakly continues today) probably started along the northern basal slopes. While wind appears to have been the primary agent of erosion, lithology, diagenetic alteration, and weathering (rock fracture) influenced the pattern and pace of erosion (Day and Kocurek (2016) highlight the importance of weathering influence on wind erosion).

Lithology influences wind erosion in several ways. Vertical erosion through the hard Stimson cap that sits on the relatively soft Mt. Sharp group sediments, leads to lateral retreat driven by the erosion of the exposed underlying softer sediment (Day and Kocurek, 2016). This forms the common hillslope profile seen in arid regions on Earth, of a flat- topped bluff, the slopes of which are lined with blocks left by the retreating cap. Given the resistance to wind erosion of the Stimson cap, progressive wind incision through it to initiate bluff retreat must have been a slow process, strongly influenced by sand supply and the strength of winds. Craters larger than 30 m in diameter were probably needed to penetrate to the underlying soft sediments, but these may not have been large enough to allow winds to erode rather than fill. In the Murray Buttes region there is an east-west trend to some of the bluff faces. Whether this reflects dominant erosive winds or some stratigraphic structure in the Stimson that influenced erodibility is unknown. The absence of Stimson bluffs to the east of Greenheugh pediment may reflect early exposure of the basal softer sediment with winds attacking the distal edges of the pediment, a thinner cap, or perhaps less strongly cemented Stimson.

Figure 26 shows mosaics of Tower butte and Quela base that illustrate how blocks on the bluffs form not only an erosional shield on the underlying softer sediments, but they also generate a momentum defect that causes the coarse dark sand to collect, further covering the slopes from abrasive wind action. This covering must strongly slow the pace of lateral slope retreat. As illustrated in a cartoon (Fig. 27), along the pediment escarpment and at the isolated Stimson capped bluffs to the north, the large blocks are not found at any significant distance across the floor of the retreating surface. The downslope termination of block coverage is abrupt and the blocks near that termination point do not show exceptional abrasive wear by wind (ventifacts). Yet, the simplest hypothesis for this striking pattern is that once the blocks become exposed beyond the protective shield of other blocks, wind abrasion with sufficient sand makes relatively quick work of eliminating the block. It may also be the case that for some significant period of time, as suggested by the billion-year exposure age date at Quela, wind stress and perhaps sediment supply, has not been sufficient to attack blocks still clustered with the rest on the bluff slope, but on more exposed blocks away from the bluff, abrasion could persist. This analysis differs some from the erosional sequence proposed by Day and Kocurek (2016) which was based on hillslopes observed early in the mission. We highlight both the retarding effects on lateral slope retreat by the colluvial mantle and sand accumulation, and the sudden complete removal of blocks beyond the base of the slope.

Blocky scree patches along the bluff slopes lining the Greenheugh pediment indicate that this process has also been episodic (Figs. 15; S4 in Supporting Information S1). Patchy removal could be due to just internal dynamics, but given the sensitivity to wind strength and the dependence of that on obliquity, these patches may be another indicator of small episodic climate shifts.

The northern edge of the Greenheugh pediment has an arcuate shape that could suggest a fan origin (Figs. 1b, 2, 5) (e.g., Anderson and Bell, 2010). We suggest however, that this shape is more likely due to a combination of the shaped diagenetically-hardened emergent ridge (Vera Rubin ridge) and an upslope highly erodible mudstone that wind has eroded into a trough and organized into periodic bedrock ridges (Stack et al., 2022). The shape of emergent VRR essentially set the shape of the pediment escarpment. Hence, the shape has nothing to do with a fan, but rather the interplay of various lithology resistance and wind
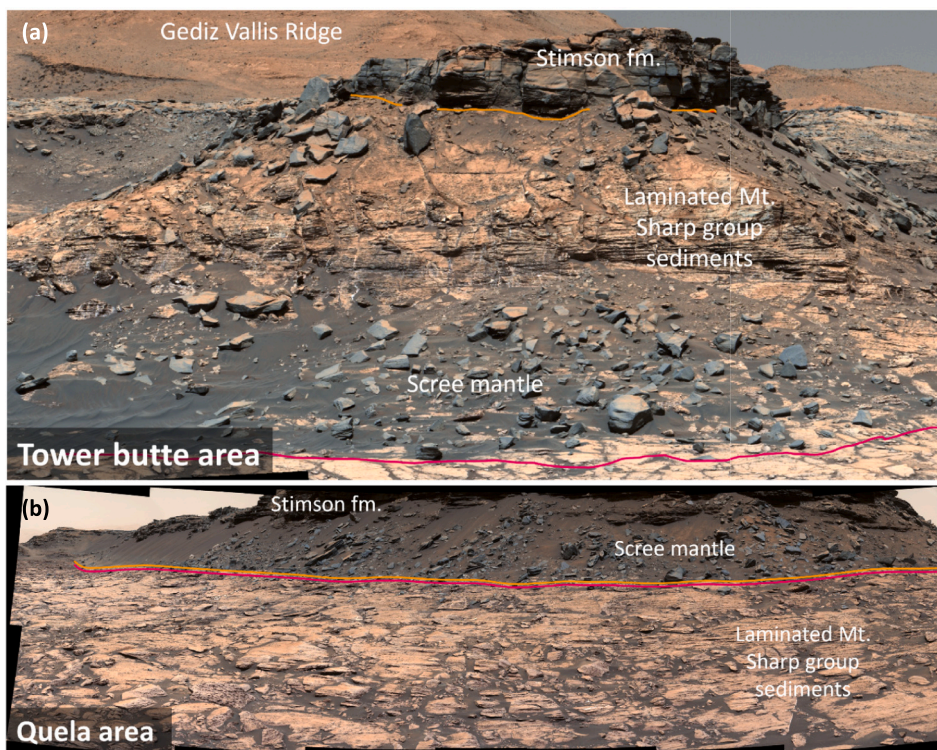
Fig. 26. Fallen Stimson boulders with associated wind-blown sand flanking steep-sided buttes at Tower butte (a) and Quela area (Butte M12). Note the absence of sand and boulders away from the base of each butte. Mastcam image credit: NASA/JPL-Caltech/MSSS. See Table S1 in Supporting information S3 for image sequence identifiers.
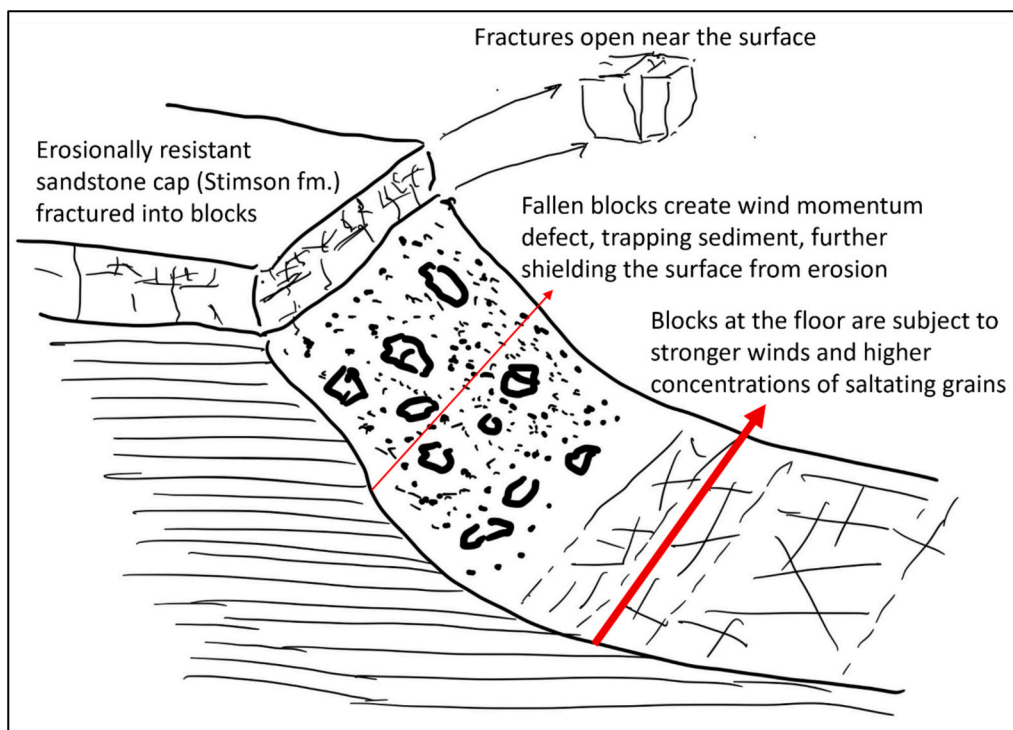

Fig. 27. Schematic diagram showing relationship between fallen Stimson boulders and local sand accumulation characteristic of the steep side slopes flanking many of the buttes observed by Curiosity. Boulder and associated sand mantling retard scarp retreat. Enhanced wind abrasion removes blocks at the base of retreating buttes.

erosion.

One other important lithologic control on erosion is bedrock fracturing. All of the bedrock along the footslopes of Mt. Sharp is fractured. These fractures arise from many processes including hydrofracturing (e. g., Schieber et al., 2017; Kronyak et al., 2019), impact cratering, and differential compaction. In addition, large scale topographic induced stresses may be important (e.g., Moon et al., 2017). Yardang development in which concentrated erosion on either side of an emergent streamlined form can produce convex hillslopes that, should the rock be sufficiently brittle, will experience tensile stresses at subcritical levels that over time led to fracture propagation. This process, however, may be dampened by anisotropy in the strength of the convex hillslopes due to their layered stratigraphy. Periglacial processes may have also contributed to fracturing (Hallet et al., 2022), perhaps during high obliquity conditions. Day and Kocurek (2016) suggested thermal stresses contributed to fracturing. High fluid pressures during burial/ diagenesis was also likely common (e.g. Cosgrove et al., 2022). The ground temperature monitor on the Curiosity rover documents that on a daily basis surface rocks typically experience 80 degree C temperature variation (e.g., −70 C to +10 C on the southern ascent on the pediment) (Pla-Garcia et al., 2016). Despite the low air humidity levels, over the probable billions of years of exposure these oscillations could induce subcritical stress crack growth (e.g., Eppes and Keanini, 2017). Combinations of pre-erosion fracturing and, then erosion and further possibly topographic induced fracture opening, cause rocks to become more erodible, and to release blocks down slopes where wind abrasion can remove them. A wind-driven landscape evolution model will need to include these processes to account for the pace of change and resulting landscape form.

5.5. Diagenesis associated with the pediment surface (SPg unconformity)

Numerous observations throughout the MSL mission indicate an extensive and complex diagenetic history experienced by the sediments of Mt. Sharp. At both the Emerson and Naukluft plateaus (Figs. 1b; 2), Rampe et al. (2020a) report extensive fracturing and associated halos (characterized by silica enrichment and deposition crystalline silica). These features were observed to crosscut the Murray and the overlying Stimson, and were interpreted to have formed through multiple fluid events likely originating deep below the surface. At least one of these fluid events postdated the lithification of the Stimson (Yen et al., 2017; Frydenvang et al., 2017). Within the lowermost Stimson in these areas, occasional nodule formation was also observed (Banham et al., 2018, 2021).

Fraeman et al. (2020) proposed a diagenetic origin for Vera Rubin ridge (VRR), the top of which is hypothesized to have been within a meter of the pediment surface (Fig. 23; Bryk et al., 2020). Multiple diagenetic fluid events (leading to increased hardness) generated iron recrystallization of iron bearing minerals, the formation of nodules and crystal pseudomorphs, extensive calcium sulfate veination, the formation of patches of red and gray hematite, and resulted in significant cementation and hardening of the rock (Bennett et al., 2021; Das et al., 2020; David et al., 2020; Frydenvang et al., 2020; Horgan et al., 2020; L'Haridon et al., 2020; McAdam et al., 2020; Rampe et al., 2020a, 2020b; Thompson et al., 2020; Wong et al., 2020). Rampe et al. (2020b) found evidence for crystalline silica in VRR, marking the third location near (but not crossing) the unconformity where the team identified quartz polymorphs. With the Stimson absent at VRR, it was not possible to assess whether there was extensive fluid exchange across the unconformity like there was downslope. However, several authors identified evidence such as hematite recrystallization (Rampe et al., 2020b), and nodule formation (Sun et al., 2020) that likely formed through late-stage diagenetic fluids that postdated at least the lithification of the Murray, and so could have influenced the Stimson at this location. While the origin and number of diagenetic fluid events that formed VRR remains poorly constrained, several authors hypothesized alteration on

the ridge was in part due to fluid flow along the SPg unconformity (see Fraeman et al., 2020 and refs therein).

The stratigraphic interval of alteration extending from the SPg unconformity down <3 m (informally termed the 'Hutton Interval') is characterized by extensive dark and light-toned veins that do not cross the unconformity, extensive nodularization, as well as chemical, mineralogical, and spectral differences from typical Glasgow member below (O'Connell-Cooper et al., 2022; Thompson et al., 2022b; Gasda et al., 2022; Dehouck et al., 2022; Thorpe et al., 2022; Sutter et al., 2022; Rudolph et al., 2022). These characteristics were observed both at the top of Western butte and at Tower butte.

ChemCam LIBS and APXS data indicate the veins and nodules below the unconformity as well as the bulk bedrock are enriched in Fe, Mg, and Mn with respect to elsewhere in the Glasgow member (Thompson et al., 2022b; Gasda et al., 2022). In addition to elevated Fe, Mn, and Mg, the Hutton interval bedrock very close to the unconformity was also enriched in mobile elements Ca and Na, depleted in S (Thompson et al., 2022b), and had low values of Chemical Index of Alteration (CIA) (Dehouck et al., 2022). Mineralogically, the interval contained low clay abundance and a significant component of crystalline silica (Thorpe et al., 2022).

In contrast to the bedrock below the unconformity, the Stimson above it showed generally less evidence for diagenetic alteration except for directly above the contact. Directly above the unconformity the Stimson does contain elevated S possibly associated with the event that depleted the strata directly below the unconformity (Thompson et al., 2022b). The lower Stimson (Gleann Beag interval) also contains extensive centimeter-scale nodules, but their chemistry is indistinguishable from the adjacent Stimson bedrock. (Fig. S6 in Supporting Information S1; Thompson et al., 2022b). Several meters above the unconformity, the Edinburgh drill sample had relatively abundant olivine, potassium feldspar, and phyllosilicates, and indicated redox disequilibrium in Iron sulfides/sulfates consistent with relatively less diagenetic alteration than elsewhere (Sutter et al., 2022).

The light-toned veins in the underlying Glasgow member observed near Tower butte crosscut the dark toned veins suggesting the fluid event that produced light-toned ($CaSO_4$-rich) veins post-dates the emplacement of the dark (Fe and Mn-rich veins) (Gasda et al., 2022). Neither light- nor dark-toned veins were observed crossing the unconformity, suggesting both the light- and dark-toned veins predate pedimentation (Fig. 12; Fig. S5 in Supporting Information S1; Gasda et al., 2022). The similarity in chemistry among the veins, nodules, and the country rock in the Hutton interval suggests a possible timing relationship. Gasda et al. (2022) hypothesize that the nodules formed early – perhaps during initial burial as they are cross-cut by light-toned veins. The dark-toned veins, although chemically similar, must have developed after lithification of the Glasgow member. Given that the veins do not cross the unconformity this brackets their timing to between the lithification of the Glasgow member and pedimentation, which could be a large period of time. Enrichment of the uppermost Glasgow member in mobile elements Ca and Na suggest Hutton interval bedrock alteration was not due to surface weathering, which would more likely result in concentrations of immobile elements (Thompson et al., 2022b). This is supported by the possible depletion of S directly below the unconformity with enriched S directly above it, and further suggests that this fluid event must have occurred after the deposition of the Stimson. It is unclear if this event is related to the apparently isochemical formation of nodules in the lowermost Stimson or whether it pre-or post-dates lithification of the Stimson (Thompson et al., 2022b).

As noted above, the soft sediment deformation within the Stimson observed near Maria Gordon (Fig. 16) notch and at the Blackcraig ascent (Fig. 18; Banham et al., 2024) is not obviously related to any of the diagenetic events suggested above. In particular, nodules were not observed in deformed Stimson and the chemistry of the deformed Stimson is identical to undeformed Stimson at the same stratigraphic level at Maria Gordon notch area. The Blackcraig fluidized sediments did

have elevated Cr and slightly elevated Fe. The deformation event however, can be constrained to the time after deposition of the Stimson but prior to its lithification – with the water perhaps originating as springs from the Gediz Vallis catchment or elsewhere higher on Mt. Sharp. Siebach and Grotzinger (2014) suggest spring activity leading to boxwork formation may have occurred far upslope from the pediment. It is possible this is the precursor to, or part of the event which lead to the lithification of the Stimson.

Alteration features along the SPg unconformity observed at the pediment (and indirectly at VRR) contain some similarities with diagenetic evidence at the Naukluft and Emerson plateaus. For example, similar spectral and chemical trends were observed within several meters of the unconformity at the Emerson plateau (Thompson et al., 2022b), and nodules like those at Tower butte often occurred in the basal Stimson at the Naukluft and Emerson plateaus (Banham et al., 2018, 2021). However, there were also notable differences between the pediment and the outcrops downslope (Naukluft and Emerson plateaus). Extensive fracture networks (Kronyak et al., 2019) and associated fracture halos, containing crystalline silica, cross the unconformity. Yen et al. (2017) and Frydenvang et al. (2017) suggest a fluid origin from deep in the basin. This is supported by Bristow et al. (2021), who suggest fluids derived at depth (primarily due to interactions with basalt and basalt-derived sediments) would likely be enriched in silica. In contrast, the opal-CT/cristobalite found on VRR and at the Hutton drill site likely formed through the recrystallization of in-situ silicate minerals (e.g., feldspars and phyllosilicates) rather than an 'enrichment' of silica from saturated fluids (Thompson et al., 2022b; Dehouck et al., 2022; Gasda et al., 2022). The temperature under which this happened remains under debate.

This review suggests four important observations regarding the timing of diagenetic events relative to pedimentation and Stimson deposition. First, the dark and light toned veins in the Glasgow member are truncated by the Greenheugh pediment erosional unconformity. Second, downslope of the contiguous Greenheugh pediment, the projected pediment surface and Stimson mantle exposed in local bluffs are crossed by fractures with crystalline silica halos. Third, before the aeolian sediments of the Stimson were lithified, groundwater was present in places, leading to soft sediment deformation. Fourth, nodularization of the basal Stimson and some of the chemistry on either side of the erosional boundary suggests some fluid transport did cross the pediment boundary. Hence, despite the geomorphic and stratigraphic record of aeolian erosion and deposition of a large dune field (the Stimson) under arid conditions, liquid water was present before, during, and after these events unfolded.

5.6. Climatic history recorded by Greenheugh pediment formation and subsequent erosion

Our observations suggest along the base of Mt. Sharp there has been a fluctuating environment of alternating erosion and deposition that may have been influenced by internal dynamics, but likely records external climatic forcing. Table 1 lists process steps, starting after the building and the onset of net erosion of Mt. Sharp, that led to the contemporary stratigraphy and topography along the footslopes of Mt. Sharp. It is meant as a summary of observations and interpretations organized to reveal the apparent time sequence of alternating erosion, deposition and apparent periods of wet and dry.

Our table begins with the active erosion of the northern face of Mt. Sharp, hence a period after net accumulation of sediment to build Mt. Sharp, when wind erosion then swept vast quantities of sediment out of the crater. This erosion revealed sediments that had experienced strong diagenetic alteration, including hydrofracturing (e.g., Caswell and Milliken, 2017; De Toffoli et al., 2020), intensive nodularization (e.g., Stack et al., 2014; Sun et al., 2019), and secondary mineral deposition (e.g., Bridges et al., 2015; Bristow et al., 2021). All of this indicates active groundwater alteration preceding the erosional stripping of Mt. Sharp

Table 1

Proposed timeline of events (1–9) from the onset of Mt. Sharp denudation, through pediment formation, to the modern. All ages approximate except for the 1 billion year age derived from cosmogenic data (Martin et al., 2021).

Step	Process	Comment
9	Present **erosion rate slowly continues along the footslope**	*Current low wind speed and low sediment supply* *Bluff slope patchy colluvial deposits record local episodic erosion*
8	Progressive, **deep wind erosion** upslope of Vera Rubin ridge	*Second contemporary bedrock erosion surface formed across the lithified top surface of the Stimson and adjacent exposed Mt. Sharp group sediment*
7	**Erosion nearly ceases** in northern slopes	*May be due to local burial by dune field* *Renewed wind erosion on the northern footslopes, **likely before 1 billion years ago***
6	**Fluvial/debris flow fan** deposition on the pediment and deposition on eroded floors of Murray buttes. (Gediz Vallis ridge is a remnant fan deposit)	latest Hesperian (~3.1 Ga)?
5	**Wind erosion** advances along northern footslopes	*Vera Rubin ridge exposed at the surface but still connected to upslope pediment* *Slow incision through pediment and slow lateral retreat*
4	Groundwater and vadose zone **water** cement Stimson sediment	*Soft sediment deformation, then cementation, and deposition ceases*
3	Wind reworking of Stimson surface producing finer scales marking the wa**shboard pattern**	
2	Aeolian sediment **deposition** of the Stimson formation on footslopes in large dune field, preserving pediment surface at that time	*Groundwater present* *Transport direction varied laterally and vertically*
1	Wind **erosion** of northern front of Mt. Sharp	*Pediment formation on footslopes of Mt. Sharp,* **late Hesperian (> 3.4 Ga)?** *Strong winds remove nearly all eroded sediment from the crater; significant groundwater alteration of sediments preceding erosion*

(Fraeman et al., 2020). Many studies have focused on this early phase of Mt. Sharp sedimentary construction (e.g., Thomson et al., 2011; Deit et al., 2013) and its climatic implications.

The wind erosion exhuming Gale along the base of Mt. Sharp, which is mostly composed of lake deposits, had produced a low relief, gentle sloping surface, i.e., a pediment (**Step 1**). The net erosion and retreat of Mt. Sharp may have been for a considerable period of time given the volume of net sediment removal. It continues presently, albeit at likely a much slower pace (e.g., Kite and Mayer, 2017). Hence, the pediment surface of the Greenheugh pediment does not record an individual event, instead it was just an actively eroding boundary on in-place Mt. Sharp sediment during a probably extended climatic period that provided strongly erosive winds. The event that is preserved and records some local to perhaps global change is the onset of net deposition of aeolian sediments across the exposed pediment. As documented by Banham et al. (2018, 2021, 2022) it is a depositional sequence, recording various scales, bedforms, and transport directions, developed as part of a large dune field (the Stimson formation) (**Step 2**). As reported above, the outcrop and stratigraphic evidence suggest that this dune field was confined to the footslopes likely neither extending far upslope onto upper Mt. Sharp, nor crossing significantly across the floor of Gale crater. Though the field was then at least 4 km wide and

probably more than 10 km in length, it was a very small area relative to Gale crater. Given its relatively small size, in an area of active wind erosion, and sand size dominated, compared to much of the exposed bedrock on which it deposited, there is a possibility that the dune field was a concentrated residual of the wind evacuation of Gale which was swept to the base of Mt. Sharp. Changing wind fields with Gale exhumation and relative emergence of Mt. Sharp could lead to wind directions that favor sand accumulation along the flanks along Mt. Sharp. In this case the climatic signature the Stimson records is sufficient strong winds that were oriented favorably to build large scale active bedforms of sediment. A thickness of at least ~10 m was deposited. As mentioned above, Bridges et al. (2017) suggested that the present wind strengths in Gale may not easily support aeolian migration/accumulation required to halt erosion.

Alternatively, this burial event could record a period of increased sand influx into Gale crater due to changing sediment availability external to Gale (such as the drying up of fluvial systems). Paleo-wind direction would suggest a sediment source from the north. It would then seem likely that other coincident deposits would be left in Gale. Such sediment may now be part of the mound skirting units mapped by Anderson and Bell (2010). In either case, the Stimson dune field appears to require an atmosphere more capable of producing winds that can transport medium sand into large scale dunes than currently is experienced in Gale. The variable transport directions recorded in the Stimson stratigraphy may record the interplay of variable regional and locally controlled wind patterns.

The surface of the Stimson sequence was probably reworked and possibly partially eroded by perhaps weaker winds into a field of smaller bedforms leading to a washboard surficial appearance (**Step 3**). The wavelength was not unlike that which is currently active on the exposed bedrock to the east of the Greenheugh pediment edge (Fig. S16 in Supporting Information S1). During the Stimson sediment accretion, groundwater was likely present, contributing to local soft sediment deformation and diagenetic alteration, perhaps including lithification of the sandstone (**Step 4**). Later, along the northern most footslopes, groundwater likely traveled up through the underlying Murray and into the lithified Stimson along fractures creating distinct, strongly depleted fracture halos in the bedrock (Yen et al., 2017) and silica enrichment (Frydenvang et al., 2017). Under the intact Greenheugh pediment upslope of Vera Rubin ridge, we did not see veins nor reaction halos crossing into the Stimson cap. Here groundwater was probably arriving from upslope sources on Mt. Sharp likely at more than one time and traveling along the much less permeable boundary with the underlying Mt. Sharp bedrock (e.g., Siebach and Grotzinger, 2014). The likely presence of groundwater during **Step 4** (and possibly **Step 2**) indicates that near surface temperatures were much warmer than present. The groundwater influence here could be sourced far outside Gale (for the footslope fracture flows) or be more locally driven, such as subsurface runoff from Mt. Sharp through the Stimson deposit (e.g., Salese et al., 2019; Fraeman et al., 2020). Taken together these observations suggest that the Stimson may record at least locally more erosive (density and possibly speed) winds and warmer temperatures than present, although wind strength may have declined during the later phase of the Stimson reworking. The Stimson formation conditions need not have had stronger winds nor wetter conditions than the period of net erosion that preceded it. It is unclear if during the period of exhumation forming roughly the current topography (**Step 1**) whether groundwater flows were concurrent. This seems likely given continued activity in subsequent steps (e.g., soft sediment deformation shortly after Stimson deposition).

The Stimson surface shifted from accretion to net erosion after lithification and this erosional process may have advanced first along the northern basal slopes (**Step 5**). This reversal from accretion to dissection is puzzling. The one clear correlation is that the Stimson by the time of incision had been lithified, forming a hard cap on the underlying Mt. Sharp group. For erosion to proceed, sufficient wind shear stress,

availability of particles (to drive wear) and exposure of the bedrock is needed (e.g., Kok et al., 2012). Perhaps the final lithification of the Stimson happened during a less intense wind period, and sometime after lithification high wind intensity returned with sufficient sediment to attack the pediment surface but did not have enough sediment supply to bury it for the given wind stress levels. Day and Kocurek (2016) propose that dominant paleowind direction in Gale where the Stimson deposit lay was from the north. This is opposite to the inferred transport direction for much of the Stimson (Banham et al., 2022), suggesting either changes in paleowind direction during Stimson deposition or local topographic effects on wind direction. If the eroded Stimson bluff orientation at Murray buttes is indicative of erosion wind direction rather than being related to the depositional system, then east-west winds, similar to that produced currently by wind being forced around the base of the mountains (Day and Kocurek, 2016) may have prevailed.

After considerable erosion of the northern most footslopes, the heterolithic gravel was transported into the footslope area (Wiens et al., 2020). The arrival of the gravels in the eroded Stimson capped topography indicates a clear wet period of surface water that postdates Stimson formation, lithification and erosion North of Vera Rubin ridge. These gravels may be remnants of once extensive fan deposit across the pediment, now preserved as the narrow remnant, Gediz Vallis ridge. The stratigraphy suggests that the fan was built by a combination of debris flow and fluvial processes (Bryk et al., 2019b; Bryk et al., 2024). Palucis et al. (2016) identified a sequence of three deep lakes, that occupied much of the northern half of Gale Crater up to a depth of 700 m. They suggested the two lower lakes, whose level cross the Gediz Vallis ridge deposits may have been coincident with the fan construction period. Palucis et al. (2020) proposed, based on crater counting, that the deepest and oldest lake may have formed over 3 billion years ago.

After deposition, wind erosion continued in the northern slopes but then according to exposure age dating effectively stopped in this area, at least 1 billion years ago (**Step 7**; Martin et al., 2021). Yet, wind erosion swept the northern edge of the Greenheugh pediment towards the south and narrowed laterally the extent of the pediment (**Step 8**). Lateral retreat at the northern edge was at least 400 m and vertical erosion exceeds 100 m at the southern edge on the upslope hills. As proposed above, the cessation of erosion at the northern footslopes may be best explained as being due to burial by a long narrow dune field (essentially a larger, deeper version of the current Bagnold dune field). If so, the 1 billion years may be an underestimate as to how long-ago erosion substantially slowed there. Much of that dune sediment may then have been progressively swept to the west side of the crater floor where presently lies a large dune field (Day and Kocurek, 2016). This erosion period also caused net loss of the washboard along the outer boundaries of the Greenheugh pediment, thus forming across that surface a second beveled bedrock surface (top of the Stimson) also formed through aeolian processes and partially capped by the Gediz Vallis ridge. It may be that the Gediz Vallis ridge topography deflected wind and reduced thereby the washboard erosion near it. Pediment bluff retreat appears to have locally been episodic, associated with the buildup and then stripping of the boulder cover on the underlying exposed Mt. Sharp group bedrock. Current wind and sediment transport along the footslope, as measured and calculated by Bridges et al. (2017), suggest that contemporary erosion rates are slow (**Step 9**). Gediz Vallis ridge deposits lack craters indicating continued active erosion and the current strong outcrop exposure on the east facing side versus the west suggests wind erosion has been stronger from the east.

Taken together **Steps 7 to 9** record an extended dry period with winds (and available sediment) sufficient to drive erosion, but perhaps at a diminishing rate overall, and essentially ceasing in the northern area. The proposed transient reburial of the northern footslopes by an expanded dune field, again calls for the buildup of sediment (**Step 7**). Perhaps this records the wind-swept concentration of sediment from the distal margins of the Gediz Vallis deposit, although paleo and current local wind directions do not indicate transport towards the north. A

pulse of wind derived sediment off the plains to the north of the crater is potentially another source.

In summary, **Steps 1 to 4** indicate a strong wind dominated period, but with groundwater likely near the surface, in which the footslope area shift from net erosion to net deposition may have been driven by internal dynamics of coarse sediment accumulation during crater erosion and topographic evolution driving wind patterns or by delivery to the crater externally. In either case, wind strength needed to be great enough to actively erode and then build a large dune field, and temperatures had to permit near surface groundwater. The ceasing of deposition, and the lithification and then onset of net erosion (**Steps 4 to 5**) may record at first a reduction of wind intensity (or sand sediment supply to the crater) and then a return to active wind erosion. In **Step 6**, a significant (but possibly relatively short lived) wet period developed leading to deposition of gravel and boulder rich sediment now visible in the Gediz Vallis ridge and possibly forming coincident with lakes, gullies, and fan-delta deposits found elsewhere in Gale crater. This may have been preceded by a regional influx of groundwater that led to a delta on the southern crater wall (Palucis et al., 2016), that records a lake level that was 700 m deep over the Gale northern floor. This was followed by an extended dry period with no evidence of either surface or subsurface free water (**Step 7 to 9**). However, Palucis et al. (2016) suggest that the Peace Vallis fan on the northern crater wall formed after Gediz Vallis ridge and related deposits. Grant et al. (2014); Grant and Wilson (2019) and Palucis et al. (2020), using different approaches also suggest it was a more recent event.

Together, this suggests that Mt. Sharp footslope exposures record a rich history of varying intensity of erosion, reversals from erosion to deposition to erosion, a probable early period with ground water near the surface, followed by the wet period of lakes and fluvial (and possibly deltaic) sedimentation, only to return to dry conditions perhaps with progressively diminishing wind strength, and a local deposition phase along the northern base that is currently being slowly stripped away.

There are a few dates of varying specificity that puts these events in a time frame sequence. Crater counting on the ejecta blanket indicate an impact age of ~3.6 to 3.8 billion (Thomson et al., 2011) or more narrowly ~3.55 Ga and ~ 3.65 Ga (Le Deit et al., 2013). In either case, this places it at the late Noachian/early Hesperian time frame when there is ample evidence of extensive hydrogeomorphic activity across Mars (e.g., Fassett and Head III, 2008; Grant et al., 2014; Grant and Wilson, 2019; Haberle, 2022). To estimate the time when Gale erosion had reached close to current topography and then slowed greatly, four different groups have conducted crater counts on the floor and walls of Gale, all counting different locations and different aerial extents. Thomson et al. (2011) combined a patch of the northern Gale floor with a few craters counted on the southern floor and footslopes of Mt. Sharp to arrive at an exposure age of early Hesperian. Le Deit et al. (2013) counted craters on two small areas on the northern floor and reported an age of 3.46 Ga. The age may be problematic however because of the small area and uncertain erosion rate (e.g., Palucis et al., 2020). Grotzinger et al. (2015) report a crater count (using data from Grant et al., 2014) which combined two areas totaling 570 km^2 of ~3.3 to 3.1 Ga. The surveyed areas included Peace Vallis fan and other areas with apparent late surface inverted-channel features. Palucis et al. (2016) counted craters for the entire 14, 200 km^2 floor and lower crater walls, and used only the 33 craters that were greater than 1 km to arrive at an exposure age of 3.3 Ga to 3.5 depending on the isochron system used.

The wide difference in these estimates of when geomorphic activity greatly slowed likely reflect differences in the size of area for which crater counting was done and the relative importance of crater walls that experienced late geomorphic activity versus crater floor regions that did not. Counts in nearby Garu crater by Putnam and Palucis (2021) indicate a formation age of ~3.5 Ga and yet this crater does not have a built-up central mound that presumably would have formed if wind deposition and mound construction had been active in Gale as late as 3.5 Ga. They suggest that Mt. Sharp deposition was, therefore, accomplished by ~3.5

Ga.

There is a reasonably consistent analysis here. The impactor likely hit between 3.6 and 3.8 Ga, with 3.6 Ga being perhaps more likely. Mt. Sharp built and then eroded back to close to its current form by ~3.3 Ga years ago, but significant erosional and depositional activity may have extended to 3.1 Ga, i.e., late Hesperian. Such a timing for decline is consistent with estimates across Mars (e.g., Haberle (2022). Holo et al. (2018) that suggest that since the late Hesperian, Mars obliquity has been on average relatively low, which, as summarized by Haberle (2022) would lead to low surface pressures and reduced near-surface atmospheric densities such that erosion would be greatly reduced. Kite and Mayer (2017) calculate erosion rates on the light toned upper Mt. Sharp bedrock from crater retention analysis as equivalent to ~500 m averaged over the most recent 3 Ga years. This is far too small to explain the deep and extensive erosion of Mt. Sharp, thus supporting a large decrease in erosion rates in the Amazonian period.

Thomson et al. (2011) counted craters on the actively eroding Mt. Sharp and concluded an age of late Hesperian to early Amazonian. Grant and Wilson (2019) combined 6 well-preserved depositional features to obtain a survey area of 429 km^2 and argued that these features reveal hydrogeomorphic activity possibly younger than 2 Ga ago. Palucis et al. (2020) however concluded that one of the features selected (Pancake Delta) is most likely older than 3 billion, while another feature (Peace Vallis fan) could be as young as Grant and Wilson (2019) proposed, but erosional rates create relatively large uncertainty. It is likely that Stimson deposition and lithification (and thus erosion resistance) preceded the Pancake delta lake (which would have risen above the Stimson deposit).

We have the unique direct exposure age dating (at two sites) of 1 billion years which tells us that most of the events on the Mt. Sharp footslope (Stimson formation, partial erosion, gravel deposition in exposed valley floors) significantly predates that time. That there is a fair chance that the exposure age sample area was buried by the equivalent of an expanded Bagnold dune field, implies the actual date of erosion cessation could be much older. Palucis et al. (2016) proposed that the lake that led to the Pancake Delta formation preceded subsequent lakes. This delta most likely formed as a consequence of regional groundwater flow to the north that caused characteristic canyons in the southern walls of the craters that terminate in distinct deltas in many craters in the Gale crater region (Palucis et al., 2016; Rivera-Hernández and Palucis, 2019). The subsequent lakes and deltas in Gale are clearly associated with runoff from the northern crater walls and Mt. Sharp, indicating locally driven hydrogeomorphic events. The >3 Ga age of the Pancake delta (Palucis et al., 2020), and the minimum of 1 billion exposure age, which occurs well after gravel deposition in the eroded northern footslopes, would suggest that the Gediz Vallis depositional events may be early Amazonian (e.g., Holo et al., 2021). Wind erosion was significant after the Gediz Vallis depositional event, as the pediment edge retreated and 100+ meters and incision into upslope topography occurred. That erosion wave may have started before the Amazonian period atmospheric conditions changed and led to much slower erosion rates

Our analysis and the logic presented above places this sequence of events as likely occurring in the late Hesperian to early Amazonian. The climatic variability that drove this rich history of relatively small-scale events could be a signal of infrequent, chaotic transitions in mean obliquity (e.g. Laskar et al., 2004; Kite et al., 2015) that would cause transient changes in atmospheric density and wind strength (driving aeolian erosion and deposition cycles), and possibly sand supply to Gale crater. In addition, groundwater was present during Stimson formation and lithification, and lakes, deltas, and the Gediz Vallis fan deposition occurred before a shift to a cold, dry and wind erosive state developed. A likely brief period of limited surface erosion and fan formation led to Peace Vallis fan deposition and possibly other small features in the Amazonian.

6. Conclusion

The rover-based inspection of the Greenheugh pediment has provided compelling evidence that fluvial processes played no role, leaving wind erosion responsible for the erosional beveling of the underlying bedrock that formed the pediment surface along the footslopes of Mt. Sharp. This suggests that unlike what has been commonly concluded on Earth, pediments on Mars may also form through aeolian processes and consequently their form alone does not necessarily indicate past fluvial activity. Unexpectedly, we have found that the footslope of Mt. Sharp is a telltale environment for recording climate dynamics and the pediment is key piece of the history. Cutting of the pediment surface came after a long period of excavation of Gale and the back wearing of Mt. Sharp that could have initiated as early as 3.5 Ga and likely mostly ceased by ~3.3 Ga. The pediment was capped by a dune field (the Stimson formation) that formed along the sloping footslopes of Mt. Sharp (but not likely extending across the entire crater floor). This burial halted the bedrock erosion, preserving the local topographic surface at that time. That time is not the time of the onset of a global climate shift from wet to dry conditions (which stared perhaps as early as 3.5 Ga), but rather it records a time of renewed sedimentation along the base of Mt. Sharp. The location, composition, and timing of the dune field suggests that the arriving sand could have been derived from the coarse residual of the massive wind excavation of Gale or from an increased supply from an external source. In either case, the development of the field along the base of Mt. Sharp is consistent with regional and topographically-induced wind patterns. These winds were likely stronger than what is possible under present atmospheric density. Importantly, during the period of active sand dunes, groundwater was present, causing local soft-sediment deformation, and contributing to diagenesis and lithification. Later groundwater was emerging from the underlying Mt. Sharp group sediments into the then lithified capping Stimson (creating reactive halos along fractures) in the northern most footslopes, and in the upper footslopes groundwater may have also been flowing within the Stimson along the pediment boundary. When active, this near surface hydrologic activity would require much warmer conditions under a denser atmosphere than present.

The environmental conditions that caused the progressive change from net sediment accretion, to lithification, and then to a net erosional environment that was initiated in the northern slopes are uncertain. Erosion rates may have been fairly low because of the highly resistant Stimson sandstone cap, which had to be breached, and even when vertical erosion cut beneath it into much less resistant Mt. Sharp bedrock, the resultant bluff slope would be mantled by sandstone blocks which would retard lateral erosion. Erosive winds supplied with sufficient loose abrading sediment would be necessary. Exposure ages at the foot of these bluffs indicate that by 1 Ga in the northern slopes lateral erosion nearly ceased and under current atmospheric conditions with its relatively weak winds, erosion rates are exceptionally slow.

Gravel delivery to the floor of the eroded northern footslopes likely signals surface water runoff sometime during a possible extended period of hydrogeomorphic events marked by lakes, deltas, and fans and the buildup of the Gediz Vallis ridge boulder deposits on top of the Stimson bedrock. The earliest, deepest lake (well above the Stimson capped Greenheugh pediment) may have developed >3 Ga, likely formed after Stimson lithification, and was driven by large flows arriving from the south. Subsequent lakes record local surface runoff and erosion. Importantly, gravel deposited in the eroded northern slopes became locally elevated due to local wind erosion, and this happened before the 1 Ga exposure age. Furthermore, after near cessation of the northern slope erosion, wind erosion continued in the south, causing emergence of Vera Rubin ridge and the retreat of the Greenheugh pediment to its current extent. Simultaneously south of the pediment more than 100 m of erosion occurred, creating canyons into the Mt. Sharp bedrock. We hypothesize that the cessation of northern erosion while erosion continued in the south was due to partial burial of the northern slopes by the equivalent of an expanded Bagnold dune field. This would then make the 1 Ga exposure age a potentially significant underestimate of the onset of reduced erosion rate. These observations collectively suggest a late Hesperian to early Amazonian surface runoff period followed by a long period of wind erosion.

Taken together we propose this event sequence: erosion of diagenetically altered bedrock (pediment formation), deposition (Stimson), groundwater-driven diagenesis and lithification (Stimson), erosion that initiates in the north, surface runoff and gravel deposition across the eroded floor of the landscape and deposition on the Greenheugh pediment to the north (and deposition of the Gediz Vallis ridge sediment), wind erosion under dry conditions that spreads from north to south, and a transient reburial by a dune field and then partial exhumation of the northern slopes. This sequence likely records both the global atmospheric density decline and drying into the Amazonian and the obliquity-driven perturbations creating transient periods of sedimentation, liquid water in the subsurface and surface erosion, strong wind erosion and finally a contemporary dry, relatively weakly erosive climate condition in the current low obliquity setting.

Supplementary data to this article can be found online at https://doi.org/10.1016/j.icarus.2024.116445.

CRediT authorship contribution statement

A.B. Bryk: Writing – review & editing, Writing – original draft, Visualization, Software, Project administration, Methodology, Investigation, Formal analysis, Conceptualization. **W.E. Dietrich:** Writing – review & editing, Supervision, Project administration, Methodology, Investigation, Funding acquisition, Conceptualization. **K.A. Bennett:** Writing – review & editing, Investigation, Conceptualization. **V.K. Fox:** Writing – review & editing, Investigation, Conceptualization. **C.M. Fedo:** Writing – review & editing, Supervision, Investigation, Conceptualization. **M.P. Lamb:** Writing – review & editing, Investigation, Conceptualization. **E.S. Kite:** Writing – review & editing. **Lucy M. Thompson:** Writing – review & editing, Visualization, Investigation. **S.G. Banham:** Writing – review & editing, Methodology, Investigation, Conceptualization. **Juergen Schieber:** Writing – review & editing, Investigation. **J.A. Grant:** Writing – review & editing, Investigation. **A.R. Vasavada:** Writing – review & editing, Supervision, Project administration, Methodology, Investigation, Funding acquisition, Conceptualization. **A.A. Fraeman:** Conceptualization, Investigation, Supervision. **L.A. Edgar:** Investigation, Writing – review & editing. **P.J. Gasda:** Writing – review & editing, Investigation. **R.C. Wiens:** Writing – review & editing, Resources, Investigation. **J.P. Grotzinger:** Supervision, Investigation, Conceptualization. **R.E. Arvidson:** Supervision, Investigation, Conceptualization. **O. Gasnault:** Resources, Investigation. **S. Le Mouélic:** Writing – review & editing, Investigation. **S. Gupta:** Supervision, Investigation. **R.M.E. Williams:** Writing – review & editing, Investigation. **R.Y. Sheppard:** Writing – review & editing, Investigation. **K.W. Lewis:** Writing – review & editing, Methodology, Investigation. **D.M. Rubin:** Methodology, Investigation, Formal analysis, Conceptualization. **W. Rapin:** Resources, Investigation. **M.N. Hughes:** Investigation. **M. Turner:** Visualization, Investigation. **S.A. Wilson:** Writing – review & editing. **J.M. Davis:** Writing – review & editing. **R.E. Kronyak:** Resources, Investigation. **Laetitia Le Deit:** Resources, Investigation. **Linda C. Kah:** Writing – review & editing, Investigation. **Jens Frydenvang:** Visualization, Resources, Methodology, Investigation. **Robert J. Sullivan:** Resources, Investigation. **Candice C. Bedford:** Investigation, Conceptualization. **Erwin Dehouck:** Resources, Investigation. **Horton E. Newsom:** Resources, Investigation, Conceptualization. **Michael C. Malin:** Supervision, Software, Resources, Project administration, Methodology, Investigation, Funding acquisition, Formal analysis, Data curation, Conceptualization.

Declaration of competing interest

The authors declare that they have no known competing financial interests or personal relationships that could have appeared to influence the work reported in this paper.

Acknowledgements

Data availability

Image data are available on NASA's Planetary Data System

References

Anderson, R.B., Bell, J.F., 2010. Geologic mapping and characterization of Gale Crater and implications for its potential as a Mars science laboratory landing site. Mars J. 5, 76–128. https://doi.org/10.1555/mars.2010.0004.

Banham, S.G., Gupta, S., Rubin, D.M., Watkins, J.A., Sumner, D.Y., Edgett, K.S., et al., 2018. Ancient Martian aeolian processes and palaeomorphology reconstructed from the Stimson formation on the lower slope of Aeolis Mons, Gale crater, Mars. Sedimentology 65 (4), 993–1042. https://doi.org/10.1111/sed.12469.

Banham, S.G., Gupta, S., Rubin, D.M., Edgett, K.S., Barnes, R., Van Beek, J., et al., 2021. A rock record of complex Aeolian Bedforms in a Hesperian Desert landscape: the Stimson formation as exposed in the Murray buttes, Gale Crater, Mars. J. Geophys. Res.: Planets 126 (4). https://doi.org/10.1029/2020JE006554.

Banham, S.G., Gupta, S., Rubin, D.M., Bedford, C.C., Edgar, L.A., Bryk, A.B., et al., 2022. Evidence for fluctuating wind in shaping an ancient Martian dune Field: the Stimson formation at the Greenheugh pediment, Gale Crater, Mars. J. Geophys. Res.: Planets 127 (9). https://doi.org/10.1029/2021JE007023.

Banham, S.G., Roberts, A.L., Gupta, S., Davis, J.M., Thompson, L.M., Rubin, D.M., et al., 2024. Ice? Salt? Pressure? Sediment deformation structures as evidence of late-stage shallow groundwater in Gale crater, Mars. Geology. https://doi.org/10.1130/G51849.1.

Barchyn, T.E., 2018. Modeling the mechanisms behind Yardang evolution. J. Geophys. Res. Earth 123 (4), 618–621. https://doi.org/10.1002/2018JF004629.

Bedford, C.C., Schwenzer, S.P., Bridges, J.C., Banham, S., Wiens, R.C., Gasnault, O., et al., 2020. Geochemical variation in the Stimson formation of Gale crater: provenance, mineral sorting, and a comparison with modern Martian dunes. Icarus 341, 113622. https://doi.org/10.1016/j.icarus.2020.113622.

Bedford, Candice C., Banham, S.G., Bridges, J.C., Forni, O., Cousin, A., Bowden, D., et al., 2022. An insight into ancient Aeolian processes and post-Noachian aqueous alteration in Gale Crater, Mars, using ChemCam geochemical data from the Greenheugh capping unit. J. Geophys. Res.: Planets 127 (9), e2021JE007100. https://doi.org/10.1029/2021JE007100.

Bell III, J.F., Godber, A., McNair, S., Caplinger, M.A., Maki, J.N., Lemmon, M.T., et al., 2017. The Mars science laboratory curiosity rover Mastcam instruments: preflight and in-flight calibration, validation, and data archiving. Earth Space Sci. 4 (7), 396–452. https://doi.org/10.1002/2016EA000219.

Bennett, K.A., Rivera-Hernández, F., Tinker, C., Horgan, B., Fey, D.M., Edwards, C., et al., 2021. Diagenesis revealed by fine-scale features at Vera Rubin ridge, Gale crater, Mars. J. Geophys. Res.: Planets 126 (5). https://doi.org/10.1029/2019JE006311.

Bennett, K.A., Fox, V.K., Bryk, A., Dietrich, W., Fedo, C., Edgar, L., et al., 2023. The curiosity Rover's exploration of Glen Torridon, Gale Crater, Mars: an overview of the campaign and scientific results. J. Geophys. Res.: Planets 128 (1). https://doi.org/10.1029/2022JE007185.

Blake, D., Vaniman, D., Achilles, C., Anderson, R., Bish, D., Bristow, T., et al., 2012. Characterization and calibration of the CheMin mineralogical instrument on Mars science laboratory. Space Sci. Rev. 170 (1), 341–399. https://doi.org/10.1007/s11214-012-9905-1.

Bretzfelder, J.M., Stack, K.M., Fraeman, A.A., Day, M., Dietrich, W.E., Bryk, A.B., 2024. Aeolian bedrock ridges in Gale crater, Mars. Icarus 408, 115855. https://doi.org/10.1016/j.icarus.2023.115855.

Bridges, J.C., Schwenzer, S.P., Leveille, R., Westall, F., Wiens, R.C., Mangold, N., et al., 2015. Diagenesis and clay mineral formation at Gale Crater, Mars. J. Geophys. Res.: Planets 120 (1), 1–19. https://doi.org/10.1002/2014JE004757.

Bridges, N.T., Sullivan, R., Newman, C.E., Navarro, S., van Beek, J., Ewing, R.C., et al., 2017. Martian aeolian activity at the Bagnold dunes, Gale Crater: the view from the surface and orbit. J. Geophys. Res.: Planets 122 (10), 2077–2110. https://doi.org/10.1002/2017JE005263.

Bristow, T.F., Grotzinger, J.P., Rampe, E.B., Cuadros, J., Chipera, S.J., Downs, G.W., et al., 2021. Brine-driven destruction of clay minerals in Gale crater. Mar. Sci. 373 (6551), 198–204. https://doi.org/10.1126/science.abg5449.

Bryk, A.B., Dietrich, W.E., Lamb, M.P., Grotzinger, J.P., Vasavada, A.R., Stack, K.M., Arvidson, R., Fedo, C., Bennett, K., et al., 2019a. In: Curiosity's Path: The Geomorphology and Stratigraphy of the Greenheugh Pediment and Gediz Vallis Ridge in Gale Crater. Presented at the 50th Annual Lunar and Planetary Science Conference, p. 2263.

Bryk, A.B., Dietrich, W.E., Lamb, M.P., Grotzinger, J.P., Vasavada, A.R., Stack, K.M., Arvidson, R., Fedo, C.M., Fox, V.K., et al., 2019b. In: What was the Original Extent of the Greenheugh Pediment and Gediz Vallis Ridge Deposits in Gale Crater, Mars? Presented at the Ninth International Conference on Mars, vol. 2089, p. 6296.

Bryk, A.B., Dietrich, W.E., Fox, V.K., Bennett, K.A., Banham, S.G., Lamb, M.P., et al., 2020. In: The Stratigraphy of Central and Western Butte and the Greenheugh Pediment Contact. Presented at the 51st Annual Lunar and Planetary Science Conference, p. 2612.

Bryk, Alexander B., Dietrich, W.E., Fedo, C., Caravaca, G., Davis, J.M., Lamb, M.P., et al., 2024. In Situ Investigation of the Gediz Vallis Ridge: A remnant Late-Stage Debris Flow Dominated Fan Deposit in Gale Crater. In: 55th Lunar and Planetary Science Conference. Lunar and Planetary Institute, The Woodlands (Texas), United States, p. 1770. Retrieved from. https://hal.science/hal-04442711.

Buz, J., Ehlmann, B.L., Pan, L., Grotzinger, J.P., 2017. Mineralogy and stratigraphy of the Gale crater rim, wall, and floor units: Gale Crater mineralogy and stratigraphy. J. Geophys. Res.: Planets 122 (5), 1090–1118. https://doi.org/10.1002/2016JE005163.

Calef III, F.J., Parker, T., 2016. MSL Gale Merged Orthophoto Mosaic (25 Centimeter per Pixel Scale). NASA Planetary Data System (PDS) Annex, U.S. Geological Survey. http://bit.ly/MSL_Basemap.

Caswell, T.E., Milliken, R.E., 2017. Evidence for hydraulic fracturing at Gale crater, Mars: implications for burial depth of the Yellowknife Bay formation. Earth Planet. Sci. Lett. 468, 72–84. https://doi.org/10.1016/j.epsl.2017.03.033.

Cawley, J.C., Irwin III, R.P., 2018. Evolution of escarpments, pediments, and plains in the Noachian highlands of Mars. J. Geophys. Res.: Planets 123 (12), 3167–3187. https://doi.org/10.1029/2018JE005681.

Cosgrove, J.W., Banham, S.G., Gupta, S., Barnes, R., 2022. The origin of the fracture networks in the mudstones of Gale Crater Mars; their implications regarding the state of stress and fluid pressure during their formation and the depth to which they were buried. J. Geophys. Res.: Planets 127 (12), e2022JE007313. https://doi.org/10.1029/2022JE007313.

Das, D., Gasda, P.J., Wiens, R.C., Berlo, K., Leveille, R.J., Frydenvang, J., et al., 2020. Boron and Lithium in calcium sulfate veins: tracking precipitation of diagenetic materials in Vera Rubin ridge, Gale Crater. J. Geophys. Res.: Planets 125 (8), e2019JE006301. https://doi.org/10.1029/2019JE006301.

David, G., Cousin, A., Forni, O., Meslin, P.-Y., Dehouck, E., Mangold, N., et al., 2020. Analyses of high-Iron sedimentary bedrock and diagenetic features observed with ChemCam at Vera Rubin ridge, Gale Crater, Mars: calibration and characterization. J. Geophys. Res.: Planets 125 (10), e2019JE006314. https://doi.org/10.1029/2019JE006314.

Day, M., Kocurek, G., 2016. Observations of an aeolian landscape: from surface to orbit in Gale Crater. Icarus 280, 37–71. https://doi.org/10.1016/j.icarus.2015.09.042.

De Toffoli, B., Mangold, N., Massironi, M., Zanella, A., Pozzobon, R., Le Mouélic, S., et al., 2020. Structural analysis of sulfate vein networks in Gale crater (Mars). J. Struct. Geol. 137, 104083. https://doi.org/10.1016/j.jsg.2020.104083.

Dehouck, E., Cousin, A., Mangold, N., Frydenvang, J., Gasnault, O., Forni, O., et al., 2022. Bedrock geochemistry and alteration history of the clay-bearing Glen Torridon region of Gale crater, Mars. J. Geophys. Res.: Planets 127 (12), e2021JE007103. https://doi.org/10.1029/2021JE007103.

Deit, L.L., Hauber, E., Fueten, F., Pondrelli, M., Rossi, A.P., Jaumann, R., 2013. Sequence of infilling events in Gale Crater, Mars: results from morphology, stratigraphy, and mineralogy: sedimentary infilling in Gale Crater. J. Geophys. Res.: Planets 118 (12), 2439–2473. https://doi.org/10.1002/2012JE004322.

Dietrich, W.E., Bryk, A.B., Banham, S.G., Rubin, D.M., Thompson, L.M., Caravaca, G., Williams, R.M.E., 2022. In: Climate and Diagenetic Implications of Possible Soft Sediment Deformation of the Basal Aeolian Stimson Sediments in Gale Crater. Presented at the 53rd Lunar and Planetary Science Conference, vol. 2678, p. 1263.

Dohrenwend, J.C., Parsons, A.J., 2009. Pediments in arid environments. In: Parsons, Anthony J., Abrahams, A.D. (Eds.), Geomorphology of Desert Environments. Springer Netherlands, Dordrecht, pp. 377–411. https://doi.org/10.1007/978-1-4020-5719-9_13.

Dromart, G., Le Deit, L., Rapin, W., Gasnault, O., Le Mouélic, S., Quantin-Nataf, C., et al., 2021. Deposition and erosion of a light-toned Yardang-forming unit of Mt sharp, Gale crater, Mars. Earth Planet. Sci. Lett. 554, 116681. https://doi.org/10.1016/j.epsl.2020.116681.

Edgett, K.S., Yingst, R.A., Ravine, M.A., Caplinger, M.A., Maki, J.N., Ghaemi, F.T., et al., 2012. Curiosity's Mars hand Lens imager (MAHLI) investigation. Space Sci. Rev. 170 (1), 259–317. https://doi.org/10.1007/s11214-012-9910-4.

Ehlmann, B.L., Edgett, K.S., Sutter, B., Achilles, C.N., Litvak, M.L., Lapotre, M.G.A., et al., 2017. Chemistry, mineralogy, and grain properties at Namib and high dunes, Bagnold dune field, Gale crater, Mars: a synthesis of curiosity rover observations. J. Geophys. Res.: Planets 122 (12), 2510–2543. https://doi.org/10.1002/2017JE005267.

Eppes, M.-C., Keanini, R., 2017. Mechanical weathering and rock erosion by climate-dependent subcritical cracking. Rev. Geophys. 55 (2), 470–508. https://doi.org/10.1002/2017RG000557.

Fairbridge, R.W., Finkl, C.W., 1980. Cratonic erosional unconformities and Peneplains. J. Geol. 88 (1), 69–86.

Fassett, C.I., Head III, J.W., 2008. The timing of Martian valley network activity: Constraints from buffered crater counting. Icarus 195 (1), 61–89.

Fedo, C.M., Bryk, A.B., Edgar, L.A., Bennett, K.A., Fox, V.K., Dietrich, W.E., et al., 2022. Geology and stratigraphic correlation of the Murray and Carolyn shoemaker formations across the Glen Torridon region, Gale Crater, Mars. J. Geophys. Res.: Planets 127 (9). https://doi.org/10.1029/2022JE007408.

Fraeman, A.A., Arvidson, R.E., Catalano, J.G., Grotzinger, J.P., Morris, R.V., Murchie, S. L., et al., 2013. A hematite-bearing layer in Gale Crater, Mars: mapping and implications for past aqueous conditions. Geology 41 (10), 1103–1106. https://doi.org/10.1130/G34613.1.

Fraeman, A.A., Ehlmann, B.L., Arvidson, R.E., Edwards, C.S., Grotzinger, J.P., Milliken, R.E., et al., 2016. The stratigraphy and evolution of lower Mount sharp from spectral, morphological, and thermophysical orbital data sets: stratigraphy and evolution of Mount sharp. J. Geophys. Res.: Planets 121 (9), 1713–1736. https://doi.org/10.1002/2016JE005095.

Fraeman, A.A., Edgar, L.A., Rampe, E.B., Thompson, L.M., Frydenvang, J., Fedo, C.M., et al., 2020. Evidence for a diagenetic origin of Vera Rubin ridge, Gale Crater, Mars: summary and synthesis of *curiosity* 's exploration campaign. J. Geophys. Res.: Planets 125 (12). https://doi.org/10.1029/2020JE006527.

Frydenvang, J., Gasda, P.J., Hurowitz, J.A., Grotzinger, J.P., Wiens, R.C., Newsom, H.E., et al., 2017. Diagenetic silica enrichment and late-stage groundwater activity in Gale crater, Mars: silica enriching diagenesis, Gale, Mars. Geophys. Res. Lett. 44 (10), 4716–4724. https://doi.org/10.1002/2017GL073323.

Frydenvang, J., Mangold, N., Wiens, R.C., Fraeman, A.A., Edgar, L.A., Fedo, C.M., et al., 2020. The Chemostratigraphy of the Murray formation and role of diagenesis at Vera Rubin ridge in Gale Crater, Mars, as observed by the ChemCam instrument. J. Geophys. Res.: Planets 125 (9), e2019JE006320. https://doi.org/10.1029/2019JE006320.

Gasda, P.J., Comellas, J., Essunfeld, A, Das, D., Bryk, A.B., Dehouck, E., et al., 2022. Overview of the morphology and chemistry of diagenetic features in the clay-rich Glen Torridon unit of Gale Crater, Mars. J. Geophys. Res.: Planets 127 (12), e2021JE007097. https://doi.org/10.1029/2021JE007097.

Gellert, R., Clark III, B.C., MSL and MER Science Teams, 2015. In situ compositional measurements of rocks and soils with the alpha particle X-ray spectrometer on NASA's Mars rovers. Elements 11 (1), 39–44. https://doi.org/10.2113/gselements.11.1.39.

Grant, J.A., Wilson, S.A., 2019. Evidence for late alluvial activity in Gale Crater, Mars. Geophys. Res. Lett. 46 (13), 7287–7294. https://doi.org/10.1029/2019GL083444.

Grant, J.A., Wilson, S.A., Mangold, N., Calef III, F., Grotzinger, J.P., 2014. The timing of alluvial activity in Gale crater, Mars. Geophys. Res. Lett. 41 (4), 1142–1149. https://doi.org/10.1002/2013GL058909.

Grotzinger, J.P., Gupta, S., Malin, M.C., Rubin, D.M., Schieber, J., Siebach, K., et al., 2015. Deposition, exhumation, and paleoclimate of an ancient lake deposit, Gale crater, Mars. Science 350 (6257), aac7575. https://doi.org/10.1126/science.aac7575.

Haberle, R.M., 2022. Martian Paleoclimate. In: Haberle, R.M. (Ed.), Oxford Research Encyclopedia of Planetary Science. Oxford University Press. https://doi.org/10.1093/acrefore/9780190647926.013.122.

Haberle, R.M., Murphy, J.R., Schaeffer, J., 2003. Orbital change experiments with a Mars general circulation model. Icarus 161 (1), 66–89. https://doi.org/10.1016/S0019-1035(02)00017-9.

Hall, S.R., Farber, D.L., Audin, L., Finkel, R.C., Mériaux, A.-S., 2008. Geochronology of pediment surfaces in southern Peru: implications for quaternary deformation of the Andean forearc. Tectonophysics 459 (1), 186–205. https://doi.org/10.1016/j.tecto.2007.11.073.

Hallet, B., Sletten, R.S., Malin, M., Mangold, N., Sullivan, R.J., Fairén, A.G., et al., 2022. Active ground patterns near Mars' equator in the Glen Torridon region of Gale Crater. J. Geophys. Res.: Planets 127 (10), e2021JE007126. https://doi.org/10.1029/2021JE007126.

Head, J.W., Neukum, G., Jaumann, R., Hiesinger, H., Hauber, E., Carr, M., et al., 2005. Tropical to mid-latitude snow and ice accumulation, flow and glaciation on Mars. Nature 434 (7031), 346–351. https://doi.org/10.1038/nature03359.

Holo, S.J., Kite, E.S., Robbins, S.J., 2018. Mars obliquity history constrained by elliptic crater orientations. Earth Planet. Sci. Lett. 496, 206–214. https://doi.org/10.1016/j.epsl.2018.05.046.

Holo, S.J., Kite, E.S., Wilson, S.A., Morgan, A.M., 2021. The timing of alluvial fan formation on Mars. Planet. Sci. J. 2 (5), 210. https://doi.org/10.3847/PSJ/ac25ed.

Horgan, B.H.N., Johnson, J.R., Fraeman, A.A., Rice, M.S., Seeger, C., Bell III, J.F., et al., 2020. Diagenesis of Vera Rubin ridge, Gale Crater, Mars, From Mastcam Multispectral Images. J. Geophys. Res.: Planets 125 (11), e2019JE006322. https://doi.org/10.1029/2019JE006322.

Howard, A.D., 1997. Badland morphology and evolution: interpretation using a simulation model. Earth Surf. Process. Landf. 22 (3), 211–227. https://doi.org/10.1002/(SICI)1096-9837(199703)22:3<211::AID-ESP749>3.0.CO;2-E.

Hughes, M.N., Arvidson, R.E., Grant, J.A., Wilson, S.A., Howard, A.D., Golombek, M.P., 2019. Degradation of Endeavour crater based on orbital and rover-based observations in combination with landscape evolution modeling. J. Geophys. Res.: Planets 124 (6), 1472–1494. https://doi.org/10.1029/2019JE005949.

Kah, L.C., Rubin, D.M., Gupta, S., Lewis, K.W., Kocurek, G.A., Grotzinger, J.P., 2013. In: Origin of the Low-Albedo Mound Skirting Unit in the Region of the MSL Landing Ellipse, and Implications for the Relative Age of Glenelg Strata. Presented at the 44th Annual Lunar and Planetary Science Conference, p. 1121.

Karlstrom, K.E., Timmons, J.M., 2012. Many unconformities make one 'Great Unconformity.'. In: Timmons, In J.M., Karlstrom, K.E. (Eds.), Grand Canyon Geology: Two Billion Years of Earth's History. Geological Society of America. https://doi.org/10.1130/2012.2489(04).

King, L.C., 1953. Cannons of landscape evolutioln. GSA Bull. 64 (7), 721–752. https://doi.org/10.1130/0016-7606(1953)64[721:COLE]2.0.CO;2.

Kite, E.S., Mayer, D.P., 2017. Mars sedimentary rock erosion rates constrained using crater counts, with applications to organic-matter preservation and to the global dust cycle. Icarus 286, 212–222. https://doi.org/10.1016/j.icarus.2016.10.010.

Kite, E.S., Lewis, K.W., Lamb, M.P., Newman, C.E., Richardson, M.I., 2013. Growth and form of the mound in Gale Crater, Mars: slope wind enhanced erosion and transport. Geology 41 (5), 543–546. https://doi.org/10.1130/G33901.1.

Kite, E.S., Howard, A.D., Lucas, A.S., Armstrong, J.C., Aharonson, O., Lamb, M.P., 2015. Stratigraphy of Aeolis dorsa, Mars: stratigraphic context of the great river deposits. Icarus 253, 223–242. https://doi.org/10.1016/j.icarus.2015.03.007.

Kite, E.S., Sneed, J., Mayer, D.P., Lewis, K.W., Michaels, T.I., Hore, A., Rafkin, S.C.R., 2016. Evolution of major sedimentary mounds on Mars: buildup via anticompensational stacking modulated by climate change. J. Geophys. Res.: Planets 121 (11), 2282–2324. https://doi.org/10.1002/2016JE005135.

Kok, J.F., Parteli, E.J.R., Michaels, T.I., Karam, D.B., 2012. The physics of wind-blown sand and dust. Rep. Prog. Phys. 75 (10), 106901. https://doi.org/10.1088/0034-4885/75/10/106901.

Kronyak, R.E., Kah, L.C., Miklusicak, N.B., Edgett, K.S., Sun, V.Z., Bryk, A.B., Williams, R. M.E., 2019. Extensive polygonal fracture network in Siccar point group strata: fracture mechanisms and implications for fluid circulation in Gale Crater, Mars. J. Geophys. Res.: Planets 124 (10), 2613–2634. https://doi.org/10.1029/2019JE006125.

Laskar, J., Correia, A.C.M., Gastineau, M., Joutel, F., Levrard, B., Robutel, P., 2004. Long term evolution and chaotic diffusion of the insolation quantities of Mars. Icarus 170 (2), 343–364. https://doi.org/10.1016/j.icarus.2004.04.005.

Lewis, K.W., Peters, S., Gonter, K., Morrison, S., Schmerr, N., Vasavada, A.R., Gabriel, T., 2019a. A surface gravity traverse on Mars indicates low bedrock density at Gale crater. Science 363 (6426), 535–537. https://doi.org/10.1126/science.aat0738.

Lewis, K.W., Peters, S., Gonter, K., Morrison, S., Schmerr, N., Vasavada, A.R., Gabriel, T., 2019b. A surface gravity traverse on Mars indicates low bedrock density at Gale crater. Science 363 (6426), 535–537. https://doi.org/10.1126/science.aat0738.

L'Haridon, J., Mangold, N., Fraeman, A.A., Johnson, J.R., Cousin, A., Rapin, W., et al., 2020. Iron mobility during diagenesis at Vera Rubin ridge, Gale Crater, Mars. J. Geophys. Res.: Planets 125 (11), e2019JE006299. https://doi.org/10.1029/2019JE006299.

Mahaffy, P.R., Webster, C.R., Cabane, M., Conrad, P.G., Coll, P., Atreya, S.K., et al., 2012. The sample analysis at Mars investigation and instrument suite. Space Sci. Rev. 170 (1), 401–478. https://doi.org/10.1007/s11214-012-9879-z.

Maki, J., Thiessen, D., Pourangi, A., Kobzeff, P., Litwin, T., Scherr, L., et al., 2012. The Mars science laboratory engineering cameras. Space Sci. Rev. 170 (1), 77–93. https://doi.org/10.1007/s11214-012-9882-4.

Malin, Michael C., Edgett, K.S., 2000. Sedimentary rocks of early Mars. Science 290 (5498), 1927–1937. https://doi.org/10.1126/science.290.5498.1927.

Malin, Michael C., Bell III, J.F., Cantor, B.A., Caplinger, M.A., Calvin, W.M., Clancy, R.T., et al., 2007. Context camera investigation on board the Mars reconnaissance orbiter. J. Geophys. Res.: Planets 112 (E5). https://doi.org/10.1029/2006JE002808.

Malin, Michal C., Ravine, M.A., Caplinger, M.A., Tony Ghaemi, F., Schaffner, J.A., Maki, J.N., et al., 2017. The Mars science laboratory (MSL) mast cameras and descent imager: investigation and instrument descriptions. Earth Space Sci. 4 (8), 506–539. https://doi.org/10.1002/2016EA000252.

Martin, P.E., Farley, K.A., Malespin, C.A., Mahaffy, P.R., Edgett, K.S., Gupta, S., et al., 2021. Billion-year exposure ages in Gale crater (Mars) indicate Mount sharp formed before the Amazonian period. Earth Planet. Sci. Lett. 554, 116667. https://doi.org/10.1016/j.epsl.2020.116667.

Maurice, S., Wiens, R.C., Saccoccio, M., Barraclough, B., Gasnault, O., Forni, O., et al., 2012. The ChemCam instrument suite on the Mars science laboratory (MSL) rover: science objectives and mast unit description. Space Sci. Rev. 170 (1), 95–166. https://doi.org/10.1007/s11214-012-9912-2.

McAdam, A.C., Sutter, B., Archer, P.D., Franz, H.B., Wong, G.M., Lewis, J.M.T., et al., 2020. Constraints on the mineralogy and geochemistry of Vera Rubin ridge, Gale Crater, Mars, from Mars science laboratory sample analysis at Mars evolved gas analyses. J. Geophys. Res.: Planets 125 (11), e2019JE006309. https://doi.org/10.1029/2019JE006309.

McEwen, A.S., Eliason, E.M., Bergstrom, J.W., Bridges, N.T., Hansen, C.J., Delamere, W. A., et al., 2007. Mars reconnaissance Orbiter's high resolution imaging science experiment (HiRISE). J. Geophys. Res.: Planets 112 (E5). https://doi.org/10.1029/2005JE002605.

Milliken, R.E., Grotzinger, J.P., Thomson, B.J., 2010. Paleoclimate of Mars as captured by the stratigraphic record in Gale Crater: STRATIGRAPHY OF GALE CRATER. Geophys. Res. Lett. 37 (4). https://doi.org/10.1029/2009GL041870.

Milliken, R.E., Ewing, R.C., Fischer, W.W., Hurowitz, J., 2014. Wind-blown sandstones cemented by sulfate and clay minerals in Gale Crater, Mars. Geophys. Res. Lett. 41 (4), 1149–1154. https://doi.org/10.1002/2013GL059097.

Moon, S., Perron, J.T., Martel, S.J., Holbrook, W.S., St. Clair, J., 2017. A model of three-dimensional topographic stresses with implications for bedrock fractures, surface

processes, and landscape evolution. J. Geophys. Res. Earth 122 (4), 823–846. https://doi.org/10.1002/2016JF004155.

Oberlander, T.M., 1974. Landscape inheritance and the pediment problem in the Mojave Desert of southern California. Am. J. Sci. 274, 849–875. https://doi.org/10.2475/ajs.274.8.849.

O'Connell-Cooper, C.D., Thompson, L.M., Spray, J.G., Berger, J.A., Gellert, R., McCraig, M., VanBommel, S.J., Yen, A., 2022. Statistical analysis of APXS-derived chemistry of the clay-bearing Glen Torridon region and Mount Sharp group, Gale crater, Mars. J. Geophys. Res. Planets 127, e2021JE007177. https://doi.org/10.1029/2021JE007177.

Palucis, M.C., Dietrich, W.E., Williams, R.M.E., Hayes, A.G., Parker, T., Sumner, D.Y., et al., 2016. Sequence and relative timing of large lakes in Gale crater (Mars) after the formation of Mount sharp: LARGE LAKES IN GALE POST MOUNT SHARP. J. Geophys. Res.: Planets 121 (3), 472–496. https://doi.org/10.1002/2015JE004905.

Palucis, M.C., Jasper, J., Garczynski, B., Dietrich, W.E., 2020. Quantitative assessment of uncertainties in modeled crater retention ages on Mars. Icarus 341, 113623. https://doi.org/10.1016/j.icarus.2020.113623.

Parker, T., Calef III, F.J., 2016. MSL Gale Merged Digital Elevation Model, Publisher: PDS Annex. U.S. Geological Survey. URL: http://bit.ly/MSL_DEM.

Parsons, A.J., Abrahams, A.D., 1984. Mountain mass denudation and piedmont formation in the Mojave and Sonoran deserts. Am. J. Sci. 284, 255–271. https://doi.org/10.2475/ajs.284.3.255.

Pelletier, Jon D., 2018. Controls on Yardang development and morphology: 2. Numerical modeling. J. Geophys. Res. Earth Surf. 123 (4), 723–743. https://doi.org/10.1002/2017JF004462.

Pelletier, Jon D., Kapp, P.A., Abell, J., Field, J.P., Williams, Z.C., Dorsey, R.J., 2018. Controls on Yardang development and morphology: 1. Field observations and measurements at ocotillo Wells, California. J. Geophys. Res. Earth 123 (4), 694–722. https://doi.org/10.1002/2017JF004461.

Pelletier, Jon.D., 2010. How do pediments form?: a numerical modeling investigation with comparison to pediments in southern Arizona, USA. Geol. Soc. Am. Bull. 122 (11–12), 1815–1829. https://doi.org/10.1130/B30128.1.

Pla-Garcia, J., Rafkin, S.C.R., Kahre, M., Gomez-Elvira, J., Hamilton, V.E., Navarro, S., et al., 2016. The meteorology of Gale crater as determined from rover environmental monitoring station observations and numerical modeling. Part I: comparison of model simulations with observations. Icarus 280, 103–113. https://doi.org/10.1016/j.icarus.2016.03.013.

Pohjola, J., Turunen, J., Lipping, T., 2009. Creating High-Resolution Digital Elevation Model Using Thin Plate Spline Interpolation and Monte Carlo Simulation, p. 60. Finland.

Rampe, E.B., Blake, D.F., Bristow, T.F., Ming, D.W., Vaniman, D.T., Morris, R.V., et al., 2020a. Mineralogy and geochemistry of sedimentary rocks and eolian sediments in Gale crater, Mars: a review after six earth years of exploration with curiosity. Geochemistry 80 (2), 125605. https://doi.org/10.1016/j.chemer.2020.125605.

Rampe, E.B., Bristow, T.F., Morris, R.V., Morrison, S.M., Achilles, C.N., Ming, D.W., et al., 2020b. Mineralogy of Vera Rubin ridge from the Mars science laboratory CheMin instrument. J. Geophys. Res.: Planets 125 (9), e2019JE006306. https://doi.org/10.1029/2019JE006306.

Rivera-Hernández, F., Palucis, M.C., 2019. Do deltas along the crustal dichotomy boundary of Mars in the Gale Crater region record a Northern Ocean? Geophys. Res. Lett. 46 (15), 8689–8699. https://doi.org/10.1029/2019GL083046.

Rudolph, A., Horgan, B., Johnson, J., Bennett, K., Haber, J., Bell III, J.F., et al., 2022. The distribution of clay minerals and their impact on diagenesis in Glen Torridon, Gale Crater, Mars. J. Geophys. Res.: Planets 127 (10), e2021JE007098. https://doi.org/10.1029/2021JE007098.

Salese, F., Pondrelli, M., Neeseman, A., Schmidt, G., Ori, G.G., 2019. Geological evidence of planet-wide groundwater system on Mars. J. Geophys. Res.: Planets 124 (2), 374–395. https://doi.org/10.1029/2018JE005802.

Schieber, J., Bish, D., Coleman, M., Reed, M., Hausrath, E.M., Cosgrove, J., et al., 2017. Encounters with an unearthly mudstone: understanding the first mudstone found on Mars. Sedimentology 64 (2), 311–358. https://doi.org/10.1111/sed.12318.

Siebach, K.L., Grotzinger, J.P., 2014. Volumetric estimates of ancient water on Mount sharp based on boxwork deposits. Gale Crater, Mars. J. Geophys. Res.: Planets 119 (1), 189–198. https://doi.org/10.1002/2013JE004508.

Souness, C., Hubbard, B., 2012. Mid-latitude glaciation on Mars. Progr. Phys. Geogr.: Earth Environ. 36 (2), 238–261. https://doi.org/10.1177/0309133312436570.

Stack, K.M., Grotzinger, J.P., Kah, L.C., Schmidt, M.E., Mangold, N., Edgett, K.S., et al., 2014. Diagenetic origin of nodules in the Sheepbed member, Yellowknife Bay formation, Gale crater, Mars. J. Geophys. Res.: Planets 119 (7), 1637–1664. https://doi.org/10.1002/2014JE004617.

Stack, K.M., Cofield, S.M., Fraeman, A.A., 2017. In: Geologic Map of the MSL Curiosity Rover Extended Mission Traverse of Aeolis Mons, Gale Crater, Mars. Presented at the 48th Annual Lunar and Planetary Science Conference, p. 1889.

Stack, K.M., Dietrich, W.E., Lamb, M.P., Sullivan, R.J., Christian, J.R., Newman, C.E., et al., 2022. Orbital and in-situ investigation of periodic bedrock ridges in Glen Torridon, Gale Crater, Mars. J. Geophys. Res.: Planets 127 (6), e2021JE007096. https://doi.org/10.1029/2021JE007096.

Stein, N.T., Quinn, D.P., Grotzinger, J.P., Fedo, C., Ehlmann, B.L., Stack, K.M., Edgar, L.A., Fraeman, A.A., Deen, R., 2020. Regional structural orientation of the Mount

Sharp group revealed by in situ dip measurements and stratigraphic correlations on the Vera Rubin ridge. J. Geophys. Res. Planets 125, e2019JE006298. https://doi.org/10.1029/2019JE006298.

Sun, V.Z., Stack, K.M., Kah, L.C., Thompson, L., Fischer, W., Williams, A.J., Johnson, S.S., Wiens, R.C., Kronyak, R.E., Nachon, M., House, C.H., VanBommel, S., 2020. Late-stage diagenetic concretions in the Murray formation, Gale Crater, Mars. Earth Planet. Sci. Lett. 552, 116587. https://doi.org/10.1016/j.epsl.2020.116587.

Sutter, B., McAdam, A.C., Wong, G.M., Clark, J.V., Archer, P.D., Franz, H.B., et al., 2022. Constraining alteration processes along the Siccar point group unconformity, Gale Crater, Mars: results from the sample analysis at Mars instrument. J. Geophys. Res.: Planets 127 (11), e2022JE007387. https://doi.org/10.1029/2022JE007387.

Thompson, L., Spray, J., Gellert, R., Williams, R., Berger, J., O'Connell-Cooper, C., et al., 2022a. In: APXS-determined Compositional Diversity of Eolian Siccar Point Group Sandstones, Gale crater Mars: Implications for Provenance and Timing of Events, EPSC2022-1184. Presented at the European Planetary Science Congress. https://doi.org/10.5194/epsc2022-1184.

Thompson, L.M., Berger, J.A., Spray, J.G., Fraeman, A.A., McCraig, M.A., O'Connell-Cooper, C.D., et al., 2020. APXS-derived compositional characteristics of Vera Rubin ridge and Murray formation, Gale Crater, Mars: geochemical implications for the origin of the ridge. J. Geophys. Res.: Planets 125 (10), e2019JE006319. https://doi.org/10.1029/2019JE006319.

Thompson, L.M., Spray, J.G., O'Connell-Cooper, C., Berger, J.A., Yen, A., Gellert, R., et al., 2022b. Alteration at the base of the Siccar point unconformity and further evidence for an alkaline provenance at Gale Crater: exploration of the Mount sharp group, Greenheugh pediment cap rock contact with APXS. J. Geophys. Res.: Planets 127 (11), e2021JE007178. https://doi.org/10.1029/2021JE007178.

Thomson, B.J., Bridges, N.T., Milliken, R., Iii, J.F.B., Calvin, W.C., Weitz, C.M., 2008. New Constraints on the Origin and Evolution of the Layered Deposits in Gale.

Thomson, B.J., Bridges, N.T., Milliken, R., Baldridge, A., Hook, S.J., Crowley, J.K., et al., 2011. Constraints on the origin and evolution of the layered mound in Gale Crater, Mars using Mars reconnaissance orbiter data. Icarus 214 (2), 413–432. https://doi.org/10.1016/j.icarus.2011.05.002.

Thorpe, M.T., Bristow, T.F., Rampe, E.B., Tosca, N.J., Grotzinger, J.P., Bennett, K.A., et al., 2022. Mars science laboratory CheMin data from the Glen Torridon region and the significance of Lake-groundwater interactions in interpreting mineralogy and sedimentary history. J. Geophys. Res.: Planets 127 (11), e2021JE007099. https://doi.org/10.1029/2021JE007099.

Turner, M., Lewis, K., 2023. Geologic structure of the Vera Rubin ridge, Gale Crater, Mars. J. Geophys. Res.: Planets 128 (9), e2022JE007237. https://doi.org/10.1029/2022JE007237.

Twidale, C.R., 2014. Pediments and platforms: problems and solutions. Géomorphol.: Relief, Process. Environ. 20 (1), 43–56. https://doi.org/10.4000/geomorphologie.10480.

Vail, P.R., Todd, R.G., Sangree, J.B., 1977. Seismic stratigraphy and global changes of sea level, part 5Chronostratigraphic significance of seismic Reflections[1]. In: Payton, C.E. (Ed.), Seismic Stratigraphy — Applications to Hydrocarbon Exploration. American Association of Petroleum Geologists. https://doi.org/10.1306/M26490C7

Watkins, J.A., Grotzinger, J.P., Stein, N.T., Banham, S.G., Gupta, S., Rubin, D.M., et al., 2022. Burial and exhumation of sedimentary rocks revealed by the base Stimson erosional unconformity, Gale Crater, Mars. J. Geophys. Res.: Planets 127 (7). https://doi.org/10.1029/2022JE007293.

Weitz, C.M., Lewis, K.W., Bishop, J.L., Thomson, B.J., Arvidson, R.E., Grant, J.A., et al., 2022. Orbital observations of a marker horizon at Gale Crater. J. Geophys. Res.: Planets 127 (4), e2022JE007211. https://doi.org/10.1029/2022JE007211.

Wiens, R.C., Maurice, S., Barraclough, B., Saccoccio, M., Barkley, W.C., Bell, J.F., et al., 2012. The ChemCam instrument suite on the Mars science laboratory (MSL) rover: body unit and combined system tests. Space Sci. Rev. 170 (1), 167–227. https://doi.org/10.1007/s11214-012-9902-4.

Wiens, R.C., Edgett, K.S., Stack, K.M., Dietrich, W.E., Bryk, A.B., Mangold, N., et al., 2020. Origin and composition of three heterolithic boulder- and cobble-bearing deposits overlying the Murray and Stimson formations, Gale Crater, Mars. Icarus 350, 113897. https://doi.org/10.1016/j.icarus.2020.113897.

Williams, R.M.E., Malin, M.C., Stack, K.M., Rubin, D.M., 2018. Assessment of Aeolis Palus stratigraphic relationships based on bench-forming strata in the Kylie and the Kimberley regions of Gale crater, Mars. Icarus 309, 84–104. https://doi.org/10.1016/j.icarus.2018.02.028.

Wong, G.M., Lewis, J.M.T., Knudson, C.A., Millan, M., McAdam, A.C., Eigenbrode, J.L., et al., 2020. Detection of reduced sulfur on Vera Rubin ridge by quadratic discriminant analysis of volatiles observed during evolved gas analysis. J. Geophys. Res.: Planets 125 (8), e2019JE006304. https://doi.org/10.1029/2019JE006304.

Yen, A.S., Ming, D.W., Vaniman, D.T., Gellert, R., Blake, D.F., Morris, R.V., et al., 2017. Multiple stages of aqueous alteration along fractures in mudstone and sandstone strata in Gale Crater, Mars. Earth Planet. Sci. Lett. 471, 186–198. https://doi.org/10.1016/j.epsl.2017.04.033.

Yingst, R.A., Edgett, K.S., Kennedy, M.R., Krezoski, G.M., McBride, M.J., Minitti, M.E., et al., 2016. MAHLI on Mars: lessons learned operating a geoscience camera on a landed payload robotic arm. Geoscient. Instrument. Methods Data Syst. 5 (1), 205–217. https://doi.org/10.5194/gi-5-205-2016.